



**Pilkington Library**

Author/Filing Title ..... MCDONALD .....

Vol. No. .... Class Mark ..... T .....

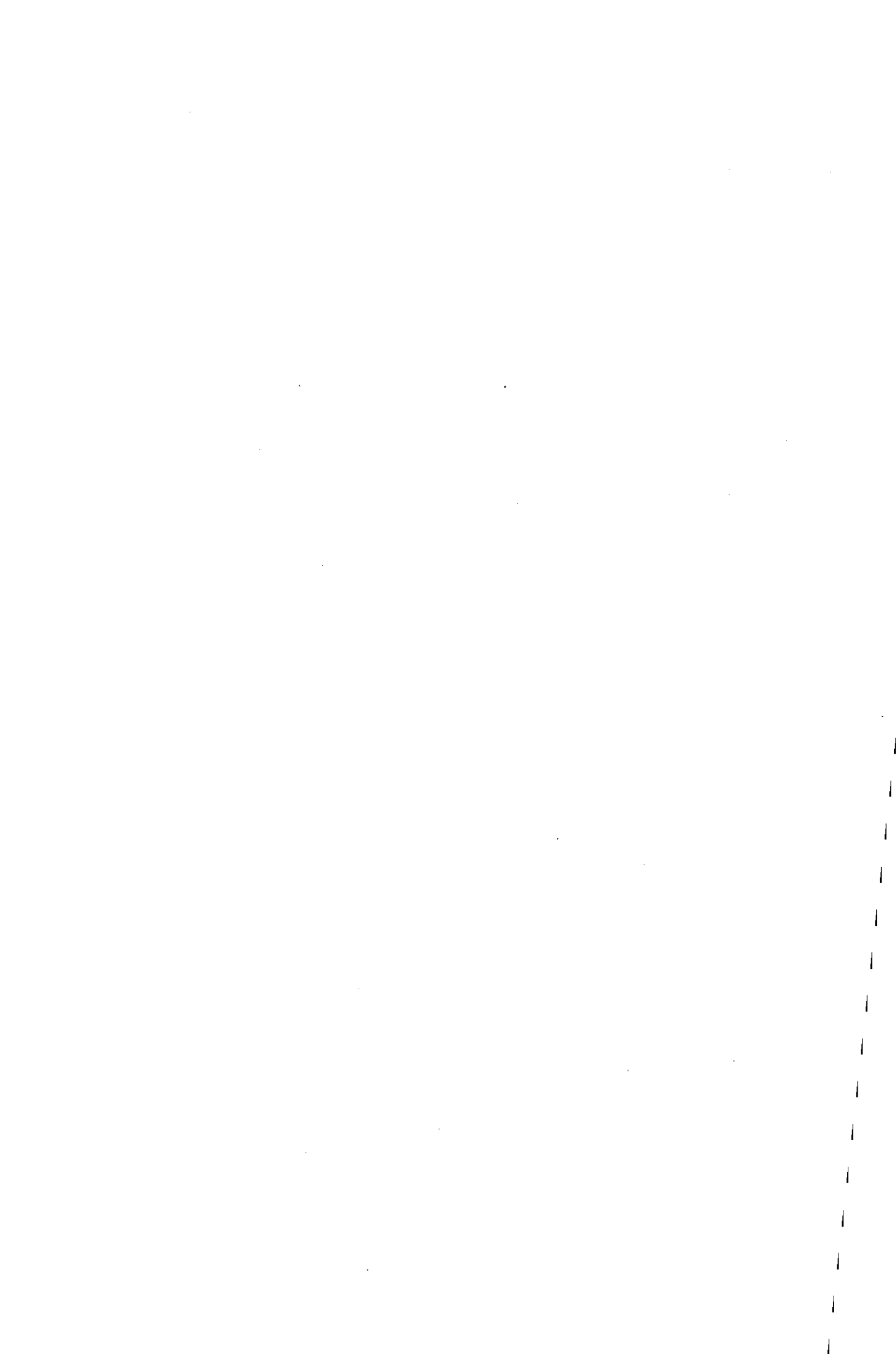
**Please note that fines are charged on ALL  
overdue items.**

OPEN SITE F COPY

0402294114



BADMINTON PRESS  
UNIT 1 BROOK ST  
SYSTON  
LEICESTER, LE7 1GD  
ENGLAND  
TEL : 0116 260 2917  
FAX : 0116 269 6639



# **OPTICAL MEASUREMENT OF PRESSURE TRANSIENT INDUCED FLOW IN HYDRAULIC SYSTEMS**

by

**Nicholas John McDonald**

**A Master of Philosophy Thesis**

**Submitted in partial fulfilment of the requirements for the award of Master of Philosophy of  
Loughborough University**

**May 2000**

**© N. J. McDonald 2000**

 Loughborough University Faculty of Science
Date Jan 01
Class
Acc. No. 040229411

M0002729LB

# CONTENTS

CONTENTS		i
ABSTRACT		v
ACKNOWLEDGMENTS		vi
CHAPTER 1	Introduction and Literature Review	1
1.1	Introduction to Solids, Liquids and Gases	1
1.2	Molecular Structure	2
1.3	Difference between Solids and Fluids - Flow	2
1.4	Viscosity - Ideal and Real Fluids	4
1.5	Background and Overview of Project Work	5
1.6	Thesis Outline	6
CHAPTER 2	Techniques for Studying Fluid and Particle Motion	8
2.1	Introduction	8
2.2	Hot-Wire Anemometry	8
2.2.1	Introduction	8
2.2.2	Anemometers and Electrical Packages	9
2.2.2.1	Anemometers	10
2.2.2.2	Electronic Packages	10
2.2.3	Experimental Usage of HWA	11
2.3	Laser Doppler Anemometry	12
2.3.1	Introduction	12
2.3.2	Doppler Shift and Optical Beating	13

2.3.3	Laser-Doppler Anemometers	14
2.3.3.1	Reference Beam Mode	14
2.3.3.2	Dual Beam Mode	15
2.3.3.3	Two Scattered Beam Mode	15
2.3.4	Experimental usage of LDA	16
2.4	Particle Image Velocimetry	17
2.4.1	Introduction	17
2.4.2	PIV Technique	18
2.4.2.1	Image Recording	18
2.4.2.2	Image Interrogation	19
2.4.3	Advances in PIV and Experimental Usage	19
CHAPTER 3	Water Hammer	22
3.1	Introduction	22
3.2	Water Hammer Causes	23
3.2.1	Valve Closure	23
3.2.2	Steam Pockets	26
3.3	Other Water Hammer Causes and Effects	28
3.4	Control of Water Hammer	30
CHAPTER 4	Study of Mechanically Induced Fluid Pressure Pulses	31
4.1	Introduction	31
4.2	Transducer and Connection to Equipment	31
4.3	Calibration Transducer	33
4.4	Transducer Testing - Cylinder Drop Experiment	34

<b>CHAPTER 5</b>	<b>Hydraulic System and Electronic Equipment</b>	<b>46</b>
5.1	Introduction	46
5.2	Hydraulic System	46
5.2.1	Hydraulic Power Pack	46
5.2.2	Accumulator	48
5.2.3	Servo valve	49
5.3	Setup of the Equipment	51
5.4	Electronic Equipment	52
5.4.1	Function Generator	52
5.4.2	Oscilloscope	53
5.5	Operating Procedure	53
<b>CHAPTER 6</b>	<b>Study I of Hydraulic System Fluid Pulses</b>	<b>55</b>
6.1	Introduction	55
6.2	Oil Seeding	55
6.3	Assembly of Optical and Imaging Equipment	56
6.3.1	Optical Equipment	56
6.3.2	Calculation of Soda Glass Window Thickness with Respect to Survival Time and Probability	57
6.3.3	Imaging Equipment	61
6.4	Initial Observations - Images and Pressure Trace Comparison	62
6.4.1	Equipment Settings	62
6.4.2	Oscilloscope Observations	62
6.4.3	Optical Observations	64
6.5	Further Work - Damaging Transducers	73
6.5.1	Increase in Valve Frequency	73
6.5.2	Use of Smaller Cross Sectional Area Fitting	75

6.5.3	Increase in Air Volume in the System	80
6.6	The Air-Standard Cycles	84
6.6.1	The Diesel and Otto Cycles - A Brief Description	84
6.6.2	The Diesel Cycle	85
6.7	Pressure, Temperature, Volume and Work Done due to Air Compression in a Dieseling Process	87
6.8	Discussion of Results and Conclusion	90
CHAPTER 7	Study II of Hydraulic System Fluid Pulses	92
7.1	Introduction	92
7.2	Testing of Laser Triggering	93
7.2.1	TTL Monostable	93
7.2.2	Equipment Assembly	94
7.3	Sequence of Images of the Transducer Diaphragm	96
CHAPTER 8	Conclusions and Possible Future Work	103
8.1	Conclusions	103
8.2	Possible Future Work	106
REFERENCES		108

# ABSTRACT

The project is concerned with observation of fluid movement and transducer diaphragm deformation, under the influence of large pressure transients of the order of 2000 PSI(140 bar). Large pressure surges often occur in hydraulic systems and this coupled with sharp rise times of the order of 100  $\mu$ s, causes damage to the surface of the transducer diaphragm or face and subsequently the pressure reading mechanisms.

CCD (Charged Coupled Device) cameras together with a suitable light source are useful optical tools to study such a process, where dramatic occurrences take place in a short time duration. A seeding technique was used to enable monitoring of the fluid movement near the transducer diaphragm, thus revealing how fluid behaves. The transducer readings can be related to the observed fluid motion and damaging mechanisms, such as water hammer, can be visualised. If the experiment is reproducible, i.e. successive pressure transients are very similar, triggered laser flashes can be used as the light source. This makes it possible to produce a picture sequence of the transducer face movement, during the pressure transient rise time.

The experiments have shown particle movement back and forth in the fluid, together with deformation of the transducer diaphragm. With high pressure changes occurring at high frequencies, air cavities form within the oil and this induces larger pressure transients with overshoot and shorter rise times. This air in the system causes severe water hammer, both in terms of noise and damage to the transducer. Dieseling of the air and oil mixture arises as a side effect and the flashes continue until the oxygen is burnt off.

# ACKNOWLEDGEMENTS

I would like to take this opportunity to express my sincere gratitude to my supervisor, Prof. David C. Emmony, for all his guidance and support, during the past year. Thanks also goes to my Director of Research, Dr. David J. Parry, for his valued advice during my course of research and also to Dr. Gerry Swallowe and Dr. Gary Critchlow for the use of equipment and sharing of knowledge.

Much appreciation goes to Steve Briggs and Peter Morgenroth of Druck Ltd. for the financial support that enabled me to undertake my research project.

I would also like to thank the following people from the Department of Physics for their utmost and professional help. Many thanks to Mr. David Insley, Mr. John Oakley and Mr. Pat Newman : for their expert work in the production of experimental fittings. Thanks also to the following staff for their assistance and support: Mr. B. Dennis, Mr. R. Pancholi, Mr. M. Pancholi, Mrs. K. Bedwell and Mr. B. K. Chavda.

My friends and colleagues at the University have been of great help and have made my time here a very informative, useful and often amusing experience. Special thanks to Ben Smith, Dr. Richard Simper, Tim Gentry, Vivi Pouli, Oscar Fernandez, Chris Cottam and Stephen Shaw for their advice and humour.

Finally, I wish to thank my family and friends for their encouragement and support, which is greatly appreciated.

# **CHAPTER 1**

## **Introduction and Literature Review**

### **1.1 Introduction to Solids, Liquids and Gases**

Matter consists of three separate states in the form of solids, liquids and gases. There is a conflict between thermal energy and intermolecular forces that determines which one of the given three forms a substance will take. Although the states are clearly different in some respects and behave in contrasting ways it is a mistake to think that solids, liquids and gases are not linked. In terms of differences solids are an example of elasticity laws, gases are an example of kinetic theory and liquids have viscosity, surface tension and bulk compressibility. This suggests that the three are completely unrelated but intermolecular forces tell us about the bulk properties of solids, liquids and gases and it is in this way that the states have something in common [1.1].

The three states can be broken down into solids and fluids. Fluids can exist in the form of gases and liquids, whereas solids are just solids. Before we can delve into the question what is a fluid, we may just as well ask ourselves what is the difference between a solid and a fluid? A simplistic answer would be that solids are hard and difficult to deform, while fluids are softer and easy to deform [1.2]. Although this might seem to be an acceptable answer, the description only touches on the subject. To gain more understanding of the difference between solids and fluids we need to examine the molecular structure of substances.

## **1.2 Molecular Structure**

All substances embody an immense quantity of molecules that are separated by empty space. There is an attraction force between all the molecules, but if the distance between them is greatly decreased to values approaching  $0.5 \times 10^{-10}$  m, there exists a repulsion force that prohibits them all joining together as one complete block. The molecules have continuous motion, but the extent of this movement is determined by the state of matter of the substance [1.3].

In solids the molecules are very close together and have strong intermolecular cohesive forces. Therefore the molecules only have slight movement (no relative movement to each other) and so solids have substantial stiffness and maintain their original shape. The molecules in liquids aren't quite as close together and the intermolecular forces are much weaker allowing more freedom of movement. However the bonds between molecules are strong enough to hold the liquid together in a definite volume [1.2]. Gases are different, with greater molecular spacing and much more molecular movement. The forces between molecules are inversely proportional to the distance they are apart and thus negligible in gases, so that the molecules are free to move away from each other indefinitely; a gas has no definite volume and will fill whatever volume it is contained in.

## **1.3 Difference between Solids and Fluids - Flow**

Although molecular structure shows the difference between solids, liquids and gases the difference between solids and fluids lies in the fact that fluids flow. Solids and liquids have a definite volume but the greater molecular spacing in liquids allows molecules to move past one another. Therefore a liquid is like a gas in that it is not rigid and can flow; liquids and gases are fluids. Fluids cannot resist shear forces when at rest. In other words they cannot sustain tangential forces, meaning that they cannot

present an enduring resistance to the displacement of one layer over another [1.3] [1.4]. The actual definition of a fluid is a substance that deforms continuously under the influence of a shearing or tangential force of any magnitude [1.2] [1.5] [1.6]. Figure 1, based on experimental observations [1.5], shows the behavior of both solids and fluids when acted upon by a constant shear or tangential force.

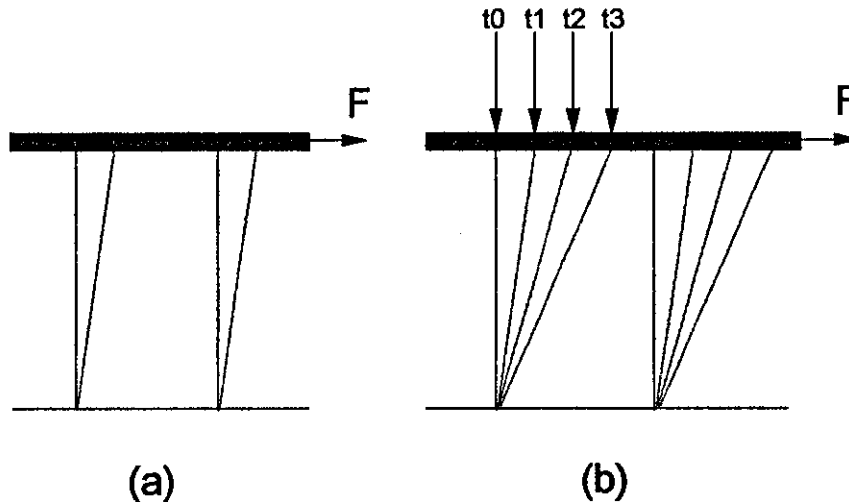


Figure 1 Response of a solid (a) and a fluid (b) under the influence of a constant tangential or shear force

In Figure 1a the solid is bonded between two plates, with the bottom plate fixed and the top plate moveable. The constant shear force  $F$  is applied to the upper plate and the block, of rectangular cross section, begins to deform. Assuming the block's elastic limit is not surpassed, it is guaranteed that the block deformation will be proportional to the applied stress [1.5]. The block will continue to deform, with the cross section forming a parallelogram. There is point where a balance is struck between the solid's built in stiffness and the shear force applied. Once this has occurred the block will stop deforming and will have a constant shape.

The experiment can be repeated with a "real" (explained in next section) fluid between the boundaries or plates, using a dye to mark out the same rectangular shape

as the solid. Figure 1b shows that with the same shear force applied, the fluid component deforms, again producing the shape of a parallelogram. Assuming the force  $F$  is continually applied the fluid element continues to change shape indefinitely, as shown by the dye outline at times  $t_0$ ,  $t_1$ ,  $t_2$  and  $t_3$  where  $t_3 > t_2 > t_1 > t_0$ .

The layer of fluid in direct contact with the solid boundary or plate will have the same velocity as the boundary itself; there is no slip at the boundary. This is an experimentally observed characteristic of fluids [1.5] and the amount or lack of slip is determined by the fluids viscosity.

## **1.4 Viscosity - Ideal and Real Fluids**

Fluids can be split into ideal and real fluids. Mathematical problems in fluid mechanics are simplified if a fluid is ideal. Ideal or perfect fluids are inviscid (have no or zero viscosity), thus they can sustain no “internal” tangential stress. It is possible for an ideal fluid to slip at a solid boundary; the velocity of the layer of fluid at the boundary is different to the velocity of the boundary itself [1.4]. An example of a near inviscid fluid is liquid nitrogen and once stirred the liquid nitrogen will continue to rotate inside the container.

Most fluids however are real fluids, have a certain viscosity value and will definitely slip at a solid boundary. Fluids with low viscosity values will flow easily, for example water has a viscosity of  $1.000 \times 10^{-3} \text{ Nsm}^{-2}$  [1.7]. Some substances however have a much higher viscosity, don't flow as easily and therefore it is often difficult to determine whether these materials are solids or liquids. These substances initially appear to behave like solids, but they might also behave like a fluid. In plastic materials such as tar and putty, either type of shear deformation will occur depending on the magnitude of the shear stress. If a low shear stress is applied to these materials they will behave as solids and will have a definite deformation. Shear stresses above a

certain critical value will induce continuous deformation and the materials experience flow. The study of such plastic solids is called rheology [1.2] [1.3] [1.6]. The fundamental distinction between solids and fluids remains. Irrespective of how thick a fluid is it will always begin and continue to flow under the smallest of net shear forces, whereas the shear force must exceed a critical value for flow to be initiated in a solid. Even then, as discussed earlier, there becomes a point where the force of moving one layer over another balances out the applied force, resulting in no further movement [1.3].

## **1.5 Background and Overview of Project Work**

Transducers are used in domestic and industrial equipment and machinery to gauge many varied factors over specific ranges. There are transducers to measure accelerations, displacements, flow in gases and liquids, forces, pressures and even humidity [1.8]. Although they are designed and function in different ways, they all serve a purpose and are all susceptible to damage, under adverse conditions and by known and unknown mechanisms.

The title of my project “Optical Measurement of Pressure Transient Induced Flow in hydraulic Systems” is quite self explanatory and during my project I have studied the behavior of pressure transducers under various conditions. Pressure transducers were first developed for use during the Industrial Revolution to measure liquid levels in piping. Next came the invention of the universal Bourdon tube and this is still a common piece of equipment used to measure pressure today [1.8]. However one of the most modern pressure transducers is one with an electrical output signal. These transducers or modules are able to measure pressures very accurately and responsively; they are able to cope with rapid fluctuations and changes in pressure. Generally the design of such transducers incorporates a diaphragm as the immediate sensing component. This is linked to some kind of electrical circuit that converts the

diaphragm deformation into an electrical signal the value of which represents the applied pressure.

Industrial processes require confirmation of actions or functions and so it is essential that the electrical signals can be sent to any part of a machine to verify that an event has successfully taken place. Problems arise when one or more transducers fail, resulting in a partial or complete breakdown in a machine or plant. Even more of a problem is that the transducers or modules are enclosed in steel pipes and fittings within high or low pressure systems and so cannot be visualised while they function or fail; the only indication that a transducer has been damaged is the lack of electrical signal.

Therefore the idea of my project is to optically monitor pressure transducers and the movement of the liquid (oil) in the immediate vicinity of the transducer diaphragm or face. It was known that the use of high pressure pulses would induce damage to both the diaphragm surface and the electric circuitry within the transducer. The pressures were of the order of 2000 PSI (140 bar or 14 MPa) with pulse frequencies of 0.25Hz or more. With the use of a specialised optical fitting and suitable optical diagnostic tools it should be possible to monitor the movement of both the transducer diaphragm and also the particles within the oil. Known and unknown hydraulic phenomena could be viewed first hand to make it possible to discover and begin to understand the cause of the damage.

## **1.6 Thesis Outline**

The following briefly describes the work carried out during the project.

Chapter 1 is an introduction to solids, liquid and gases and outlines the project.

Chapter 2 describes the different techniques used to monitor fluid and liquid movement and behavior, from late in the last century the introduction of hot wire anemometry to the present day laser doppler and particle image velocimetry techniques.

Chapter 3 gives an insight into the phenomena of water hammer. For years this mechanism has been a major cause of pipeline and valve damage. This chapter describes how water hammer arises, what effects it has and methods of its prevention or control.

Chapter 4 is a report of the initial experimental work. This involved the electrical study of mechanically induced pressure pulses and their affect on the pressure transducer.

Chapter 5 is a detailed description of the equipment used for the main experimental work. The source of the pressure pulses is a compressed air driven hydraulic power pack and the control of these pulses is provided by a 'MOOG' servovalve (a fast acting hydraulic switch) operated by a function generator.

Chapter 6 describes the main experimental work involving the optical diagnostic technique of using a suitable continuous light source, CCD camera and frame grabber. The results, obtained and problems found are included in this chapter.

Chapter 7 contains the final experimental work. A technique for monitoring the diaphragm movement, involving a laser flash pulse as the light source, is discussed and the technique is compared to the continuous light source.

Chapter 8 contains the conclusions and suggests possible future work in this field.

# **CHAPTER 2**

## **Techniques for Studying Fluid and Particle Motion**

### **2.1 Introduction**

Scientists have been studying the behavior of and measuring the velocities of fluids and particle movement for the past hundred years [2.1]. Although the equipment and methods involved have changed quite dramatically with the introduction and evolution of new technology, some basic techniques still remain today. The first measuring devices were hot-wire anemometers built in the latter part of last century and they are still produced and used today. In more recent times there has been the development of Laser Doppler Anemometry and later still the usage of CCD (Charged Coupled Device) cameras as an optical diagnostic tool in Particle Image Velocimetry. The following 3 sections of this chapter describe the basic principles behind the 3 methods and give examples of experiment in which these scientific techniques have been utilized.

### **2.2 Hot-Wire Anemometry**

#### **2.2.1 Introduction**

Hot wire anemometers were first made by enthusiasts in the late 1800s as this type of equipment was not yet commercially available [2.1]. Initially the anemometers were very primitive and all progress had to be made by the scientists themselves. The term Hot-wire anemometer suggests that the device uses a heated wire to exclusively make velocity measurements in air. This is deceptive as anemometers can be utilized for a

variety of fluids, furthermore probes using a heated metal film are often utilized, as well as wires. It was the in the early 1900s that the name was first used, when the hot wire probes were solely used for measurements in air. As time has evolved the name anemometer has prevailed, even though, as previously mentioned, they can be used in a variety of fluids; they can be used in many liquids including water, blood and oil.

With the use of hot wire anemometry it is possible to measure the direction and speed of fluid flow [2.1]. Anemometers are also efficient tools with which to measure turbulence, to make measurements in compressible flows and even to take temperature readings. Measurement of gas mixture concentrations and two-phase flows are also feasible, but only with the use of a particular and specialised approach.

### **2.2.2 Anemometers and Electronic Packages**

The hot-wire anemometer is fundamentally a thermal transducer and thus is quite a complex device [2.2]. This is because anemometers are sensitive to variations in temperature and also effects that falsify results, such as dust contamination. Another complication is that they are non linear instruments and so calibration of such instruments is extremely involved.

The following explains in quite simple terms how a typical present day anemometer operates. Current is passed through a fine filament or wire which is set in the gas or liquid at right angles to the direction of flow. When the flow rate or velocity changes, there is a variation in the heat transfer from the filament. This filament material has a temperature coefficient of resistance, meaning that as the temperature shifts a relative change in the resistance occurs. Electronic equipment observes this change in resistance and gives out electronic signals that represent the velocity or temperature of the flow. Every hot wire anemometer contains a probe, a cable and an electronics package. However, there are two main designs of anemometers and three types of electronic systems used to control them.

### **2.2.2.1 Anemometers**

#### Hot wire probe

This type of anemometer has a single thin tungsten or platinum wire sensor, approximately 1mm long and  $5\mu\text{m}$  in diameter, that is supported by two needles that are in turn mounted on a ceramic or epoxy probe body [2.1]. The wire is arc welded or soldered to the two needles and is electrically heated. When the fluid passes over the wire it is convection cooled and the amount of cooling represents the fluid velocity. At the other end of the probe is a water tight electrical connector with gold plated contacts to reduce resistance.

#### Wedge hot film probe

Another popular design is the wedge hot film probe [2.1]. This design incorporates a quartz rod that is ground to a wedge at one end with a thin metal hot film sensor, typically nickel or platinum, along the knife edge of the wedge. In most cases a thin coat of quartz is used to protect the film from chemical or abrasive damage.

### **2.2.2.2 Electronic Packages**

#### Constant Temperature Anemometer

The most familiar is the constant temperature anemometer [2.1]. The probe or sensor is one arm of a Wheatstone bridge, with one variable resistor and two fixed resistors as the other three arms. Connected to the bridge is a feedback amplifier, that has the ability to sense and correct any unbalance in the bridge. Fluid velocity fluctuations attempt to change the temperature of the probe, but sensors in the amplifier detect this and supply a heating current to the variable resistor to maintain constant sensor resistance and hence constant sensor temperature. The resultant voltage difference across the bridge is proportional to fluid velocity.

### Constant Current Anemometer

This also has a Wheatstone bridge and an amplifier, but feedback is not employed in this kind of anemometer [2.1]. Constant current is supplied to the Wheatstone bridge and so it is only balanced at one exact fluid flow velocity value; the bridge is unbalanced at any other velocity. As with the constant temperature anemometer the voltage difference across the bridge is proportional to the flow velocity.

### Pulsed Wire Anemometer

The pulsed wire anemometer contains a wire that heats the fluid around it. This portion of heated fluid is convected downstream to another wire that senses the temperature. Therefore the time taken for the heated fluid to travel from the first wire to the second is inversely proportional to the fluid velocity.

## **2.2.3 Experimental Usage of HWA**

Hot-wire anemometers are still used in a wide range of scientific experiments all over the world to make measurements in both gases and liquids. Takami [2.3] showed that by rotating a single hot-wire probe towards numerous orientations it is possible to measure 3 components of mean velocity and 6 Reynolds stress components. He also used the same technique used to measure 10 components of triple correlation and 15 components of quadruple correlation of fluctuating velocity in steady turbulent flows. Instantaneous velocity vector calculations [2.4] allow the application of similar triple- and quadruple-sensor probes, of arbitrary wire arrangement, to high level turbulence flows, without the need to align the probe axis to the mean flow direction. It was found that the 4 sensor probe gives slightly smaller errors in mean flow components but substantial improvement in determining the turbulent flow values.

Wallace et al [2.5] have also used the 4<sup>th</sup> sensor in each of the 3 arrays to an advantage. The 12 sensor is a superior tool with which to measure statistical properties of boundary layer velocity and vorticity fields. This is especially the case in

near wall measurements. Other near wall experiments have been carried out using hot-wire anemometry. In particular Khoo et al [2.6] used HWA in both turbulent channel and boundary layer flows, with Reynolds numbers up to 55000, using aluminium and perspex as the wall materials. Near wall calibration techniques and laminar flow wall correction were used to explain wall effects on hot-wire measurements, enabling true velocity fields to be produced.

Even with the invention of other high technology methods, Hot-wire anemometry has stood the test of time and this is probably due to the fact that multipoint measurements are easy to make [2.7]. The technique is also easy to adapt, i.e there are no problems with the addition or reduction of wires. HWA is a low cost science and depending on the wire material, it is possible to measure velocity fluctuations up to 30kHz. The only real disadvantages are that calibration is often quite complicated, the probe can interfere with the flow and the wires are very fragile.

## **2.3 Laser Doppler Anemometry**

### **2.3.1 Introduction**

Laser Doppler Anemometry, commonly abbreviated to LDA, was invented in the 1960s [2.8], following the arrival of lasers. It is a non intrusive optical technique for taking instantaneous local velocity measurements of particles present in fluid flow; unlike HWA and early velocity measuring techniques, LDA doesn't require equipment to be present in the fluid, such as probes, that affect the flow conditions.

The art of LDA, also known as laser anemometry, optical anemometry or laser Doppler velocimetry [2.9], was first started in 1964, by Yeh and Cummins [2.9] [2.10]. They used a technique involving the Doppler shift (explained in next section) of laser light to determine velocities, after noticing the shift of light scattered from

particles in a fully developed laminar pipe flow of water. Advances in the subject have lead to three different systems and although there are noticeable differences in the techniques used, they are in fact quite similar; irrespective of the method, the same pieces of equipment are always required to make up a laser-Doppler anemometer. These are a light source (always a laser), optical equipment arranged to transmit and collect light, a photocathode and a system to process the signal. Of the three LDA systems used, the most common utilize the “reference beam” or the “dual-beam” (fringe) modes. The third less employed arrangement is the “two-scattered beam” mode. The “Laser-Doppler Anemometers” section explains each of the three methods, but before that we must have an understanding of Doppler shift and the resultant optical beating.

### **2.3.2 Doppler Shift and Optical Beating**

Frequency changes in wave propagation can occur when there is movement of the source, receiver, propagating medium or interrupting reflector or scatterer [2.10]. These frequency changes or shifts are commonly known as “Doppler” shifts following the discovery of the phenomenon in 1842 by an Austrian Scientist. The Doppler shift is a result of the relative movement of source and receiver and this shift is also renowned for electromagnetic radiation and thus light. When light from distant galaxies reaches our earth, there is a “red” shift to lower frequencies and this is credited to the fact that the galaxies are moving away from us at great velocities. In experiments using LDA there is no relative movement of equipment so the shift is a result of particle movement that scatters light from the source to the receiver. With the kind of velocities found in fluids the Doppler shifts produced are extremely small. Therefore, the only suitable method for measuring these shifts involves heterodyning or “beating” of two frequencies.

This principle of optical beating can be applied to light beams that can be heterodyned by exposing them to a light detector in the same instant. The detector’s

output includes a component of the difference or heterodyne beat frequency. When performing optical measurements of velocity, the Doppler shifted scattered light is heterodyned with either direct unshifted light from the source or with shifted light, scattered from a different point or through a different angle.

### 2.3.3 Laser-Doppler Anemometers

#### 2.3.3.1 Reference Beam Mode

Figure 2.1 shows a typical laser-Doppler anemometer design [2.10].

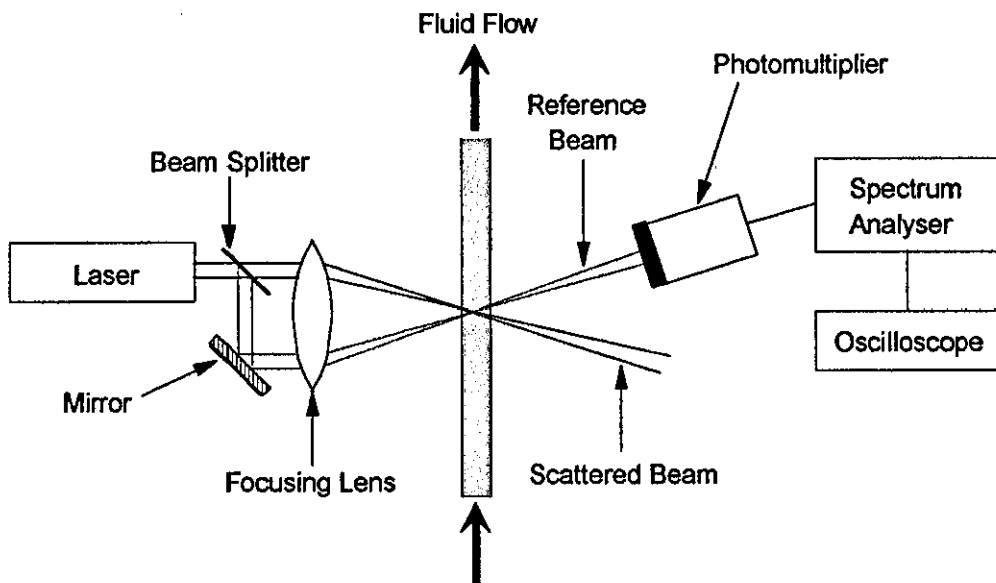


Figure 2.1 Basic LDA experiment using the "reference-beam" or "local oscillator heterodyning" mode

The system shown above employs laser Doppler beating to measure the velocity of fluid in a transparent pipe. The light from the laser is split into an intense scatter beam and a weak reference beam. The scatter beam is focused into a small region where the fluid velocity is required. This light is scattered by the particles moving in the fluid and is received by the detecting photomultiplier. The weaker reference beam

is directed straight to the detector where it beats with the stronger scattered beam. The scattered light frequency has been changed by the Doppler effect and the interference with the reference beam produces a frequency difference between the two beams, that is proportional to the particle velocity. The spectrum analyser receives this photomultiplier output signal and displays the result on the oscilloscope. For the arrangement shown in Figure 2.1, the Doppler shift frequency is given by:

$$v_D = (2v/\lambda) \sin (a/2)$$

Where  $v$  is the velocity of the particle,  $\lambda$  is the light wavelength and  $a$  is the angle of deflection of the scattered beam by the particle.

### **2.3.3.2 Dual Beam Mode**

In the dual beam system, two equal intensity intersecting light beams are used to produce a pattern within the volume of intersection. The intensity of light scattered onto the detector rises and falls as each particle passes through the fringe pattern. The rate of the intensity fluctuations is proportional to the particle velocities.

### **2.3.3.3 Two Scattered Beam Mode**

This mode uses a single focused laser beam directed into the fluid flow and light scattered by the particle in two directions is accumulated symmetrically about the axis of the system. When these two scattered beams are combined, the relative phase of their wave fronts depends on the distance of the particle to each of the light collecting apertures. Therefore as the particle passes through the beam, the beams of scattered light interfere both constructively and destructively. This leads to Doppler frequency fluctuations of the light intensity at the detector.

### 2.3.4 Experimental usage of LDA

Following the initial reference-beam LDA work of Yeh and Cummins, various scientists utilized this technique for measurements in both gases and liquids. Goldstein and Hagen [2.9] [2.11] among others applied this arrangement to turbulent water flows in 1967. The following year saw Lewis et al [2.9] [2.12] make measurements in turbulent air flows and others later studied aspects of fluid mechanics including blood flow, shock wave passage and even supersonic flows. Durst and Whitelaw [2.9] [2.13] [2.14], in 1971, mastered the dual-beam system to measure mean and fluctuating velocity components in fully developed channel water flow and air jets.

In more recent years a wider range of phenomenon have been studied. Kim et al [2.15], in 1992, looked at the kinematics of wave-fluid particles instantly before the breaking of a wave. They used a system to generate and study both extreme transient waves (representative of those found in hurricanes) and regular waves. LDA has also been used to measure boundary-layer profiles on a twin engine aircraft whilst in flight [2.16]. Several runs were made and measurements were taken both in and out of clouds. By dividing the root-mean square of the measured velocities by the mean velocity of each run, it was possible to calculate turbulence intensity levels. Durst et al [2.17] collected LDA measurements in near-wall regions of turbulent pipe-flow. They took measurements of the mean velocity and statistical moments of turbulence velocity variations in a fully developed pipe flow at low Reynolds numbers.

Finally, Kassab et al [2.18] utilized the dual-beam mode, in conditions with a Reynolds number of  $Re = 10^4$ ; the measurements were made in a turbulent jet flow. Many aspects were studied and measured including the following:

- (1) The measurement of turbulent velocity profiles.

(2) The study of the effect that upstream conditions have on the mean and turbulent velocity profiles near the jet exit.

The main advantages of LDA [2.7] [2.10] are that, as previously mentioned, it is a non intrusive technique, calibration is not necessary, there is a fast response of the order of 10 Hz and temperature variations do not affect results. Disadvantages include the fact that a transparent medium are required, contaminating scattering particles must be present in the fluid and only single point measurements are realistic as a high power laser is needed at every point of measurement.

## **2.4 Particle Image Velocimetry**

### **2.4.1 Introduction**

Particle Image Velocimetry (PIV) has been around for approximately 15 years and has become a well established technique in fluid mechanics study. As with LDA it is a non-intrusive technique for monitoring fluid flow. However unlike HWA and LDA, which are only point measurement techniques, PIV can be used to measure instantaneous 2-D fluid velocity fields from the required plane of interest [2.8] [2.19]. This means that large areas of study, with vast numbers of data points, can be examined very quickly.

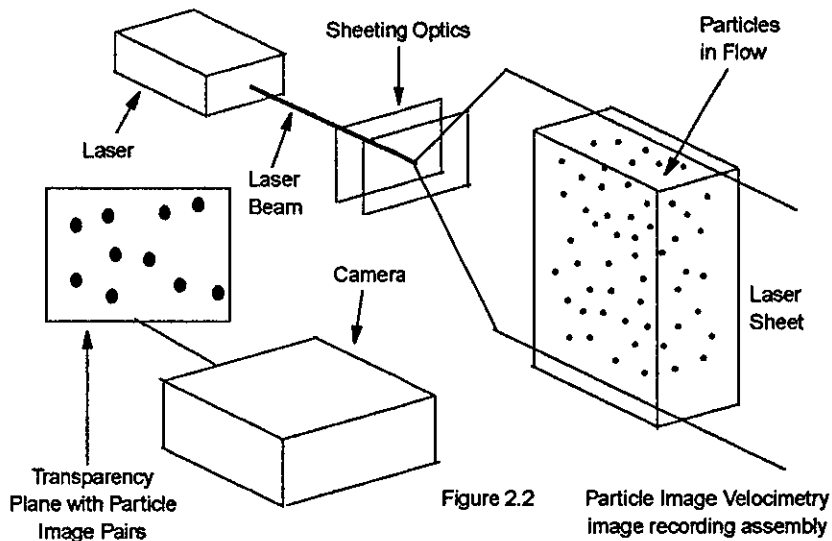
PIV has evolved from a solid mechanics technique known as Laser Speckle Photography (LSP) [2.8] [2.19]. This uses double exposure photography to obtain an image of a solid surface before and after a disturbance, leading to a speckle pattern that conveys information of the surface displacement. The equivalent technique for examination of fluid flows was called Laser Speckle Velocimetry (LSV). As with LSP, double pulsed laser light was scattered, by seeding particles within the fluid flow, producing a speckle pattern that was analysed using Young's fringe method.

The seeding densities were reduced and this produced discrete particle images on photographic film. With the use of multi-pulsed light source, with known pulse separation, it was possible to measure particle velocities from the displacement of successive particle images. This was the invention of Particle Image Velocimetry. The PIV technique consists of an image recording stage and an image interrogation stage. The following section outlines and explains the basic procedures in these stages.

## 2.4.2 PIV Technique

### 2.4.2.1 Image Recording

Figure 2.2 shows a typical PIV image recording assembly.



Light from the laser is formed into a plane of light by sheeting optics [2.8] [2.19] [2.20]. Illumination of the fluid flow is by the double pulsed light sheet and the light is scattered off the seeding particles, within the flow, towards a camera lens. The before and after positions of each particle is recorded by a camera, on photographic film, or by a digital CCD (Charged Coupled Device), oriented 90 degrees to the plane

of the sheet of light. Particle pairs show the displacement of each particle between each two consecutive laser pulses of known time separation and these are placed on a transparency, ready for interrogation.

#### **2.4.2.2 Image Interrogation**

The transparency containing the particle image pairs is analysed, point by point by the technique of spatial autocorrelation of each of the small interrogation regions. This results in the mean particle displacement of the particle images and therefore the mean velocity of each flow region. By examining each adjacent region it is possible to obtain each velocity vector over the whole field of interest and gain an overall picture of the fluid flow.

If a CCD camera has been used to store the particle image pairs then depending on the quality of the camera and also the concentration of particles, it is possible to use either particle tracking or correlation processing to produce a complete processed image of the velocity vectors [2.20]. Individual displacements of particles can be established in low concentrations, but correlation processing is normally used for high concentrations of particles. However, with the combination of particle tracking after correlation processing, high resolution particle velocity maps may be obtained.

#### **2.4.3 Advances in PIV and Experiment Usage**

PIV has moved on greatly in the last few years, as advances in lasers, cameras and image processing have lead to all electronic and digital PIV techniques. Presented in June 1996, at the New Orleans AIAA Advanced Measurements and Ground Testing Technology Conference [2.20], was an all electronic 3-D digital system that had been developed for measurements in supersonic flows. Mounted in a stereo viewing arrangement, two high resolution CCD cameras were utilized to obtain out of plane velocity components due to measurement of the difference between in-plane

velocities. Also a 3-D Photogrammetric particle tracking velocimetry method [2.21] has been used to track large numbers of particles, yielding a credible high resolution, 4-D measurement of fluid flow. The 3 components of every velocity vector are given as a function of time to enable accurate studies of different flow phenomena. The system uses commercial CCD cameras and digital image processing and tracking units to analyse up to a 1000 velocity vector fields in the same instant, with a resolution of 25 fields per second.

Kurada et al [2.22] obtained 3-D particle co-ordinates with a PC based vision system using just one CCD camera. This technique was based on photogrammetric imaging and manipulates a rare blend of stereo and orthogonal views to gather accurate positions of particles, within a cylindrical section of fluid flow. The experimental visual data was recorded on a tri-split lens CCD camera assembly, thus producing the stereo and orthogonal views. Correlation of small cubic regions, at different time instants, enabled the measurement of average particle displacements in that region.

There have been many studies of fluid turbulence including that of Hassan and Philip [2.23] who used a particle tracking neural network algorithm. Scherer's and Bernal's [2.24] holographic technique enabled them to measure velocity fields in 3-D turbulent jet flow regions. This involved the simultaneous recording of tracer particles on two in-line holograms, with two exposures on each hologram. The flow velocity was determined from the displacement between the two exposures. Holographic particle-image velocimetry has even been used in experiments in space [2.25], aboard the space shuttle Discovery.

In 1988 when PIV was still a relatively new science, Vogel and Lauterborn [2.26] combined PIV and high speed photography to investigate flow around cavitation bubbles whilst they collapsed near a solid surface or boundary. They used a high speed liquid jet impinging on a solid surface to create the cavitation of bubbles and

witnessed effects such as “Water Hammer” (Described in Chapter 3) produced by the high pressures involved.

Finally, the scope of PIV has enabled the undertaking of many more velocity fluctuation measurement experiments from three-phase fluidization systems [2.27] to studies of unsteady flows across aircraft Delta wings [2.28]. That fact that the complete instantaneous measurement of two-dimensional fields (in the basic experiments) and 3-dimensional fields (in more complicated configurations) is possible, shows that PIV is the most advanced fluid velocity measuring technique. As with LDA there is no obstruction of the flow and no calibration is required [2.7]. The only disadvantages to PIV are the high costs of equipment and the complexity of the arrangements and methods.

# CHAPTER 3

## Water Hammer

### 3.1 Introduction

Water Hammer is a familiar phenomenon associated with pressure fluctuations found in both domestic and industrial liquid filled pipeline systems. It is commonly known to be responsible for the rattling of pipes, that occurs when there is a sudden operation of water systems within the home [3.1], such as the turning on and off of taps [3.2] or when the toilet is flushed [3.3]. For many years scientists and engineers in process and chemical industries [3.4], have identified the fact that pressure surges can result in extreme stresses and subsequent bursting of pipelines.

“The phenomenon of water hammer has not been widely understood” [3.5]. This is a view held by many scientists and it is this fact that has lead to confusion of the term “water hammer.” Some scientists believe “water hammer” to be the noise that is created, as a result of large pressure surges and thus water hammer is not the destructive force itself. Weis [3.6] states “the term is the name of the noise produced when a hydraulic pressure surge suddenly closes a check valve... Sometimes hydraulic pressure surges result from water hammer, but water hammer is not always present. The surge may be a result of the condition causing the water hammer.”

Many more understand water hammer to be the actual damaging pressure surge mechanism and it occurs with or without noise, as conveyed by the following four quotes. “Water hammer is the name commonly given to the pressure fluctuations that develop in a pipe...” [3.3] “...surge pressures in pipelines - or water hammer - can lead to excessive stressing...” [3.4] “Rapid changes in flow rate require large forces that are seen as large pressures, which are usually referred to as water hammer” [3.6].

“Water hammer has a tremendous and dangerous force... Water hammer is not always accompanied by noise” [3.7].

Another view is that “Water hammer is the term used to define the destructive forces, pounding noises and vibration which develop in a piping system when a column of non-compressible liquid flowing through a pipe line at a given pressure and velocity is stopped abruptly” [3.1].

Although there are contradicting beliefs there is a general understanding that large transient pressure waves can lead to the destruction or damage of pipelines and sometimes there is an associated noise and a vibration of the system. Therefore it is conceivable to state that water hammer is a phenomenon found in liquid pipeline systems due to sudden changes in flow velocities. This results in the formation of destructive water hammer (WH) pressure surges often accompanied by WH noise and vibration. WH surges or transients can result from different circumstances: Two main causes are rapid valve closure and the presence of steam pockets within the system. These are discussed in the next section.

## **3.2 Water Hammer Causes**

### **3.2.1 Valve Closure**

The following description accompanied by the diagram in Figure 3.1 is an example to show how basic valve closure causes WH pressure surge via the production of an unsteady flow [3.1] [3.3] [3.5]. A large reservoir of water is connected to a pipe of length ‘L’ and at the other end of the pipe is a valve. Figures 3.1a shows the valve in the open position, thus allowing water to flow out of the pipe at a pressure head, due to the height of liquid contained in the reservoir.

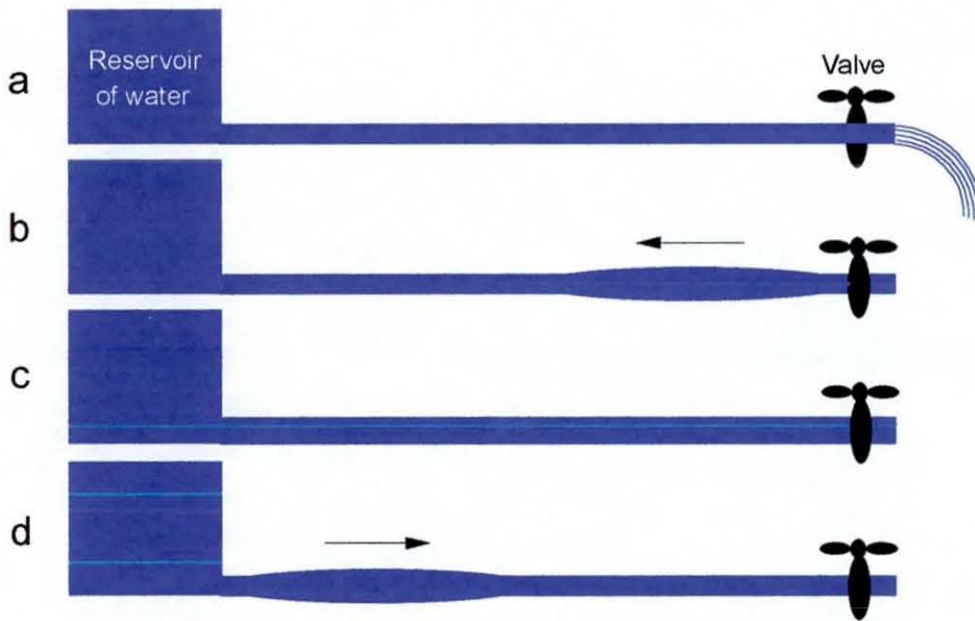


Figure 3.1 Diagram to show how basic valve closure leads to WH surges.

When the valve is slammed shut, as shown in Figure 3.1b, the liquid traveling down the pipe suddenly has no outlet. This liquid has momentum and in order to bring it to rest there must exist a force at the valve [3.3]. Pressure is this force and it applies itself uniformly over the cross-section of the pipe. Some of this energy is stored in the pipe, as the pipe expands (Figure 3.1b), but most of the pressure goes into compression of the liquid; although thought to be incompressible, water has a modulus of elasticity that is approximately 100 times less than that of steel [3.5]. This local pressure rise of the water has produced an unstable situation; the liquid next to the valve is at rest and the pressure is high, but liquid is still trying to flow down the pipe due to the reservoir head. The compressed stationary liquid travels back up the pipe towards the reservoir at a rate called the wave velocity 'A', which is the velocity of sound in that medium. The velocity of this surge will be much greater than the velocity of flow from the reservoir and thus the traveling pressure gradient momentum is large enough to stop the flow momentum. After time  $L/A$  the pressure surge has reached the reservoir.

Figure 3.1c shows the system at time  $L/A$ . Although the pressure in the pipe is uniform, it is at an increased value. Therefore the pipe pressure is higher than the reservoir head pressure and again we have an unstable situation. This causes flow to be forced into the reservoir whilst there is a reduction of pressure in the pipe to equal the pressure in the reservoir.

However this pressure reduction wavefront disturbance reverses its direction and travels back towards the valve, as shown in Figure 3.1d. On reaching the valve after time  $2L/A$  the wavefront or WH surge is again reflected back towards the reservoir. During this time of  $2L/A$  the system has been subjected to unusually large pressures and stresses. If the pipe line was frictionless and the liquid was ideal there would be no resistance to flow and thus no overall pressure drop. However, with pipe friction and elasticity the WH surge gradually diminishes until all its original momentum has been absorbed.

The above description for inducing WH surges has assumed instant closure of the valve. However, valves take a measurable amount of time to open or close. If the time taken for valve closure is less than the critical time (  $TC = 2L/A$  ), then the closure time is termed critical and water hammer will occur with a peak pressure change defined by the Joukowsky [3.1] formula:

$$P = WAV / 144g$$

Assuming that water is the liquid used in the experiment

- W Fluid Density ( 62.4 lb/ft<sup>3</sup> )
- V Velocity change of fluid ( ft/s )
- g Acceleration due to gravity ( 32.2 ft/s<sup>2</sup> )
- A Wave Velocity ( ft/s )

$$A = C / [ 1 + \{ K ( - 2 + DR ) / E \} ]$$

- C Velocity of Sound in liquid ( 4660 ft/s )
- K Modulus of Fluid ( 300,000 PSI )
- E Modulus of Material ( 29,000,000 PSI )
- DR Dimension ratio of pipe ( pipe outer diameter / pipe wall thickness)

If we assume  $V = 1$  ft/s,  $DR = 5$  then we have the following

$$A = 4660 / [ 1 + \{ 3 \times 10^5 ( - 2 + 5 ) / 2.9 \times 10^7 \} ] = 4520 \text{ ft/s}$$

$$P = 62.4 \times 4520 \times 1 / 144 \times 32.2 = 61 \text{ PSI}$$

Therefore, assuming that the valve is closed in a time less than TC, the peak pressure rise due to WH will be 61PSI for every ft/s that the water is moving at. If for example the water was moving towards the valve at 10 ft/s then the pressure rise would be over 600PSI. Such a large WH pressure surge could have a disastrous effect. For valve closure times  $TA > TC$  the corresponding WH pressure rises are much less than for  $TA < TC$  and are simply approximated to:

$$P = 0.027 \times L \times V / TA$$

Valve closure time determines whether damage will occur and therefore can have a dramatic effect on the system.

### 3.2.2 Steam Pockets

Steam bubble collapse induced WH is one of the most common causes of damage to piping and supports in steam power plants [3.8]. When hot liquid or steam contracts during cooling in a closed pipe, the pressure decreases very close to the saturation vapor pressure [3.9]. This can be very dangerous, as when there is rapid opening of a valve at one end of the pipe, the line or atmospheric pressure suddenly causes the cavity to collapse and produce an unanticipated WH surge.

Biphase systems carry water and steam in different parts of the machinery and problems are likely to occur when these systems don't operate as they should. Valves often fail to close properly so that steam or even water, that is hot enough to flash, leaks into a chamber or pipeline that should only contain cool water [3.8]. Flash occurs when hot water under a certain pressure is released to a lower pressure at a temperature above the boiling point for the lower pressure [3.10]. For example, water at a pressures of 10, 15 and 20 PSI will boil at approximately 193, 212 and 238° F respectively [3.11]. Once this has happened the steam is trapped by a column of the cooled liquid and this will inevitably initiate a WH surge, with or without the encouragement of pump or valve operation. The ensuing swift condensation of the steam causes the bubble to collapse and this creates severe impacts as the surrounding liquid accelerates into the resultant vacuum [3.7] [3.12]. Another steam generated WH phenomenon is when there is a lack of correct drainage ahead of a steam control valve [3.7]. On opening the valve, a slug of condensate rushes into the equipment at a high velocity and this will induce WH when it strikes the end face of the pipe.

These two kinds of steam bubble collapse induced WH are called intermediate water hammer and final water hammer respectively. Figure 3.2 shows the two mechanisms.

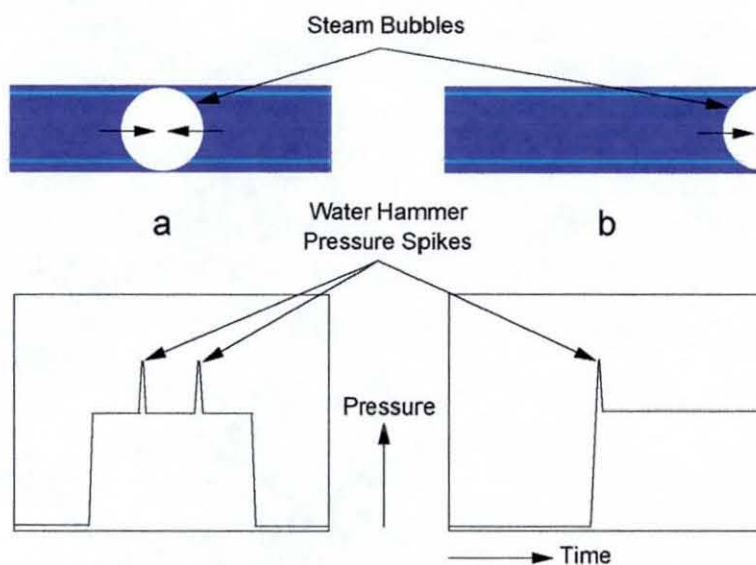


Figure 3.2 Diagram of (a) intermediate water hammer bubble and the (b) final water hammer bubble with typical corresponding pressure traces

In both cases the bubble condenses and collapses quicker if the water is very cold and this leads to the very low pressure in the bubble. With the intermediate bubble collapse, shown in Figure 3.2a, the bubble is completely surrounded by liquid. When a valve is operated the surrounding pressure will increase and the bubble will collapse and as previously stated the water accelerates towards the centre of what used to be the bubble and WH pressures are experienced. There may be more steam bubbles within the system and these may collapse at different stages during the pressure increase as shown by the two WH spike in Figure 3.2a. The final bubble collapse is different in that it takes place as a cooling cavity at the blind end of a pipe, as pictured in Figure 3.2b. When the pressure is applied the single steam bubble immediately collapses at the end face of the pipe. Therefore the liquid is instantly accelerated towards this pipe end, strikes the pipe wall, hence producing a single WH pressure transient as shown by the trace in Figure 3.2b. For both types of WH the pressures involved can be quite modest, but large bubbles collapsing at high pressures can produce enormous surges with potentially disastrous and detrimental effects.

### **3.3 Other Water Hammer Causes and Effects**

Other causes of WH within liquid carrying pipelines are ordinary trapped air slugs and also cavitation produce by pumps. Air can exist in a system in the form of bubbles or in solution [3.13]. The percentage, by volume of air, depends on the system pressure but it can be anything above 2%, so although there might not appear to be air in the system it is always present in some form. If a considerable amount of air is present in the system then the same kind of WH can occur as with steam bubble induced WH. Air can become trapped at couplings and fittings and because it is able to squeeze through minute gaps much more easily than water, it can even create seep through gaps in gaskets and sealing rings. Another problem with air is that it moves at different rates to water and this could easily initiate unstable back and forth surging of

the water. The resultant pressure transients could damage equipment including valves, gauges and pumps.

Air escapes through gaps at a much faster velocity than liquids, due to its low viscosity. However when the air has fully escaped through a sizable outlet, the rapid closure of the air valve float is possible due to the drag of the air. This would result in rapid deceleration of the water column, that was flowing behind the air pocket and WH would ensue.

Pump start up and shut down cause problems by initiating or interacting with existing cavities [3.5]. If void spaces or air cavities exist downstream from a pump and the pump is started before the cavities are removed, rapid collapse of the voids cause huge pressures. These voids can either be vapor cavities or a single large air bubble. In order to eradicate this problem, the pump should be started slowly and the flow should be increased gradually to collapse the air pockets or drive them out of the system.

The shutting down of a pump, however, causes more liquid transient problems than the case of the pump start up. Pump shut down or spin down occurs in the event of a power failure and there is a rapid deceleration through the pump. This causes an upsurge on the suction side of the pump and a down surge on the discharge side. It is the latter down surge that causes the major problem. The liquid is still flowing on the down side and this can produce a pressure drop results in “vapor column separation” [3.5]. If these cavities become large then there is a greater distance in which the separate columns can accelerate back towards each other. The large pressure head of the downstream column adds to the impact with the upstream column and this will be magnified if the pump is started at the same time.

Water hammer has been detected in experiments of cavitation. High velocity jets were fired against an object surface, such as gall stones in the technique of

Extracorporeal Shock Wave Lithotripsy [3.14]. Bubbles are formed when the local pressure inside the liquid falls below the vapor pressure at the temperature [3.15]. When the liquid pressure becomes greater than the vapor pressure some bubbles collapse due to surface tension, but some stick to the object surface [3.16]. If a bubble is on the edge of or near to the object, the object's surface exerts a drag force on the liquid that surrounds the bubble near to this surface. The drag force causes the bubble to collapse in such a way that the portion of the bubble furthest away from the object surface moves in quicker than the opposite portion. This creates a liquid jet that impinges on the surface. The resultant pitting damage to the surface is caused by either this WH jet or by the emission of a shock wave. Both have been detected in experimentation where damage occurs, but the actual cause of damage is still not decided [3.15].

### **3.4 Control of Water Hammer**

Many devices have been invented to help avoid large problems due to WH pressure transients. However it is sometimes the fault of the prevention devices that the actual phenomenon occurs [3.6]. Often though devices such as surge vessels [3.17] and accumulators (also known as closed surge tanks) are correctly fitted to protect pumps and valve against the event of a pressure surge. Just as a capacitor stores charge these devices store the built up pressure of WH and therefore the other equipment in the system isn't subject to huge transients. Air spring valves [3.18], that close gradually to allow the flow to gradually come to a halt, have also been used. Valve stroking is also used, where variable controllers are fitted to ordinary valves, so that just as with the spring valve they can be closed slowly. Alternatively they can be closed quickly then slowly, using a non-linear valve closure schedule, because the bulk of the pressure surge occurs during the second part of the valve closure [3.19].

# **CHAPTER 4**

## **Study of Mechanically Induced Fluid Pressure Pulses**

### **4.1 Introduction**

Prior to the main experimentation it was essential to test the pressure transducers and use them to gain more experience in using digital oscilloscopes and in the analysis of the transducer output traces. The transducers are used in industrial processes and are subjected to regular high pressure oil pressures up to approximately 3000 PSI. One method of simulating high pressure pulses, is to drop a weight on to a column of liquid to induce a pressure pulse. This would be a simple and effective way of testing the transducers, although the magnitude of the pulses produced would only be a fraction of those found in industry. Before this experiment could be accurately carried out, the transducers had to be connected to leads and wires in order to take readings. They also required calibration, although they have a nominal value of the relationship between the supply and output voltage and the pressure applied.

### **4.2 Transducer and Connection to Equipment**

The transducer investigated in these experiments is normally used for monitoring very high oil pressures up to 4000 PSI and it can be seen on the next page in Figure 4.1. On the surface of the transducer that is exposed to the fluid there is an extremely thin steel diaphragm. Behind the diaphragm is a small volume of oil and a tiny electronic circuit. When pressure is applied to the diaphragm the oil compresses slightly. The sensor and circuit detects this compression and gives an output signal that represents the average pressure applied to the surface.

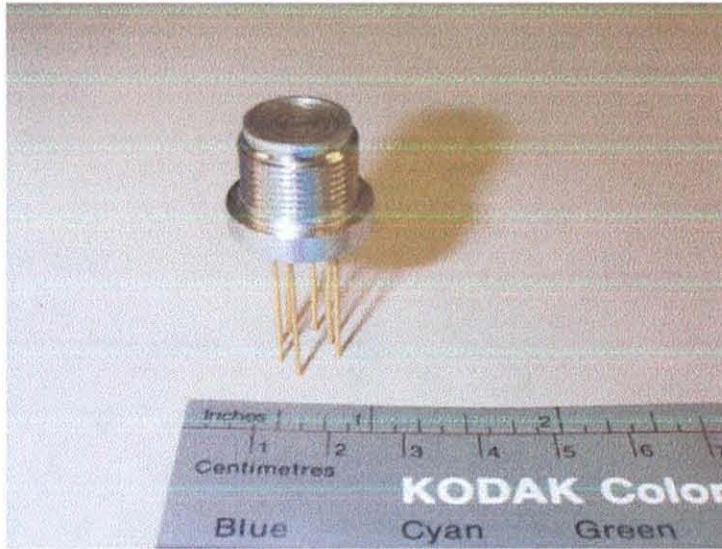


Figure 4.1 Picture of 4000PSI rated Pressure Transducer

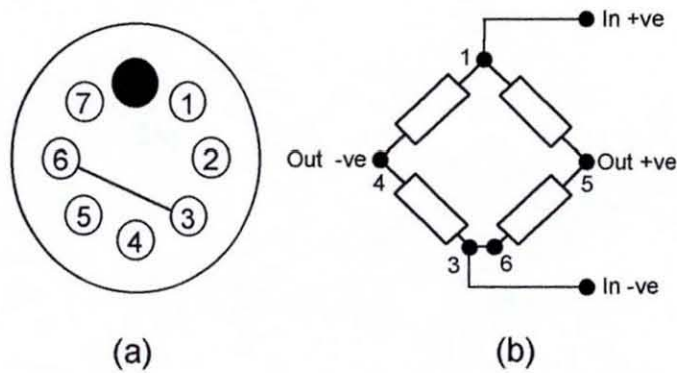


Figure 4.2 (a) is the end view of the transducer and (b) is a diagram of the transducer's wheatstone bridge

Figure 4.2a is an end view of the rear of the transducer. The 7 wires run through the entire length of the module to just behind the diaphragm. They are connected by fine wire bonds to the points on the electronic “Wheatstone Bridge” circuit shown in Figure 4.2b. The four resistors are actually strain gauges that change resistance when subjected to a strain or pressure and thus affect the voltage across the bridge.

Voltage was supplied to the input wires, Figure 4.2b, labeled In +ve and In -ve and the wires were connected to a voltmeter and later to an oscilloscope, to monitor the resultant output voltage. This was all done by the use of leads and crocodile clips. It was anticipated that the temporary output connections would be sensitive to electromagnetic pick up. If this was the case then a permanent BNC lead would take the place of the wires and clips.

### 4.3 Calibration of the Transducer

The usual operating supply voltage of the transducer is about 3V, but the transducer can comfortably operate at 10V. It was decided that a suitable supply voltage would be 5V. This translated to 5mV output for every bar of applied pressure. The variable supply voltage was monitored by a volt meter to ensure that the output was approximately 5V; the variable supply was slightly unstable and fluctuated about 5V by  $\pm 0.02V$ .

The transducer was attached to one end of a 40cm long, 1.3cm diameter copper pipe, the other end, via a 1/2inch fitting, was connected to the supply pressure. This supply was argon gas with a maximum possible operating pressure of 90PSI. The pressure was increased from 0 to 70PSI in 2PSI increments and the corresponding voltmeter readings were recorded.

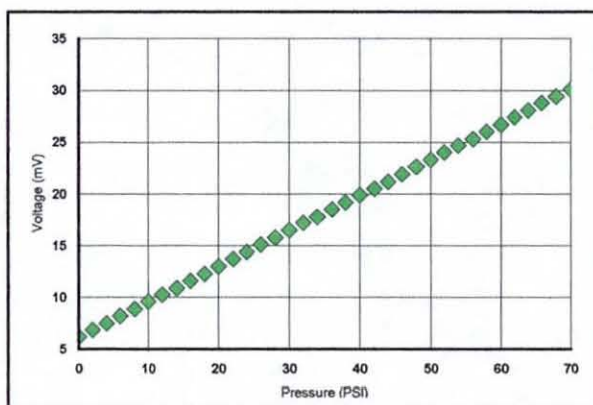


Figure 4.3 Graph to show relationship between applied pressure and corresponding voltage output of the pressure transducer.

From the graph in Figure 4.3 we can see that the relationship between pressure supplied and output voltage is linear. The voltage output reading increased by 23.9mV for the 70psi pressure rise.

Standard Atmosphere = 14.696psi

$70\text{psi} / 14.696\text{psi} = 4.763\text{bar}$

$23.9\text{mV} / 4.763\text{bar} = 5.018\text{mV}/\text{bar}$

Therefore the nominal calibration value is correct; we can use the approximation of 5mV/bar for a 5V supply.

#### **4.4 Transducer Testing - Cylinder Drop Experiment**

The half inch fitting was removed from the copper tube. Next a long copper tube of 3.8cm diameter was soldered into a connector, that was in turn soldered to the free end of the small copper tube. Water was introduced into the lower part of the system. This can be seen on the following page in Figure 4.4, together with the connection to the power pack and digital oscilloscope.

Also shown is the 9.4cm long, 3.7cm diameter steel cylinder that was dropped down the tube onto the water column. This cylinder was attached to a length of string and could be lowered or raised using the pulley that was fixed to the ceiling. As you can see the design is such that the weight is only allowed to fall as far as the connector and thus will not strike the transducer diaphragm; only the pressure wave or pulse comes into contact with the transducer.

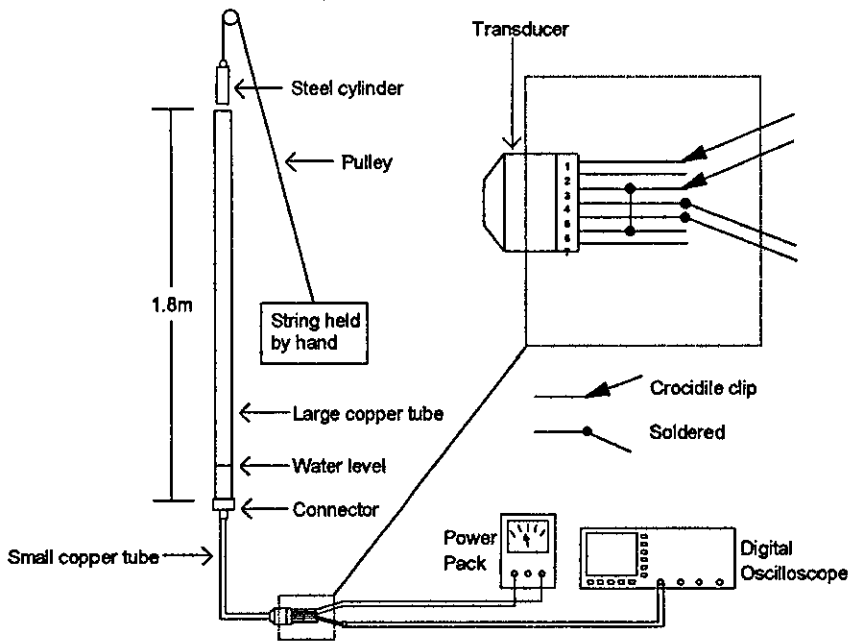


Figure 4.4 Diagram of Cylinder drop experiment set up

With the equipment set up the quiescent trace was visible on the scope as an oscillating sine wave, centred around 10mV, with an amplitude of approximately 10mV due to interference or pick up. Initially the weight was dropped from an arbitrary height and the trigger level was varied to get a pulse on screen. This was done so that the volts/division and time base settings could be set to suitable levels. The typical pulse height was about 50mV and the trigger level was set to 30mV so that the pick up didn't fire the trigger. This pick up was thought to be caused by the inductive loop of the temporary connections, but the interference still remained even when the BNC lead was used.

N.B. The main problem in these preliminary experiments was that we are dealing with low pressures and voltages. Therefore the maximum pressure values are not precise figures due to the interference sine wave. The transducers are designed for very high pressures, i.e. 200 bar would produce 1V output, so the interference would be negligible.

The cylinder was dropped from heights of 10, 20, 30, 40 and 50cm and 4 waveforms for each height were saved on the digital scope. This information was transferred via an iee488 cable to a computer and could be viewed in a DOS software program. Text files each containing 100s of co-ordinates were extracted and placed in spreadsheets so charts of the waveforms could be produced. The 4 waveforms for each height were very similar only differing slightly in the maximum voltage. Figures 4.5a to 4.5e show 1 of the 4 waveforms for each of the 5 heights.

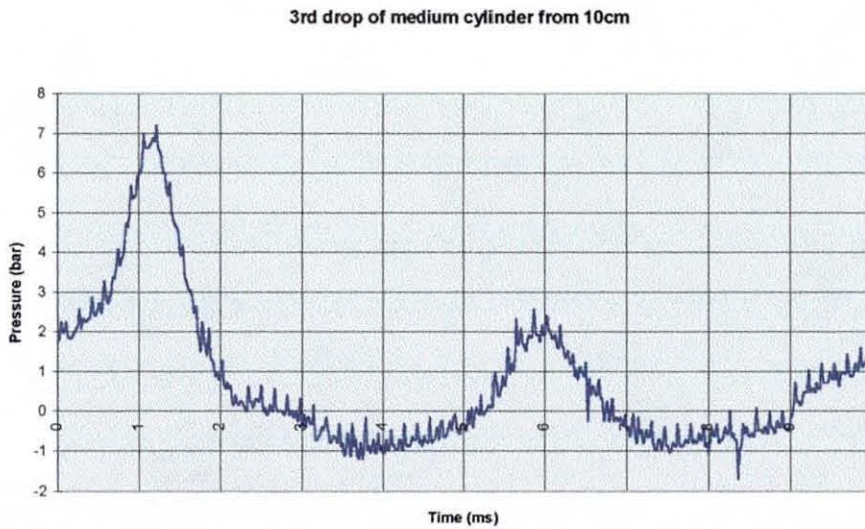


Figure 4.5a Transducer signal due to "Cylinder Drop Experiment" from a height of 10cm

3rd drop of medium cylinder from 20cm

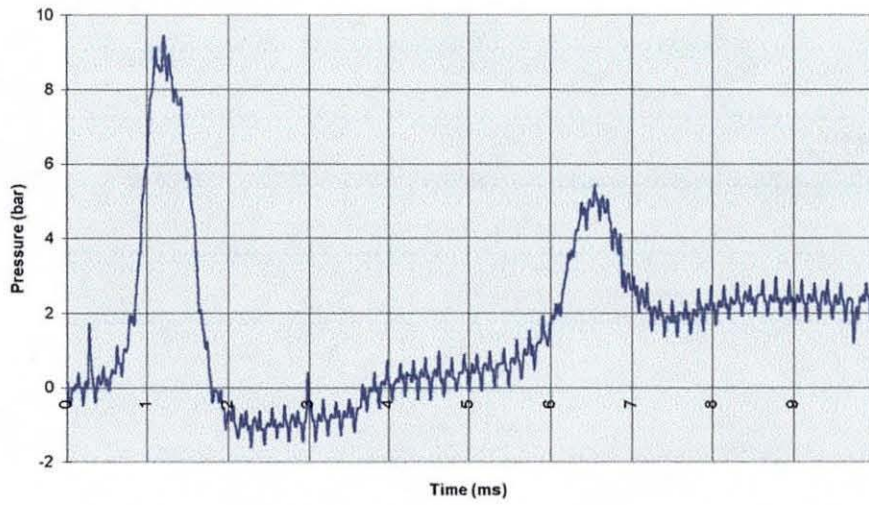


Figure 4.5b Tranducer signal due to "Cylinder Drop Experiment" from a height of 20cm

4th drop of medium cylinder from 30cm

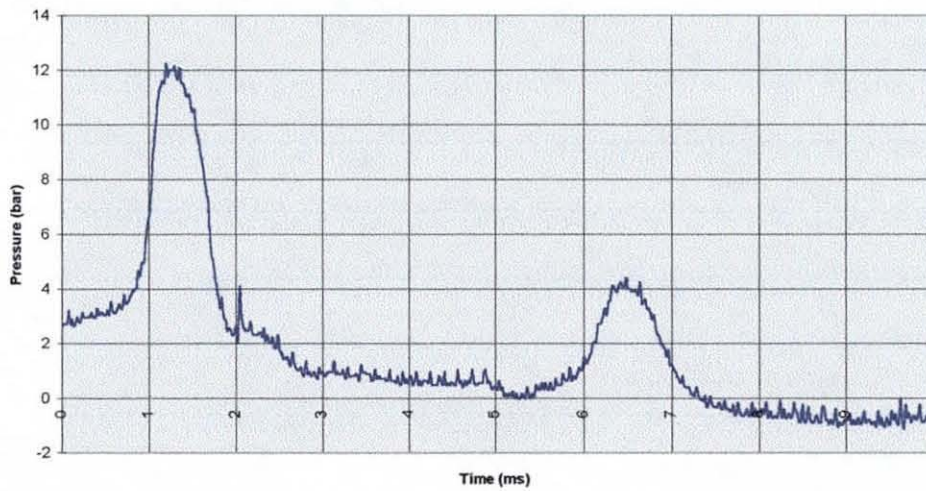


Figure 4.5c Tranducer signal due to "Cylinder Drop Experiment" from a height of 30cm

2nd drop of medium cylinder from 40cm

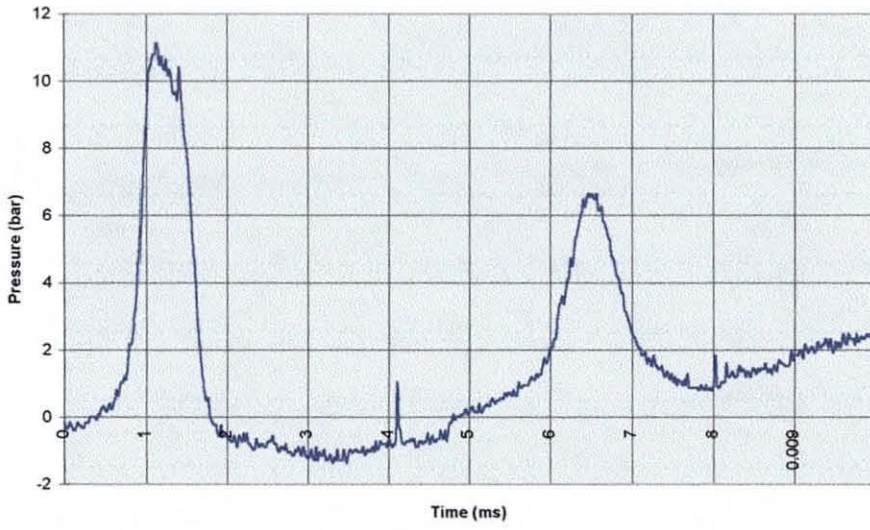


Figure 4.5d Transducer signal due to "Cylinder Drop Experiment" from a height of 40cm

4th drop of medium cylinder from 50cm

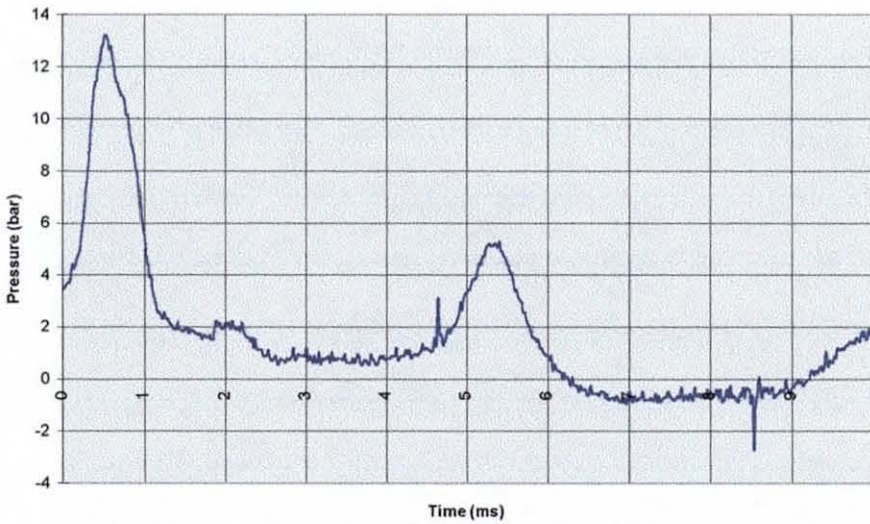


Figure 4.5e Transducer signal due to "Cylinder Drop Experiment" from a height of 50cm

Figure 4.6 explains the pulse separation and width for each height drop.

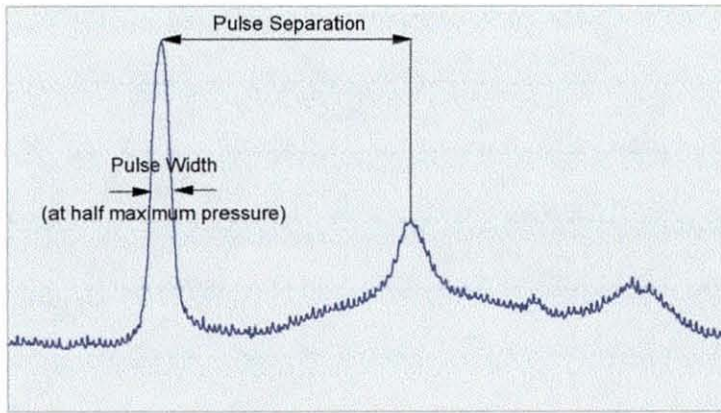


Figure 4.6 Diagram to explain Pressure Pulse Separation and Width on an example trace

Drop height	Max. Voltage	Max. Pressure	Pulse Sep.	Pulse Width
10cm	35mV	7bar	4.8ms	0.8ms
20cm	45mV	9bar	5.2ms	0.7ms
30cm	60mV	12bar	5.2ms	0.7ms
40cm	55mV	11bar	5.3ms	0.65ms
50cm	65mV	13bar	4.8ms	0.7ms

The above table contains typical values of the maximum pressure, the pulse separation and width for each height drop. The results convey the thought that the change in height doesn't affect the Pulse separation or width, but just the maximum pressure. However, the pressure created by the 30cm drop is greater than for the 40cm. This is possibly caused by the fact that there is considerable air resistance and friction in the system. When the cylinder falls it is compressing the air already in the tube, although some of the air can pass at the edge of the cylinder. There is friction between the cylinder and the inside of the pipe, which also reduces the cylinder velocity. The velocity of the cylinder for the 30cm drop must have exceeded that of the cylinder when dropped from 40cm. These peculiar results are possibly due to the irregular air resistance and friction of the cylinder drop system.

Confusion was caused by the pulse separations and widths. The continuous pulses occurred at a separation of 5ms and had half maximum pulse widths of around 0.7ms. It is difficult to see how these values arose. Did the cylinder bounce on the surface of the water at the initial impact before submerging? This wouldn't normally occur for the cylinder falling into a free volume of liquid, due to the ratio of the cylinder length to the radius. In this situation the transverse wave travels to the edge of the cylinder, displacing the water, before the longitudinal wave travels up and down the length of the cylinder. However the fact that the cylinder falls onto water in a closed system, where the water can't displace sideways, could cater for the concept of the cylinder bouncing on the surface, before sinking. If the cylinder did bounce on the water surface and we treat the impact as one between 2 solids the contact time would be as follows:

Longitudinal wave travels 0.188m (twice the cylinder length) at approximately 5000m/s (velocity of sound in a steel rod). The duration of which is only 37.6 $\mu$ s. This value doesn't correspond to the pulse separation or pulse width.

Perhaps reflections of sound waves occurred in the pipe. This might explain the pulse separation values. However at 5000m/s in copper the sound wave would travel approximately 25m over a duration of 5ms. The velocity of sound in water is 1500m/s, equating to a distance of 7.5m; the column of water in the pipe was only 0.5m in length. It could be possible that the cylinder hits the water, stays in contact with the surface for a time corresponding to the pulse width. The cylinder bounces off the surface at the same time as the water compresses and then the cylinder hits the surface for a second time producing a second pressure pulse. The cylinder then makes a third even smaller bounce or simply sinks in the liquid and rests at the connector.

Different length cylinders (half the original length and double the original length) were tested to discover if a change in dimension affected the pulse separation or width. The short cylinder however, didn't produce a clear concise waveform and

often didn't produce a large enough pulse to fire the trigger. The original medium length cylinder and the long cylinder were both dropped 4 times from 0.3m and 1m, with the waveforms saved and transferred to the computer. Figures 4.7a to 4.7d show 1 of the 4 waveforms for the 2 cylinder lengths at the 2 different height drops.

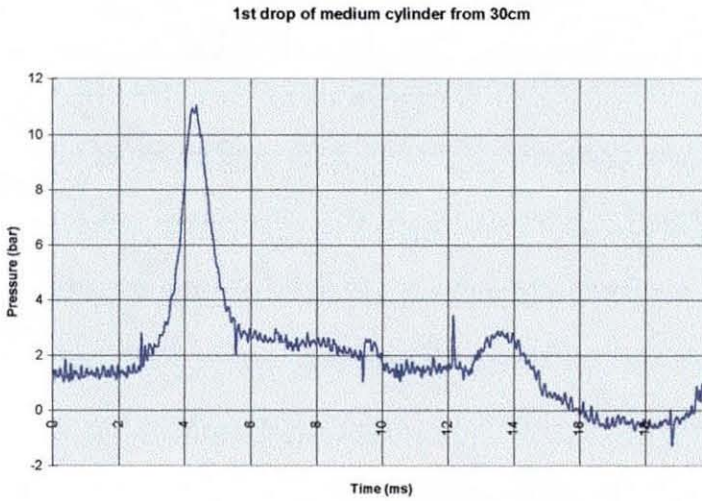


Figure 4.7a Transducer signal due to "Cylinder Drop Experiment" with medium cylinder from a height of 30cm

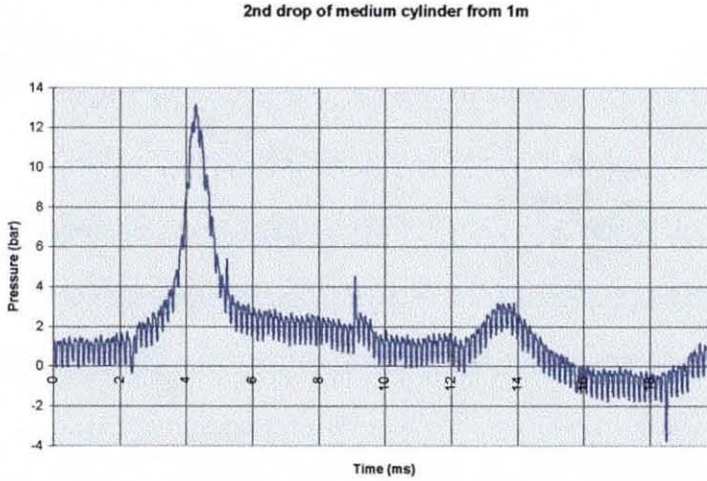


Figure 4.7b Transducer signal due to "Cylinder Drop Experiment" with medium cylinder from a height of 1m

1st drop of long cylinder from 30cm

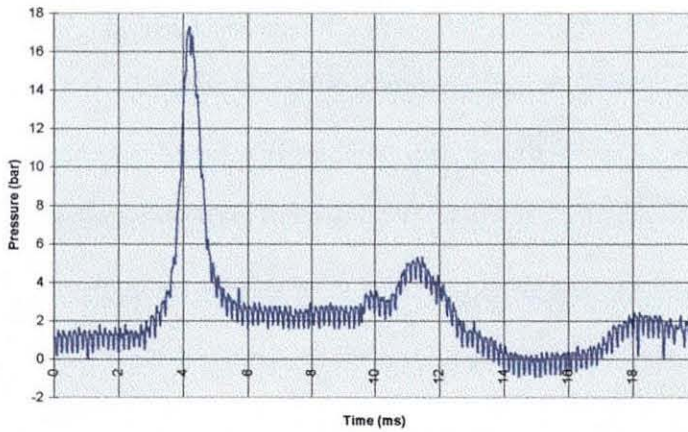


Figure 4.7c Tranducer signal due to "Cylinder Drop Experiment" with long cylinder from a height of 30cm

1st drop of long cylinder from 1m

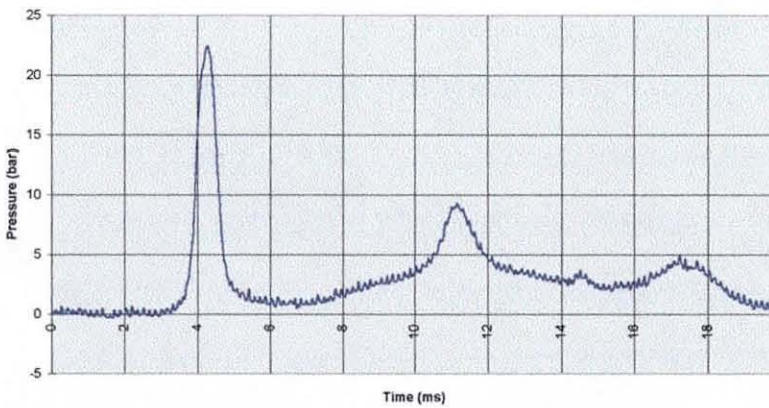


Figure 4.7d Tranducer signal due to "Cylinder Drop Experiment" with long cylinder from a height of 1m

The following gives the typical values of the maximum pressure, the pulse separation and width for each drop.

Medium cylinder

Drop height	Max. Voltage	Max. Pressure	Pulse Sep.	Pulse Width
0.3m	55mV	11bar	9ms	1.2ms
1m	65mV	13bar	9ms	0.8ms

## Long cylinder

Drop height	Max. Voltage	Max. Pressure	Pulse Sep.	Pulse Width
0.3m	85mV	17bar	7ms	0.8ms
1m	112.5mV	22.5bar	7ms	0.6ms

From these results we can see that the pulse separation is only affected by the length of the cylinder and not the height of the drop, whereas the width of the pulse is affected by both these factors. There is a non linear inverse relationship between the pulse separation and the cylinder length. Again treating the impact as one between 2 solids we expect the pulse width or contact time to be proportional to the cylinder length. However, the pulse width is significantly less for the long cylinder.

If we assume that the friction and air resistance in the pipe affects the cylinders in the same way, then they will have similar velocities at impact. However, the fact that the longer cylinder weighs more, means that it builds up more momentum so a larger pressure pulse is produced upon impact with the water surface. The greater impact of the long cylinder could have caused the shorter pulse separation and the pulse width. Why this happens is not known, but the crudeness of the experiment has probably been the cause of all the irregular occurrences.

After the above experiments, although the transducer still worked, the surface of the diaphragm was damaged. The middle of the transducer diaphragm was slightly dented and small pits were dotted randomly around the surface. This could have been caused by trapped air. However, the pressures involved are insignificant compared to typical industrial conditions, so there are again more unexplained circumstances. The transducers were later subjected to pressure pulses of over 2000 PSI, the nature of which together with the subsequent damage is explained in Chapter 6.

The following calculation shows the pressure that would be expected if the steel cylinder drop onto the water was treated as an impact between two flat solid surfaces.

The calculation will be for the long steel cylinder (length of 0.188 m) dropping from a height of 1 m, which actually produced a pressure recording of 22.5 bar.

impact Pressure = impact Force / unit Area

$$P = F / A$$

impact Force = cylinder Momentum change / Time change

$$F = dp / dt$$

$dp / dt = m (dv / dt)$      $m = 1.6 \text{ kg} = \text{cylinder mass}$

$v = \text{cylinder velocity at impact}$

$$v = (2gh)^{1/2}$$

$g = 9.81 \text{ m/s}^2 = \text{acceleration due to gravity}$

$h = 1 \text{ m} = \text{cylinder drop height}$

$$v = 4.43 \text{ m/s}$$

The cylinder goes from 4.43 m/s in the time that it takes for the speed of sound to travel twice the length of the cylinder.

$$t = 2L/w$$

$L = 0.188 \text{ m} = \text{length of cylinder}$

$w = 5000 \text{ m/s} = \text{velocity of sound in steel}$

$$t = 75.2 \mu\text{s}$$

$$dv/dt = 4.43 / 75.2 \times 10^{-6}$$

$$m (dv/dt) = 1.6 (58910) = 94256$$

$$A = \pi r^2$$

$r = 0.0185 \text{ m} = \text{cylinder radius}$

$$A = 1.075 \times 10^{-3} \text{ m}^2$$

$$P = (m (dv/dt)) / A$$

$$P = 94256 / 1.075 \times 10^{-3}$$

$$P = 8.77 \times 10^7 \text{ Pa} = 865 \text{ bar}$$

The calculated pressure of approximately 865 bar is far greater than the actual 22.5 bar that was recorded from the long cylinder drop from 1 m. This is probably due to the fact that the impact is not between two solid flat surfaces. The steel cylinder would bounce on a solid surface but in reality the cylinder splashes on to the water surface and sinks. However the calculation shows that large pressures can easily be produced and if the cylinder was dropped on to a flat solid surface a pressure of approximately 865 bar would be produced.

# CHAPTER 5

## Hydraulic System and Electronic Equipment

### 5.1 Introduction

This chapter contains a detailed account of the setup and operation of the basic mechanical and electrical equipment used in the experimental work. On the mechanical side it includes the connection of the power pack, accumulator, servovalve, transducer, hydraulic pipes and fittings. The electrical equipment consists of a function generator to power the servovalve, a battery or power pack voltage supply for the transducer and an oscilloscope connected to the transducer to monitor pressure pulse traces. Additional electrical and optical equipment are explained in Chapters 6 and 7 where the CCD camera with the aid of a bulb or laser illumination is used to study particle and transducer face movement.

### 5.2 Hydraulic System

#### 5.2.1 Hydraulic Power Pack

The hydraulic power pack is illustrated on the following page in Figure 5.1. Compressed air at pressures up to 100PSI is fed into the power pack at the "Air Supply Connection". The air enters a large air piston that is connected to a smaller hydraulic piston. The air piston is much larger in cross sectional area than the hydraulic piston and so relatively low air pressures are converted into very high hydraulic fluid pressures.

AZ SERIES HYDRAULIC POWER PACK

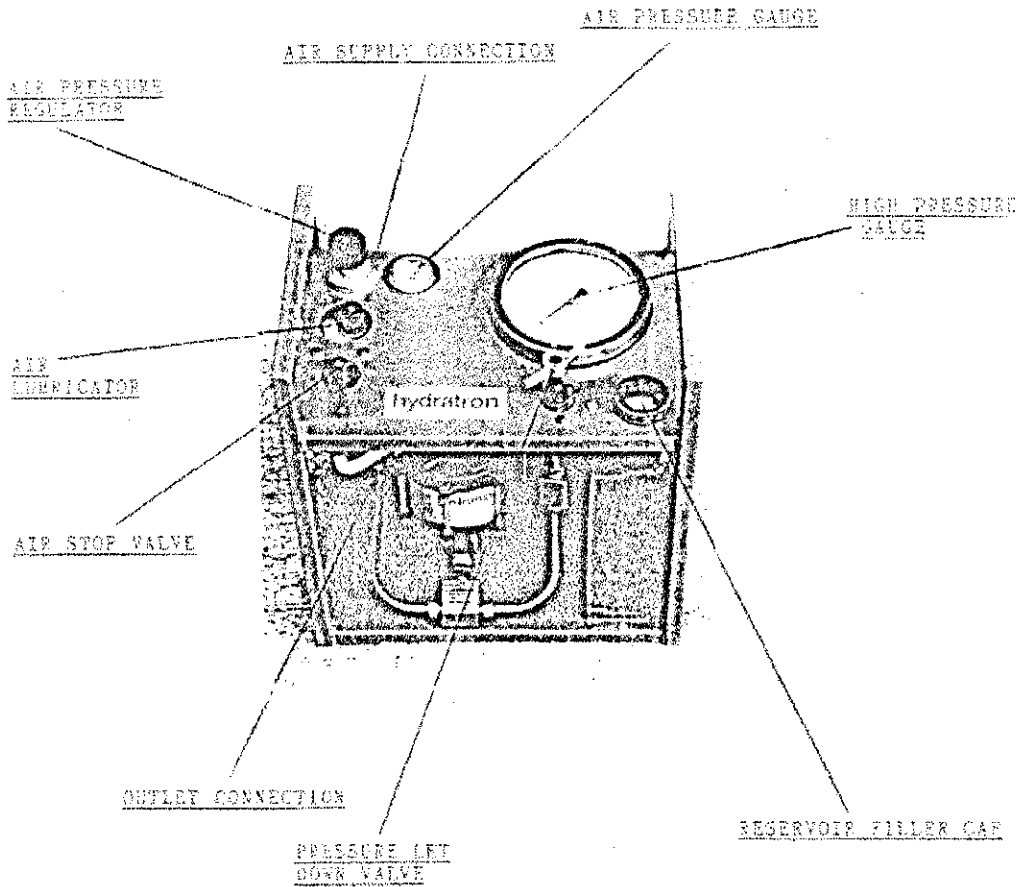


Figure 5.1 Hydratron AZ-1-36HPU hydraulic power pack. Air input pressures up to 100PSI are converted into hydraulic fluid outputs (water/oil) of up to 3600PSI.

Reprinted with permission from Hydratron Ltd. [5.1]

When air enters the power pack this acts over the surface area of a large piston. This piston pushes a smaller hydraulic piston downwards onto a volume of oil and this is known as one stroke. Upon every stroke, a fixed volume of oil proportional to the hydraulic piston diameter is then compressed and released from the power pack at a fixed pressure. This pressure should be equal to the product of the input air pressure and the large air piston area, divided by the small hydraulic piston area. However the table on the following page shows the actual output hydraulic (Hyd.) fluid pressures produced from input air (Air) pressures with the values measured in pounds / square inch (PSI) [5.1].

Air	10	20	30	40	50	60	70	80	90	100
Hyd.	250	600	1000	1400	1775	2115	2475	2825	3200	3600

The air piston is 36 times larger in cross sectional area than the hydraulic piston and so the magnitude of increase in pressure should be 36. However the data shows that the magnitude of increase is only 25 for an input of 10PSI air pressure and this increases with increasing input pressures up to 36 for an input of 100PSI.

As previously mentioned, the power pack pumps out a fixed volume of fluid per stroke. For very high pressures the pump has to work harder to compress the fluid, so it cannot produce the same numbers of strokes per minute, as it would for lower pressures; smaller volumes of fluid are pumped out at higher pressures. For example, for an input pressure of 100PSI, the power pack can pump out 183 cubic inches per minute at 2000 PSI, 143 in<sup>3</sup> /min. at 2500 PSI, 119 in<sup>3</sup> /min. at 3000 PSI and only 73 in<sup>3</sup> /min. at 3500 PSI [5.1]. The only problem with the power pack is that due to its pumping mechanism, it can't pump fluids out at a constant pressure. Therefore an accumulator is required to smooth out the flow and sustain a constant pressure within a hydraulic system.

### 5.2.2 Accumulator

Accumulators are to hydraulic systems what capacitors are to electronic circuits; capacitors store charge and therefore maintain voltage when connected to a drain resistor. In the case of the hydraulic accumulator it maintains pressure while supplying fluid flow. Hydro-pneumatic accumulators [5.2] are pressurised cylinder vessels, containing a bladder filled with nitrogen gas to some initial pressure. For this project a 1.15 litre, 207 bar (3000 PSI) rated accumulator, filled to just over 100 bar (1500 PSI) was used to smooth out the flow and sustain pressures between 1500 and 2700 PSI. At one end of the cylinder is a gas valve, to allow an increase or decrease in the initial nitrogen gas pressure. The other end of the cylinder contains a fluid port assembly that is connected to the hydraulic system.

In order for the accumulator mechanism to take effect the pressure in the hydraulic system has to be above the initial value of the accumulator, in this case 1500 PSI. Once there exists a pressure within the hydraulic system above 1500 PSI, the nitrogen bladder begins to compress so that the accumulator stores fluid. The accumulator can therefore sustain pressures when fluid is extracted from the system. However the volume of the accumulator and the pre-set nitrogen gas pressure are it's limiting factors and so the range of use of hydraulic system will determine accumulator choice.

### 5.2.3 Servovalve

The MOOG E760 series servovalves have a two stage design that combines a friction-less pilot stage that drives a spool and bushing power stage [5.3]. Figure 5.2 is a basic diagram to show how the two stages link together and thus shows how the valve operates.

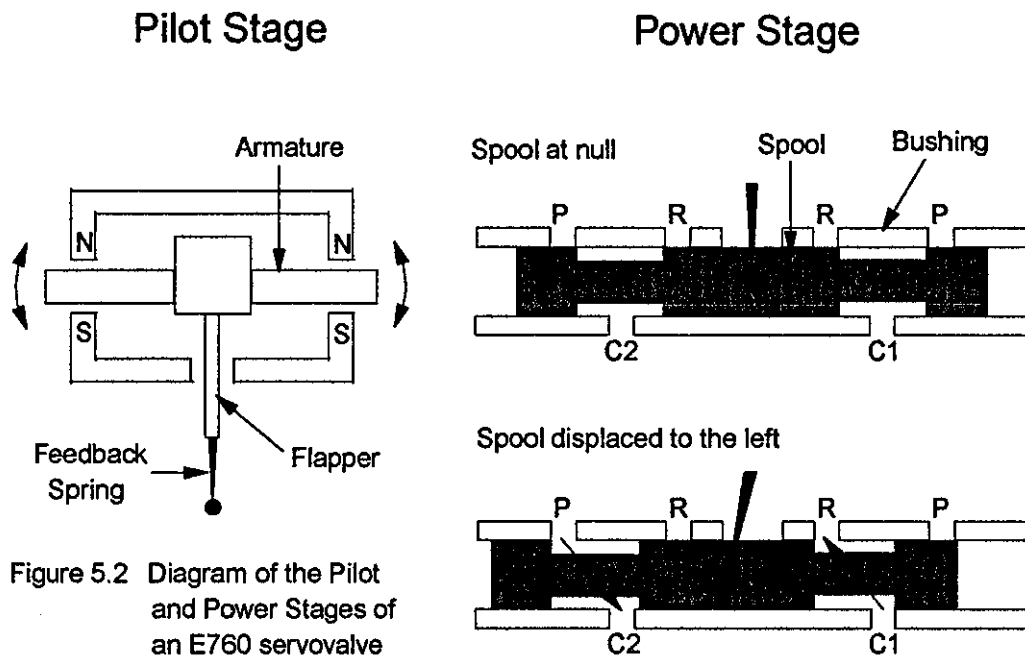


Figure 5.2 Diagram of the Pilot and Power Stages of an E760 servovalve

The pilot stage shows an armature and flapper assembly placed in a fixed magnetic field, with North (N) and South (S) poles. Although not shown in Figure 5.2, two

wires are wrapped round, to make two coils on each arm of the armature. When a current is passed through the coil, this creates a magnetic field in the armature so that one end becomes a North pole and the other a South pole. The supplied current is AC and therefore the alternating magnetism of the armature causes it to rock or rotate within the fixed magnetic component. On the end of the flapper is a feedback spring, which is linked to a spool shown in the Power Stage. The spool is contained in the bushing and the four ports of the valve are labeled as P, R, C1 and C2. Port P is the supply pressure port, R is the return flow port and ports C1 and C2 are control ports.

When no current is supplied to the coil there is no magnetism in the armature, thus the spool is at null, as shown in the power stage. When current is supplied this causes the rotating armature and flapper assembly to displace the spool via the feedback spring. The power stage shows the spool displaced to the left and this allows flow from P to C2 and from C1 to R as shown in Figure 5.3. Similarly when the spool is displaced to the right this allows flow from P to C1 and therefore flow from C2 to R.

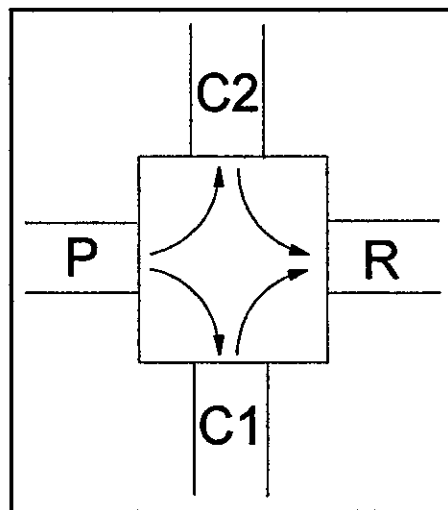


Figure 5.3 Diagram to show how the MOOG Servovalve operates

## 5.3 Setup of the Equipment

Before operating the power pack the user must check that the:

- 1 Reservoir contains a sufficient amount of fluid, in this case oil.
- 2 "Air Lubricator" contains enough lubricating oil
- 3 "Pressure Let Down Valve" is open (turn anti-clockwise).
- 4 "Air Stop Valve" is closed (turn anti-clockwise).
- 5 "Air Pressure Regulator" at a minimum (turn anti-clockwise).

The next step is to connect a suitable air supply (up to 100 PSI) to the "Air Supply Connection". Suitable high pressure rated hydraulic fittings and pipe were used to connect the hydraulic power pack to the MOOG servovalve via the accumulator. The control port marked C1 on the servovalve was blocked off using a blanking nipple and the other control port marked C2 was connected to the pressure transducer via a suitable fitting and a flexible high pressure hydraulic hose. The return port marked R, was linked to the power pack reservoir via a flexible tube. Any build up of oil, and therefore pressure, at port C1 or port C2 would flow out of port R to return to the reservoir at atmospheric pressure, hence the use of a simple flexible tube.

Figure 5.4 shows the set up of the mechanical equipment. Also shown are a Function Generator, a Digital Oscilloscope and a 9V Battery. These are discussed in the next section.

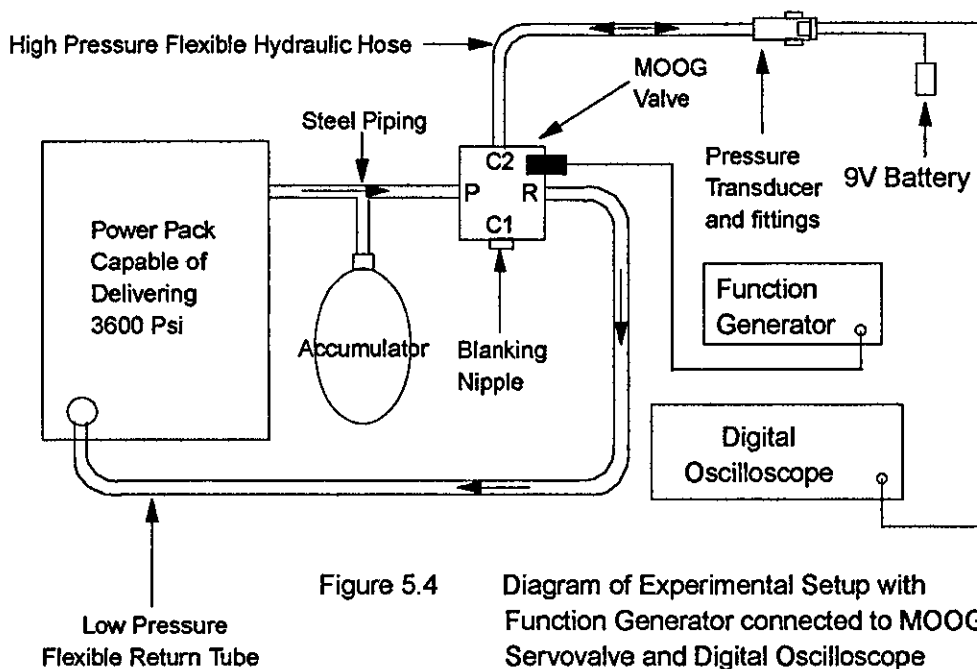


Figure 5.4 Diagram of Experimental Setup with Function Generator connected to MOOG Servo Valve and Digital Oscilloscope connected to Pressure Transducer via leads

Once all the equipment in the hydraulic system was connected the fittings were tightened and the equipment could be connected to the electrical equipment.

## 5.4 Electronic Equipment

### 5.4.1 Function Generator

A Wave or Function Generator, Figure 5.4, via the use of a 4 pin plug connector, is used to power the MOOG servovalve, the operation of which has already been described. The coils on the servovalve armature are connected in parallel and this results in a coil resistance of  $40\Omega$ . The servovalve requires a supply current of  $40\text{mA}$  and therefore the nominal voltage for that current is  $\pm 1.6\text{V AC}$ . Knowing this the function generator was set to a square wave of  $3.2\text{V}$  or more, with the lowest frequency of  $0.2\text{Hz}$ . Once the function generator is switched on the faint ticking of the

switching of the servovalve can be heard; the servovalve becomes much more audible when operating with high pressure fluids.

### **5.4.2 Oscilloscope**

The digital oscilloscope, Figure 5.4, is used to monitor the voltage produced by the transducer and hence the pressures in the fluid, experienced by the pressure transducer. As with analogue scopes the digital scope can plot a graph and has a trigger that can be used to obtain the required trace on screen. However, the digital scope unlike an analogue scope has the ability to remember thousands of x-y co-ordinates so that when triggered the trace can be saved to 1 of 4 channels. The large range of timebase settings for the x-axis is also a useful feature of the digital scope, making it an excellent tool for recording the pressure traces.

As discussed in Chapter 4 the transducer can be operated comfortably by voltages supplies of the order of 10V. Mains pick up was experienced during the cylinder drop experiment and so a 9V battery were connected to the pressure transducer instead, see Figure 5.4. The battery is connected to the transducer wires 1 and 3/6 using crocodile leads and the transducer wires 4 and 5 are connected to the oscilloscope with a croc to BNC lead.

## **5.5 Operating Procedure**

The power pack is now ready for use and any air can be extracted from the system. The transducer is at the end of the hydraulic hose. Therefore it can be made the highest point in the system and air can be released from the transducer fitting by executing the following operations.

- 1 The "Pressure Let Down Valve" is opened (turn clockwise).
- 2 The "Air Stop Valve" is opened (turn clockwise).
- 3 The "Air Pressure Regulator" is turned slowly clockwise until the pump begins to reciprocate at around 10 to 15 PSI air pressure with a corresponding oil pressure of 300 to 400 PSI.
- 4 Operate servovalve at the lowest frequency of 0.2Hz.
- 5 Gradually release the transducer fitting until air and or oil seeps from the fitting and allow air to escape.
- 6 When all air has escaped only oil will seep out of the fitting, which can now be tightened.

All the air is now out of the hydraulic system and the power pack, together with the accumulator and servovalve, can be used to create high pressure pulses. Further clockwise turning of the "Air Pressure Regulator" increases the air input pressure and thus increases the oil output pressure. The trace of the pressure pulses can be visualised on the oscilloscope. Below 1500 PSI the square wave oil pulses will be very irregular, but above 1500 PSI the accumulator takes effect and perfect square pulses are produced. The length of these pulses can be altered by changing the frequency or duty cycle on the function generator. The hydraulic system is functioning in the correct fashion and is now ready to be used to test the high pressure transducers.

# CHAPTER 6

## Study I of Hydraulic System Fluid Pulses

### 6.1 Introduction

This chapter describes the bulk of the work carried out on the study of fluid pulses, initially with a section about the type of seeding used. Following this is a description of the optical and imaging equipment assembly and a detailed calculation of the glass safety requirements. The initial oscilloscope and optical observations are next to be covered. There is a larger section on changes to the system and conditions to induce damage to the transducers. Following on from this there is a description of the dieseling process and the final section is a detailed calculation of the typical temperatures and energies involved in the experimental work.

### 6.2 Oil Seeding

Before any study of the oil could be made a suitable type of seeding particle had to be found. The particles have to be similar in density to the oil, so that they don't sink or float in the oil. Previous studies of particle movement in liquids have utilized seeding particles including conifer pollen [6.1], Potters Ballotini Spherical<sup>TM</sup> hollow glass spheres [6.2] or polystyrene spheres [6.3].

In the first experiments 20 $\mu$ m diameter polystyrene spheres and 11 and 100 $\mu$ m diameter hollow glass spheres were mixed into oil, in separate transparent containers. The containers of oil were in turn illuminated by a small tungsten lamp and the seeding particles were observed using a CCD camera that was connected to a

monitor. Agitation of the containers led to swirling of the particles within the oil. The larger hollow glass spheres sank quite quickly due to a density of  $1100 \text{ kg/m}^3$  compared with the  $865 \text{ kg/m}^3$  oil. Although smaller hollow spheres had a similar density, they sank at a slower rate in the viscous oil, but these smaller particles were quite difficult to see in the oil. However, the polystyrene spheres, although having a density of  $1050 \text{ kg/m}^3$ , were slow to settle and were easily detected. Oil impurity particles also acted as useful tracers.

The polystyrene spheres were used for seeding and so a small amount of the oil containing these spheres was sucked into a pipette tube. With the transducer removed from the optical brass fitting or cell, oil was squeezed out of the pipette, into the top of the cell. The oil level in the cell was topped up, so that there is no air in the system when the transducer was screwed back into the cell. The arrangement of the transducer, test cell and optical equipment is shown in the next section.

## **6.3 Assembly of Optical and Imaging Equipment**

### **6.3.1 Optical Equipment**

Once the seeding of the oil in the cell was completed and the mechanical and electrical equipment was set up as shown in Chapter 5, the camera and light source were assembled as shown in Figure 6.1. Light from the halogen bulb illuminated the oil and seeding particles so that the CCD camera lens could be focused onto a plain of particles within the oil.

The Optical Brass Fitting was designed so that the windows on either side were close as possible to each other to reduce the cross sectional area of the chamber; the power pack wouldn't have to work as hard to compress the oil and thus maintain pressure, as it would for a cell containing a large volume.

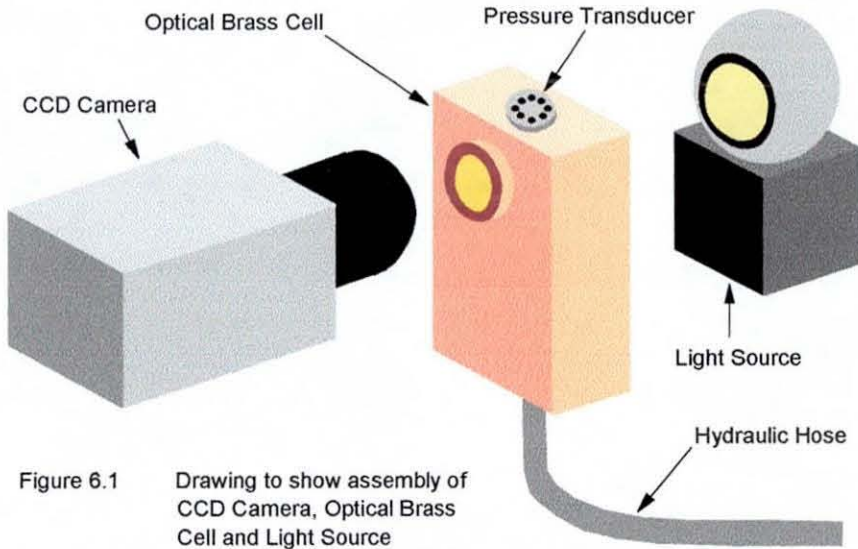


Figure 6.1 Drawing to show assembly of CCD Camera, Optical Brass Cell and Light Source

### 6.3.2 Calculation of Soda Glass Window Thickness with Respect to Survival Time and Probability

The following calculations were made to ensure the windows could sustain the large pressures, with a very low probability failure over a long duration of system operation.

$$\sigma_{\max} \approx \Delta P \cdot R^2 / t^2 \quad [6.4] \quad \text{Equation 1}$$

- $\sigma_{\max}$  = Maximum tensile stress on low-pressure face
- $\Delta P$  = Pressure difference across window
- $R$  = Radius of window
- $t$  = Thickness of window

Have to calculate design stress  $\sigma = \sigma_{\max}$ .

$$\sigma_{\max} = \sigma_r \cdot \text{SRF} \cdot \text{SFRF} \quad \text{Equation 2}$$

- $\sigma_r$  = Modulus of rupture
- SRF = Strength-reduction factor
- SFRF = Static fatigue reduction factor

The **Modulus of rupture** measures the mean glass strength for a short period bending test and has a value of 50 MPa for Soda glass.

The **Strength-reduction factor** is required by the Weibull equation (below) for a given failure probability.

$$\ln P_s(V) = - (V / V_0) \cdot (\sigma / \sigma_0)^m \quad \text{Equation 3}$$

The probability of one sample of volume  $V_0$  surviving a stress  $\sigma$  is  $P_s(V_0)$ . The probability that a batch, of  $n$  such samples, all survives the stress is only  $\{P_s(V_0)\}^n$ . If these  $n$  samples were all stuck together to give a single sample of Volume  $V = nV_0$  then its survival probability would still be  $\{P_s(V_0)\}^n$ .

- $P_s(V)$  = Probability of success of Volume  $V$
- $V$  = Volume of  $n$  samples       $V_0$  = Volume of single sample
- $\sigma$  = Stress on  $n$  samples       $\sigma_0$  = Stress on single sample

The **Static fatigue reduction factor** is essentially for the static fatigue equation in order to satisfy the required design lifetime.

$$(\sigma / \sigma_{TS})^n = t(\text{test}) / t \quad \text{Equation 4}$$

- $n$  = Slow crack growth exponent
- $\sigma_{TS}$  = Test Stress       $\sigma$  = Design stress
- $t(\text{test})$  = Test time       $t$  = Design time

The window was tested at a stress  $\sigma_{TS}$  for a test time of 10 minutes -  $t(\text{test}) = 0.166$  hours, so it will last  $t$  hours at the design stress  $\sigma$ .

We require a  $10^{-6}$  (1 in 1000000) failure probability and a design life under load of 1000 hours for a window. The pressure window separates the atmosphere from oil at pressures up to approximately 200 bar, i.e. the window has to with stand a pressure difference ( $\Delta P$ ) of 200 bar or 20MPa. Find the ratio of the window radius to the window thickness.

**Equation 3**                       $\ln P_s(V) = - (V/V_0) \cdot (\sigma/\sigma_0)^m$                       Soda glass  $m = 10$

For the ratio put                       $-(\sigma/\sigma_0)^{10} = \ln 0.999999$

$\sigma/\sigma_0 = (-1.000000500029 \times 10^{-6})^{1/10} = 0.25$

Strength-reduction factor (SRF) = 0.25

**Equation 4**                       $(\sigma/\sigma_{TS})^n = t(\text{test})/t$                       Soda glass  $n = 10$

For the ratio put                       $(\sigma/\sigma_{TS})^{10} = 0.167/1000$

$\sigma/\sigma_{TS} = (1.67 \times 10^{-4})^{1/10} = 0.42$

Static fatigue reduction factor (SFRF) = 0.42

**Equation 2**                       $\sigma_{\max} = \sigma_r \cdot \text{SRF} \cdot \text{SFRF}$

$\sigma = \sigma_{\max} = 50 \times 10^6 \cdot 0.25 \cdot 0.42$

$\sigma = 5.26 \times 10^6 \text{ Pa}$

**Equation 1**             $\sigma = \Delta P \cdot R^2 / t^2$

$$t / R = ( 20 \times 10^6 / 5.26 \times 10^6 )^{1/2} = 1.95$$

The window radius is 6mm so the window would have to be 11.7mm. Glass is very rarely made to such a thickness so the following calculations are for a window of radius 6mm and thickness 10mm.

**Equation 1**             $\sigma = \Delta P \cdot R^2 / t^2$

$$\sigma = 20 \times 10^6 \cdot ( 0.006 / 0.01 )^2$$

$$\sigma = 7.2 \times 10^6 \text{ Pa}$$

Therefore the product of Strength and the Static Fatigue Reduction Factors is

$$7.2 / 50 = 0.144$$

If we set the design time to 1000 hours this equates to a SFRF of 0.42. Therefore we can work out the probability of a 6mm thick window failing under a pressure difference of 200 bar for 100 hours; SRF is 0.34.

$$\sigma / \sigma_0 = 0.34$$

$$0.34^{10} = 2.3 \times 10^{-5}$$

$$\exp -2.3 \times 10^{-5} = 0.999976997705$$

The probability of failure is therefore 0.000023002295 or 1 in 43474.

The calculations show that for 1000 hours working life of the window there is approximately a 1 in 40000 chance of the windows cracking under the pressure of 20 MPa or approximately 2900 PSI.

### **6.3.3 Imaging Equipment**

The CCD camera was connected to a monitor via a high speed Betamax video recorder and a SUN station with a frame grabber software package. Therefore live footage that was visible on the monitor, could be recorded, with the option of obtaining an image at any instant on the SUN station system. Frames grabbed by the SUN station could be transferred to a floppy disc, in order to study the image in PC drawing and photo software packages.

The CCD camera was placed very close to the front test cell window and although the depth of focus was quite substantial the resultant image wasn't large enough. Therefore a lens tube was fitted to the CCD camera to obtain a wider field of view, which allowed the CCD camera to be placed closer to the test cell window and thus produce a better image. However, this addition of the tube resulted in a shorter depth of view. In order to make sure that the field of view was in the plane of the centre of the transducer diaphragm, the following procedure was followed. The lens was adjusted to create the largest field of view. Then the distance between the camera and the front window was adjusted and noted until marks on the front window were in focus. The process was repeated but marks on the rear window were focused on. The CCD camera was then placed at the mid point between these 2 marks so that the camera was focusing approximately on the required plane. Although the method was quite crude the required image was produced.

## **6.4 Initial Observations - Images and Pressure Traces Comparison**

### **6.4.1 Equipment Settings**

With the Power Pack running at approximately 2000 PSI and the function generator at a frequency of approximately 0.25 Hz (minimum output from generator) the MOOG servovalve completed a cycle, or switched on and off, every 4 seconds. The hydraulic pipe was seen to jolt slightly with an accompanying thumping noise every 2 seconds; the pipe expanded and contracted whilst the oil compressed and a slight “Water Hammer” noise was heard. This indicated that the 2000 PSI oil pressure was present in the pipe for 2 seconds, then the valve switched and this pressure was released into the flexible tube and returned to the reservoir. Another switch of the valve and the pressure increased in the pipe again.

### **6.4.2 Oscilloscope Observations**

The oscilloscope showed the pressure signals detected by the transducer. If the time base was switched to a suitable value, i.e. 1 second per division with 10 divisions on the scope display, a 2000 PSI amplitude square wave pulse of cycle length 4 seconds was seen on the scope screen. Figure 6.2 is a typical example of this trace and although the rise of the 130 bar (1700 PSI) pressure looks very fast there was a finite rise time of the pressure.

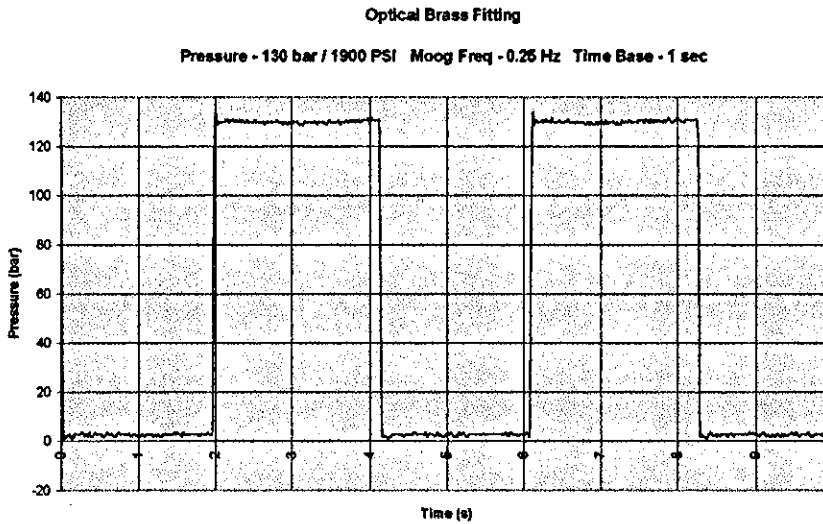


Figure 6.2 Example transducer signal trace for optical brass fitting or test cell

The time base was speeded up to 1ms per division so that the pulse rise time could be clearly seen. Figure 6.3 shows a typical trace. The pressure rise time is almost 5ms and the pressure overshoot the 140 bar (1950 PSI) supply to 160 bar (2350 PSI), probably due to the Water Hammer mechanism. Similar overshoot can be seen in Figure 6.2, as the small spikes after the pressure rises at 2ms and 6.1ms.

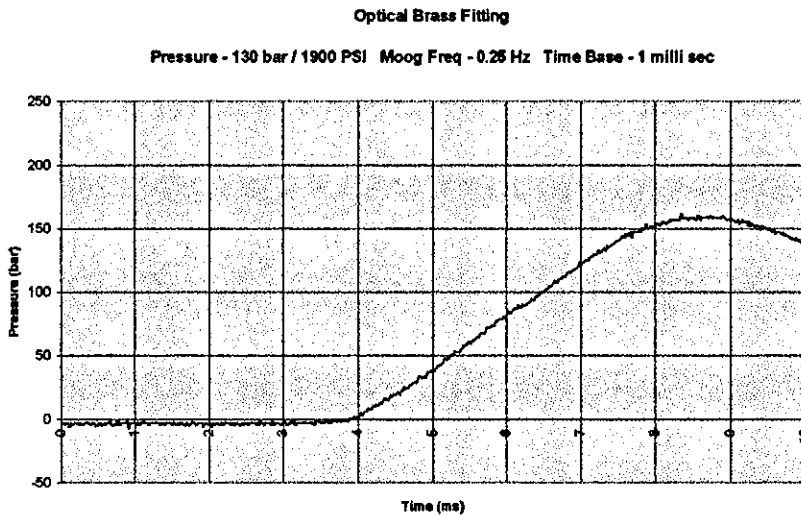


Figure 6.3 Example transducer signal trace for optical brass fitting or test cell

### 6.4.3 Optical Observations

Optical observations of this type of pressure pulse can be seen in the black and white photographs in Figures 6.4a and 6.4b. The pressures of the oil in these figures are atmospheric (before pressure pulse) and 2000 PSI (after start of pressure pulse) respectively. Although there doesn't seem to be any obvious difference between the images, there is slight deformation of the diaphragm face in 6.4b, due to the approximate pressure of 2000 PSI.

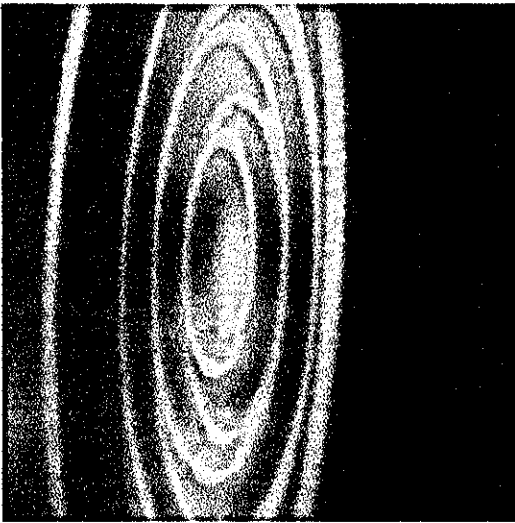


Figure 6.4a Photograph of transducer face with the oil at a pressure of 1 bar or 14.7 PSI.

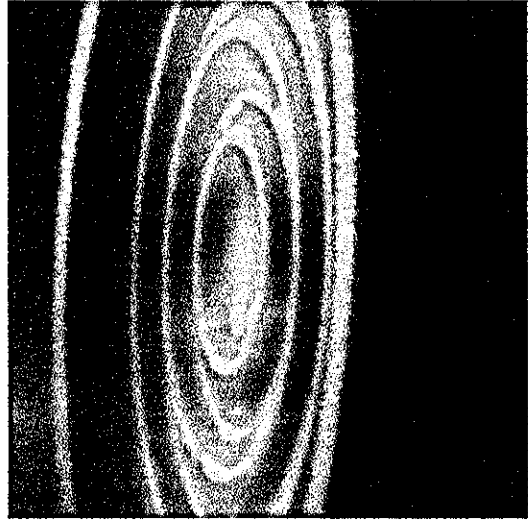


Figure 6.4b Photograph of transducer face with the oil at a pressure of 2000 PSI.

In Figure 6.5 the angle between the plane of the transducer face and the direction in which the camera points was changed from approximately 30 degrees to approximately 10 degrees. This was done so that both the face and the seeding

particles could be seen. Figure 6.5a is before the pulse at atmospheric pressure or 14.7 PSI and Figure 6.5b is after the start of the pulse with the pressure at 2000 PSI.

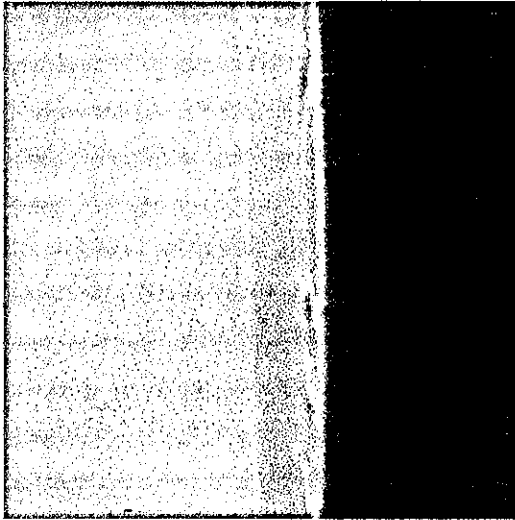


Figure 6.5a Photograph of transducer face and particles. Oil pressure of 1 bar or 14.7 PSI

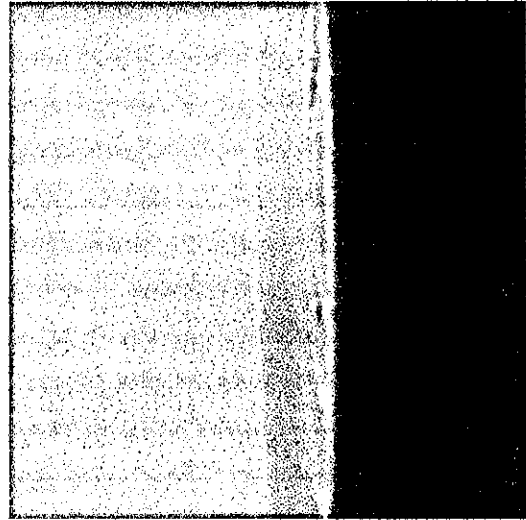


Figure 6.5b Photograph of transducer face and particles. Oil pressure of 2000 PSI.

Close examination of the images shows a slight movement of particles in various directions. Movement of the transducer face isn't noticeable. Further adjustment of the camera position and angle was made so that the focal plane was normal to the transducer face. This allowed images to be recorded showing the position and movement of the particles relative to the transducer face, with the viewing angle in the same plane as the transducer face, led to images of the particle positions. Figure 6.6a is before and 6.6b is after the start of the pressure pulse.

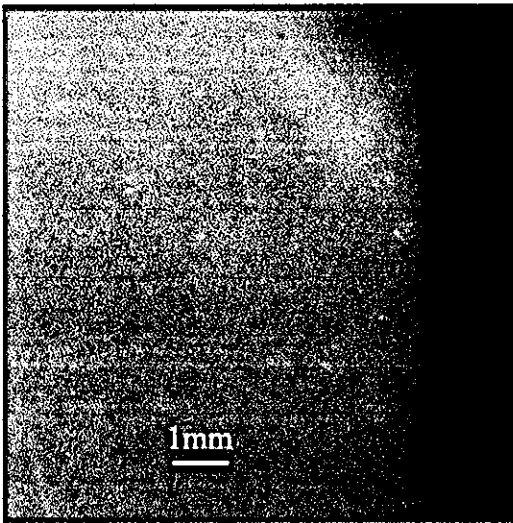


Figure 6.6a Photograph of transducer face and particles. Oil pressure of 1 bar or 14.7 PSI

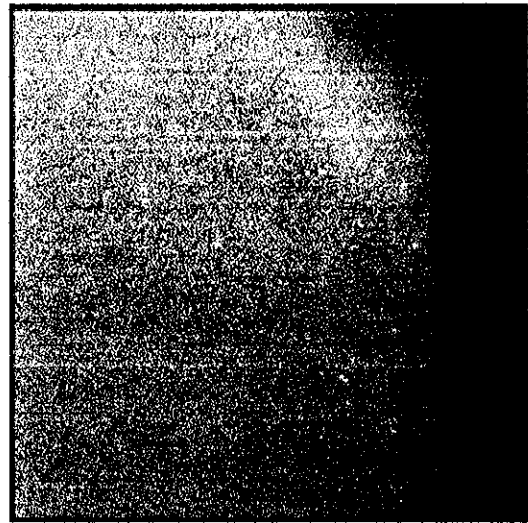


Figure 6.6b Photograph of transducer face and particles. Oil pressure of 2000 PSI.

These photographs are rather dark and manipulation of the contrast and brightness in a PC photo package led to much brighter images. This was done using the “curve” option. As you can see in Figure 6.7a, the light pixels, towards the white end of the scale, remain light and the black or dark pixels, towards the black end of the scale remain dark pixels. This is due to the linearity of the straight line “curve”. However when a point on the straight line was dragged to produce a curve there was a non linear relationship between the initial pixels and the final pixels. From Figure 6.7b, we can see that the white pixels remained white, the light pixels became white, the grey pixels became lighter, the dark pixels became grey and just the black pixels remained black. The improvement of the contrast is the equivalent of increasing the  $\gamma$  or gamma in the photographic process.

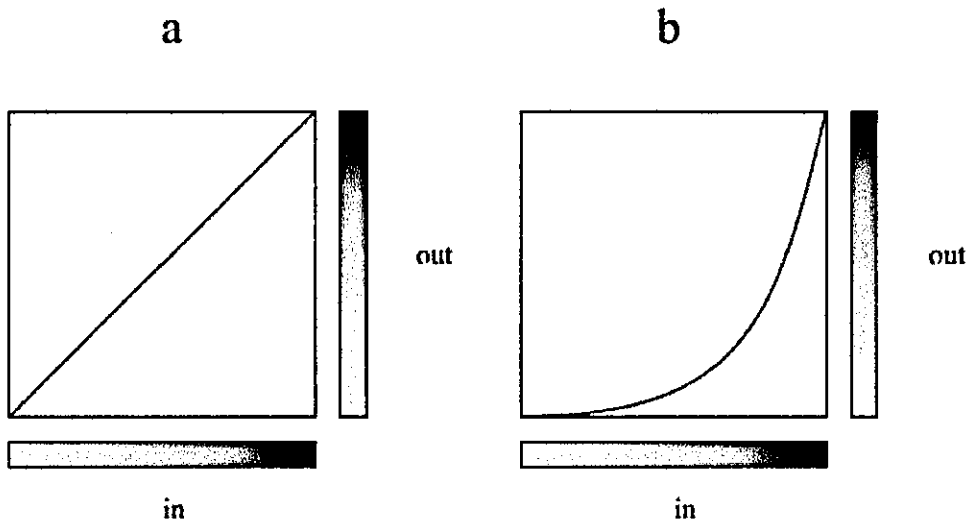


Figure 6.7 Diagram to show (a) linear and (b) non linear translation of white and black pixels.

The results of this process are shown in Figure 6.8a and 6.8b respectively.

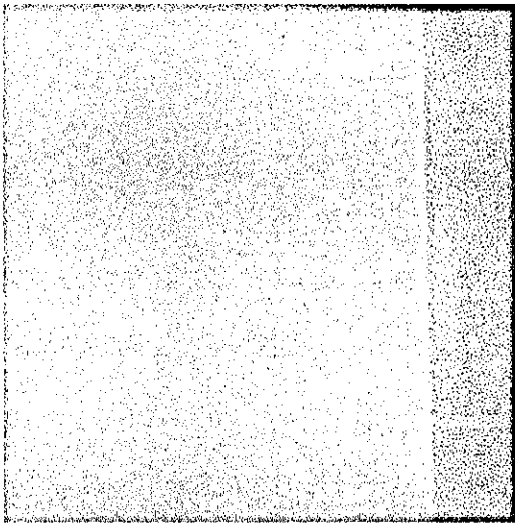


Figure 6.8a Image of transducer face and particles  
Oil pressure of 1 bar or 14.7 PSI

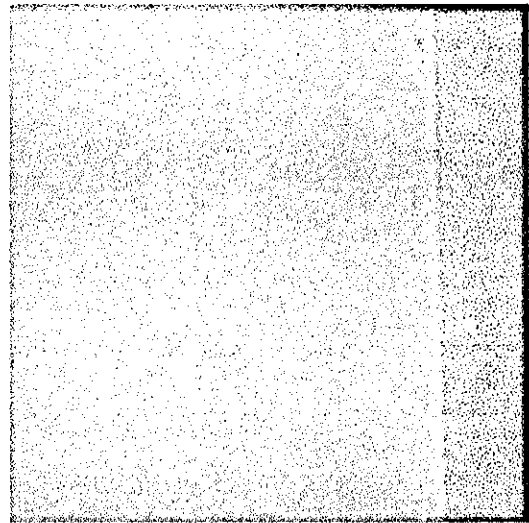


Figure 6.8b Image of transducer face and particles  
Oil pressure of 2000 PSI.

The lighter image makes the particles clearly detectable and the black transducer edge has been enhanced on the right hand side of the pictures, due to the relative brightness of the oil.

Further use of the PC photo application allowed the production of a picture with the before and after pulse positions mapped onto each other. The particle image edges were sharpened, as shown in Figure 6.9a and 6.9b. Inversion of these images, followed by increased brightness and contrast produced images portrayed in Figure 6.10a and 6.10b.

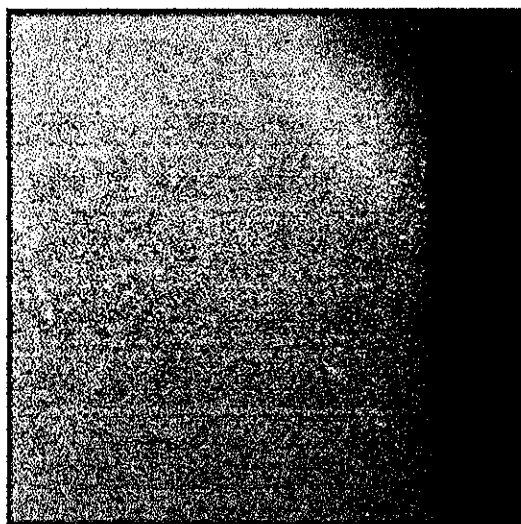


Figure 6.9a Image of transducer face and particles  
Oil pressure of 1 bar or 14.7 PSI

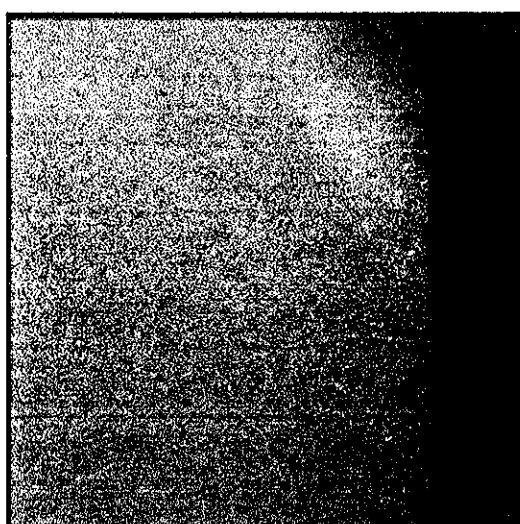


Figure 6.9b Image of transducer face and particles  
Oil pressure of 2000 PSI.

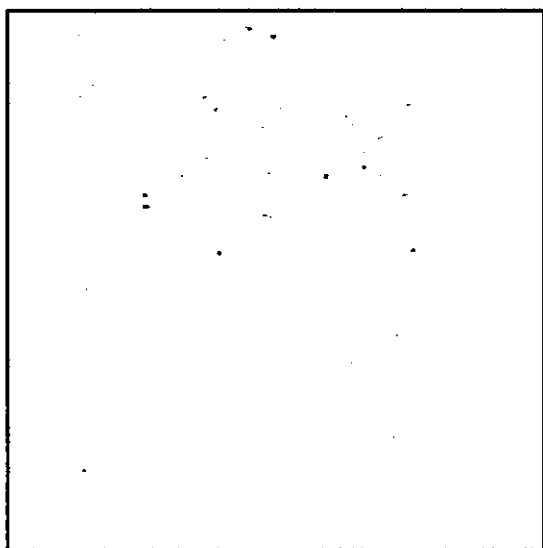


Figure 6.10a Image of particles  
Oil pressure of 1 bar or 14.7 PSI

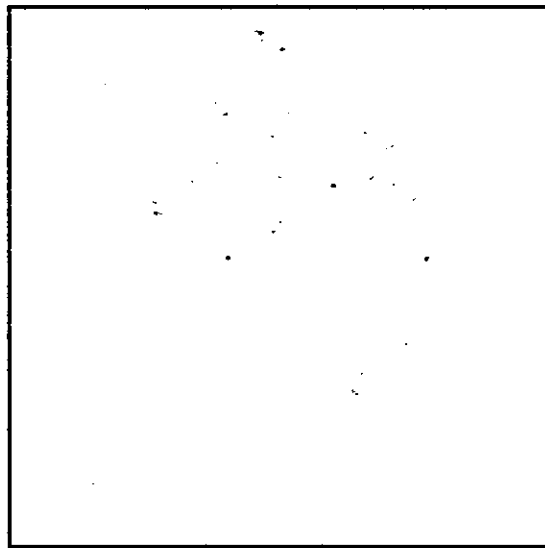


Figure 6.10b Image of particles  
Oil pressure of 2000 PSI.

The images in Figure 6.10a and 6.10b were transferred to the CorelXara2 drawing package. One of the images was made transparent and then it was positioned over the other image to produce particle image pairs, shown in Figure 6.11, similar to those produced in PIV as described in Chapter 2.

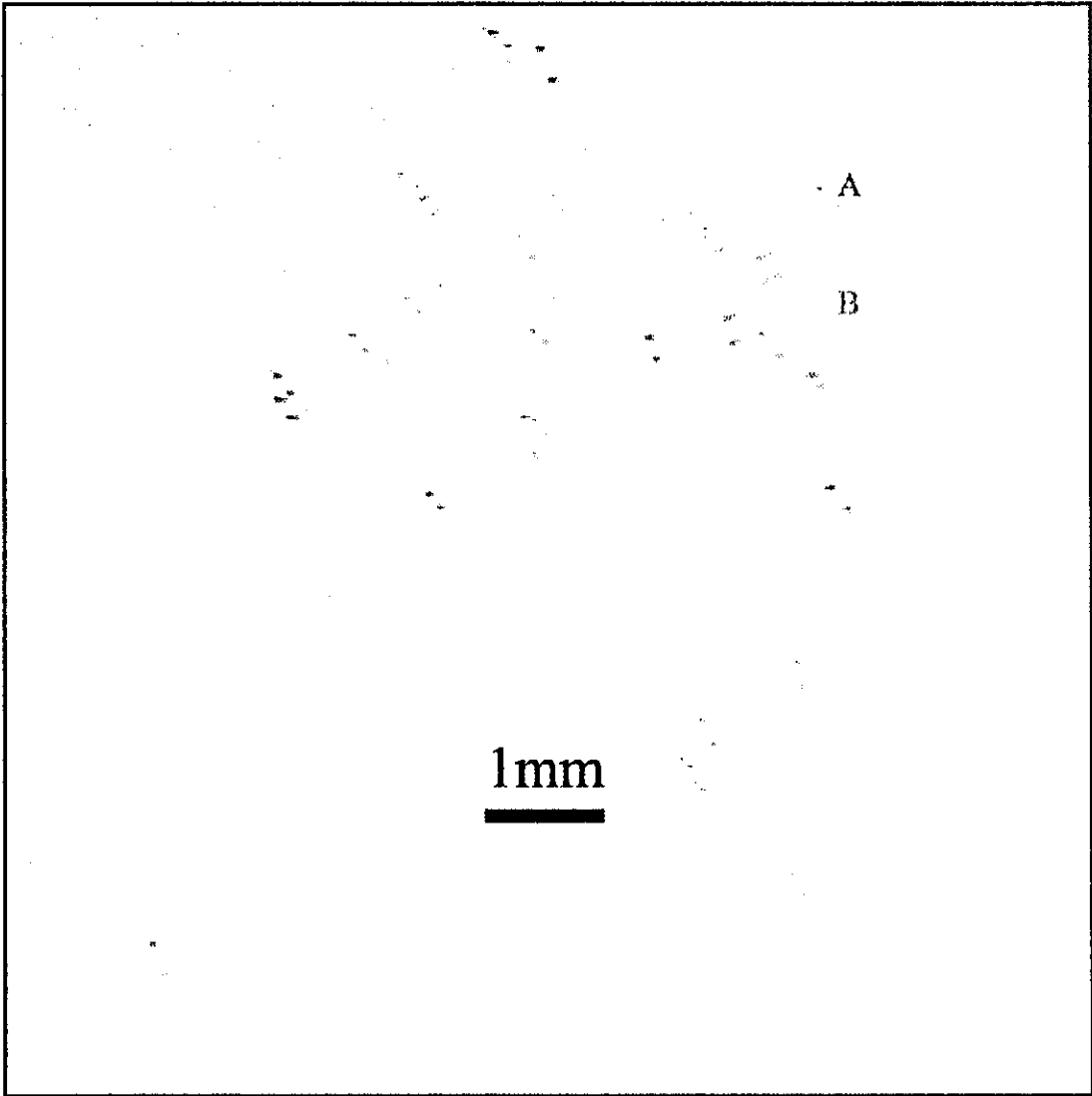
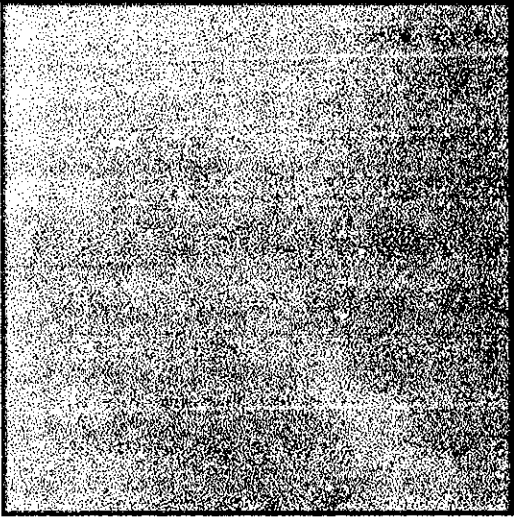
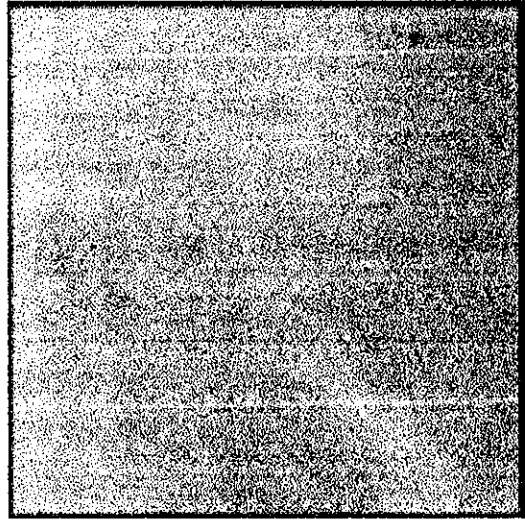


Figure 6.11 Image of the particles pairs. The blue dots show the particle positions when the oil pressure was 1 bar or 14.7 PSI and the red dots show the particle positions when the oil pressure was 2000 PSI.

Figures 6.12 to 6.16 show the different stages in the piecing together of another final image of particle pairs. In this case the transducer face is in the vertical plain but just out of view along the right hand side of the image.



**Figure 6.12a** Photograph of transducer face and particles. Oil pressure of 1 bar or 14.7 PSI



**Figure 6.12b** Photograph of transducer face and particles. Oil pressure of 2000 PSI.

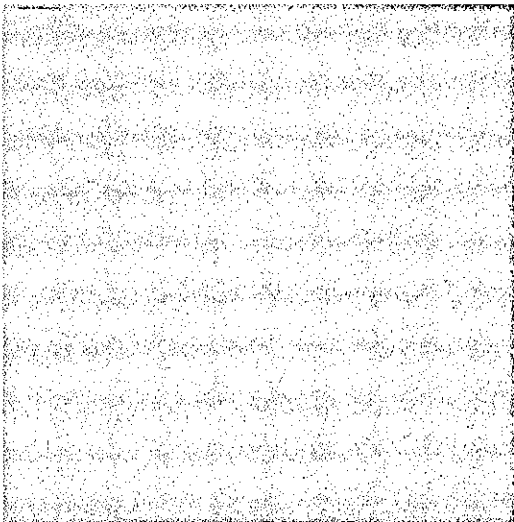


**Figure 6.13a** Image of transducer face and particles  
Oil pressure of 1 bar or 14.7 PSI

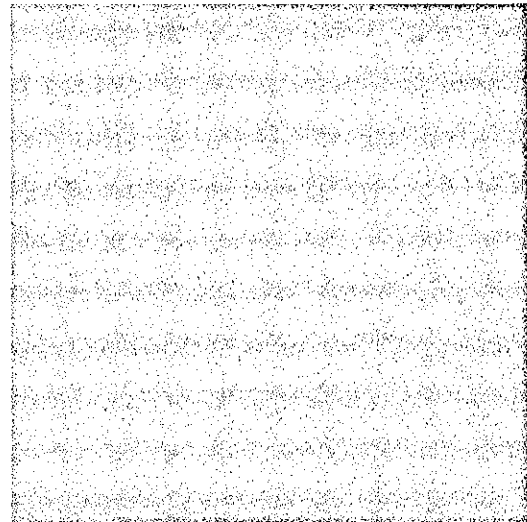


**Figure 6.13b** Image of transducer face and particles  
Oil pressure of 2000 PSI.

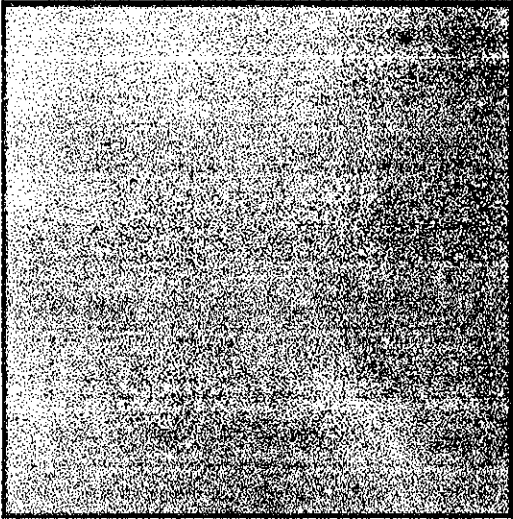


Figure 6.14a Image of transducer face and particles  
Oil pressure of 1 bar or 14.7 PSI

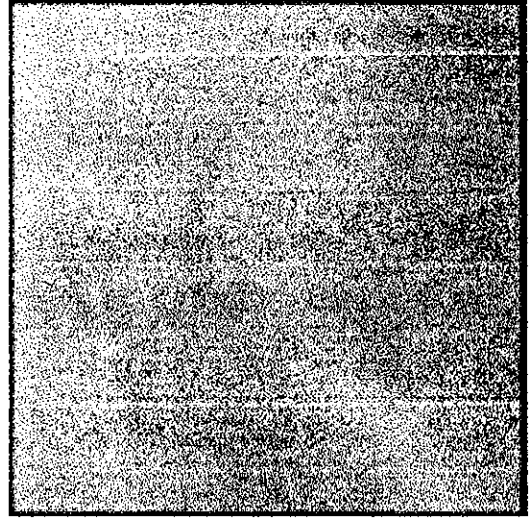


Figure 6.14b Image of transducer face and particles  
Oil pressure of 2000 PSI.

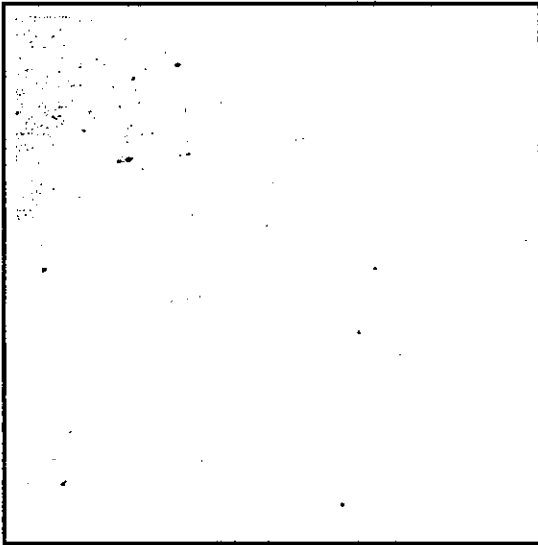


Figure 6.15a Image of transducer face and particles  
Oil pressure of 1 bar or 14.7 PSI

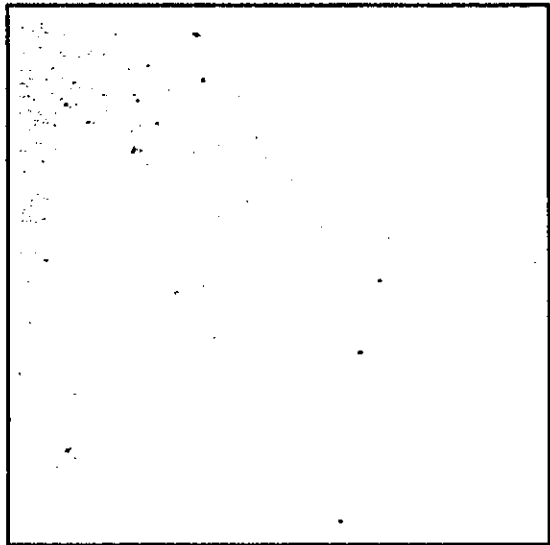


Figure 6.15b Image of transducer face and particles  
Oil pressure of 2000 PSI.

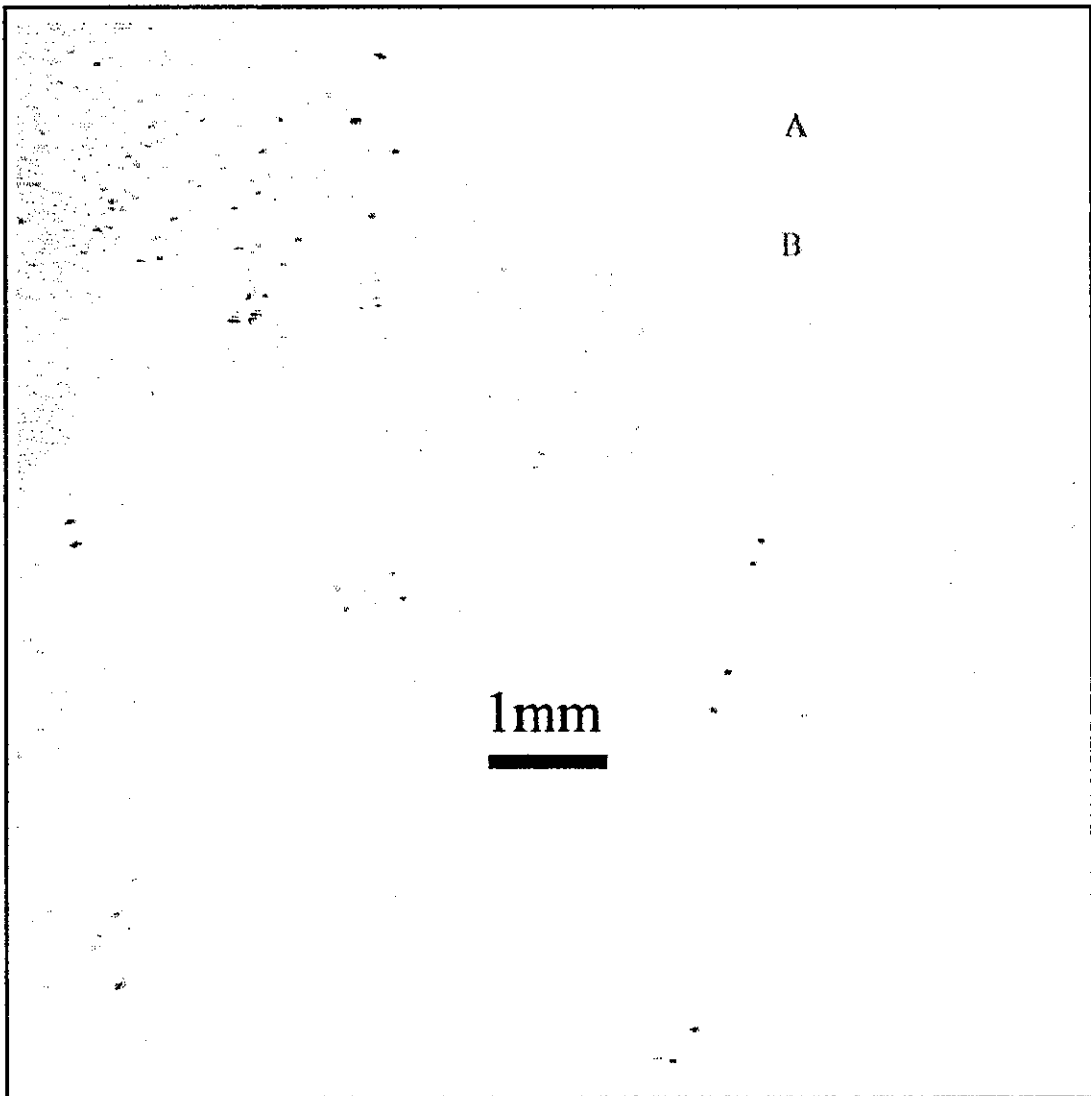


Figure 6.16 Image of the particles pairs. The blue dots show the particle positions when the oil pressure was 1 bar or 14.7 PSI and the red dots show the particle positions when the oil pressure was 2000 PSI.

From Figure 6.11 all the particles appear to have moved, in a similar direction, down and to the right towards the face of the transducer. The average displacement was approximately 0.25mm, although there may have been out of plain movement which isn't detectable. Figure 6.16 however shows that the particles moved in various directions. Particles towards the top left moved up and to the right. Whereas the particles at the right hand side near the transducer face moved down and to the left.

The whole image suggests that there was a swirling motion during the pressure pulse. The average displacement of particles was approximately 0.4mm, but some moved as much as 0.6mm.

In both instances the pressure involved was approximately 2000 PSI and the MOOG valve was operating at 0.25 Hz. Therefore the pressure pulses were also similar to the one shown in Figure 6.3, with a very steady pressure rise. In both instances no damage was made to the transducer face or electrical components of the transducer. One would expect the particles to move uniformly from the left to the right instead of the down ward motion seen in Figure 6.11 and the swirling in Figure 6.16. An explanation of this could be that if any air was trapped in the Optical test cell, the oil would obviously surge towards and compress this air. However great care was taken to extract the air from the system. For some reason the particles and thus the oil moved in an irregular fashion. This was only at a low frequency of valve operation, with no transducer damage. Damage was known to occur at high frequencies, where swifter rise times were involved so study of this followed.

## **6.5 Further Work - Damaging Transducers**

### **6.5.1 Increase in Valve Frequency**

In order to create the fast damaging rise times the MOOG servovalve frequency had to be increased. With the power pack output pressure still approximately 2000 PSI, pressure traces were recorded, Figure 6.17, for valve frequencies of (a) 0.25 Hz and (b) 16Hz. The relatively large cross sectional area of the Optical test cell meant that even at the higher frequency the rise time was still slow. However as the frequency was increased small air bubbles appeared in the optical viewing part of the brass test cell. The air could have been forced through the system after previously being trapped in a coupling or fitting. Another explanation is that the increased frequency forced the

air to come out of solution; as previously discussed in Chapter 3, at least 2% of the volume will be taken up by air within the oil.

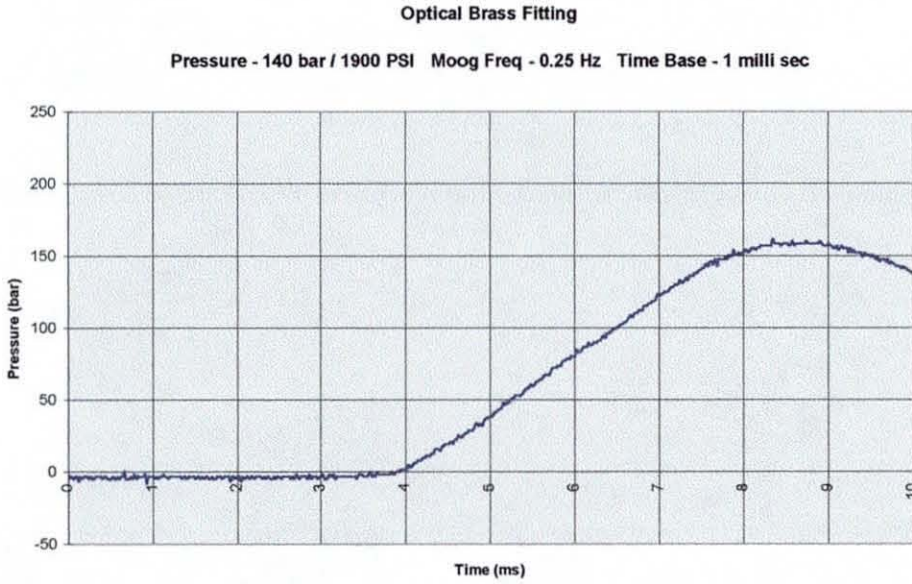


Figure 6.17a Tranducer signal trace for optical brass fitting or test cell, with MOOG frequency of 0.25Hz.

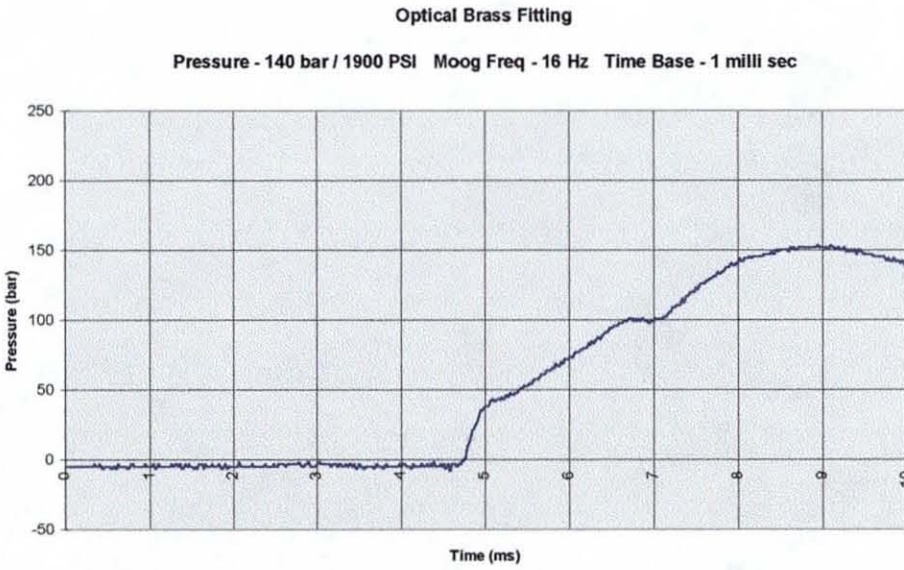


Figure 6.17b Tranducer signal trace for optical brass fitting or test cell, with MOOG frequency of 16Hz.

These air bubbles led to heating and additional vibration of the hydraulic hose as well as louder WH noise. Further observation, Figure 6.17b, showed that although the overall rise time was still as long as 4ms, the pressure rise was no longer smooth. It can be seen that there was an initial rise of approximately 40 bar (600 PSI) that took place in approximately 250 $\mu$ s. This and the heating and vibrational effects were believed to be the result of having air in the system.

## 6.5.2 Use of Smaller Cross Sectional Area Fitting

Another fitting or test cell with a smaller cross sectional area was used. This was done so that faster rise times could be guaranteed, however this meant that windows couldn't be fitted. The power pack oil pressure output was approximately 2500 PSI (170 bar) and results were recorded, Figure 6.18, again with the valve running at (a) 0.25 Hz and (b) 16 Hz.

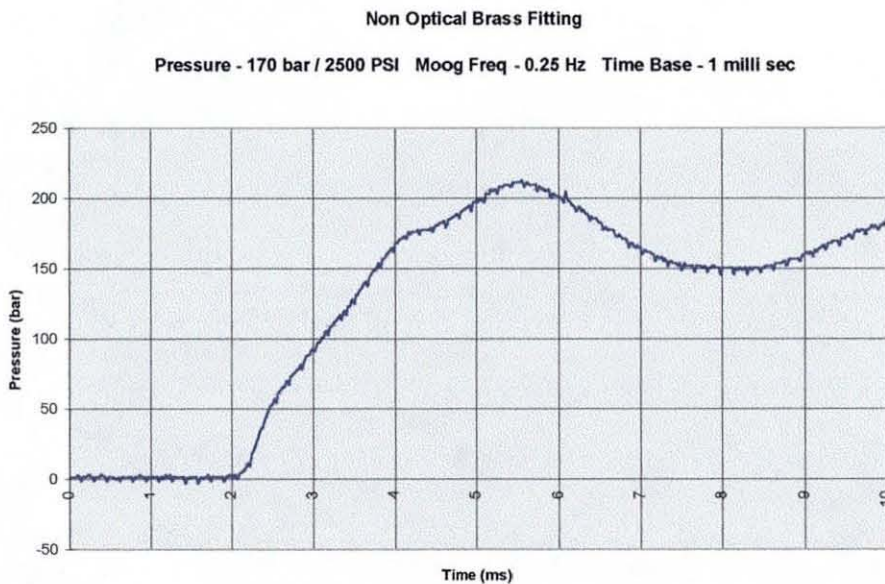


Figure 6.18a Transducer signal trace for non optical brass fitting or test cell, with MOOG frequency of 0.25Hz.

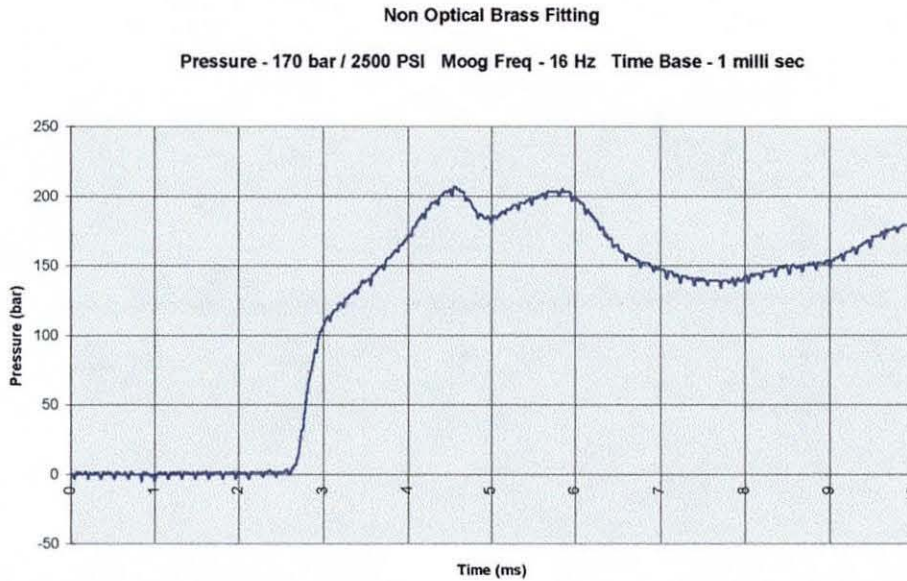


Figure 6.18b Transducer signal trace for non optical brass fitting or test cell, with MOOG frequency of 16Hz.

The rise times were noticeably shorter and the imperfections of the traces more pronounced. At the lower frequency of 0.25Hz the total rise time was approximately 3ms and there was an initial rise of 50bar (750PSI) in just under 500 $\mu$ s. The trace imperfections suggest that perhaps there were air bubbles in the system. Although this can't be visualised the WH characteristics of hose vibrations, noise and heat were more pronounced than with the optical fitting.

Changes in the trace and amplification of the WH effects occurred when the frequency was increased to 16Hz. The overall rise time was still approximately 3ms but the initial rise has increased by 100 bar (1600 PSI) in a time span of about 400 $\mu$ s. The rate of change of this initial pressure, was therefore 250000 bar/s and this created damage to the transducer electronic connections, but the surface of the diaphragm or face was relatively untouched with slight pitting of the surface. Removal of the diaphragm showed that some of the wire bonds had been ripped off resulting in a loss of signal output.

The hose expansion and contraction caused it to vibrate much more vigorously and the heat and noise produced was much greater than at 0.2Hz or with the optical test cell. Presumably the air pockets inside the hose were much larger, and this resulted in damage to the transducer and more noticeable heat, noise and vibration. Although air presence definitely led to the fast pressure rises and damage it is not clear how this happens. Perhaps the compression and subsequent collapse of the air bubbles led to damaging jets impinging on the surface of the transducer, as occurs in the cavitation process.

Figures 6.19 and 6.20 show the traces for the larger optical and smaller non optical test cell at both frequencies but with a longer time base setting to get more of the pressure wave trace.

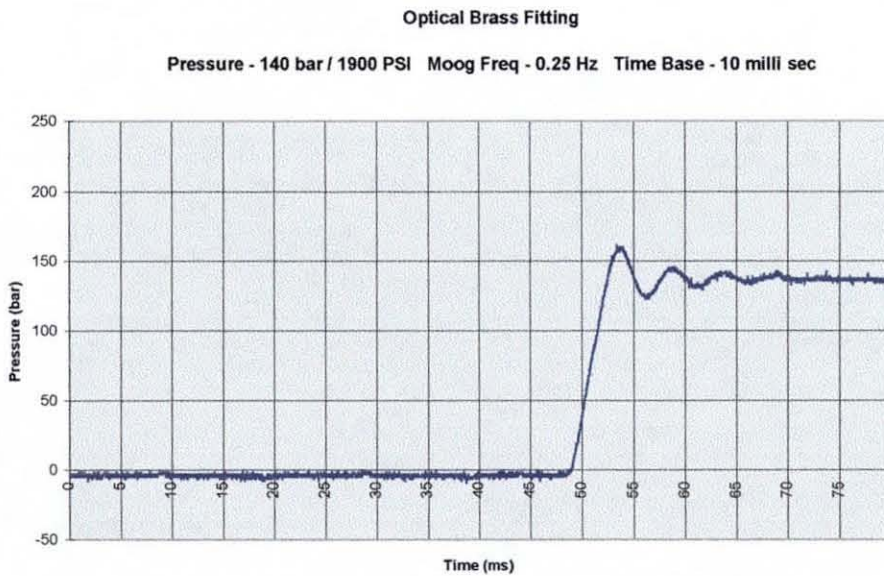


Figure 6.19a Transducer signal trace for optical brass fitting or test cell, with MOOG frequency of 0.25Hz.

### Optical Brass Fitting

Pressure - 140 bar / 1900 PSI Moog Freq - 16 Hz Time Base - 10 milli sec

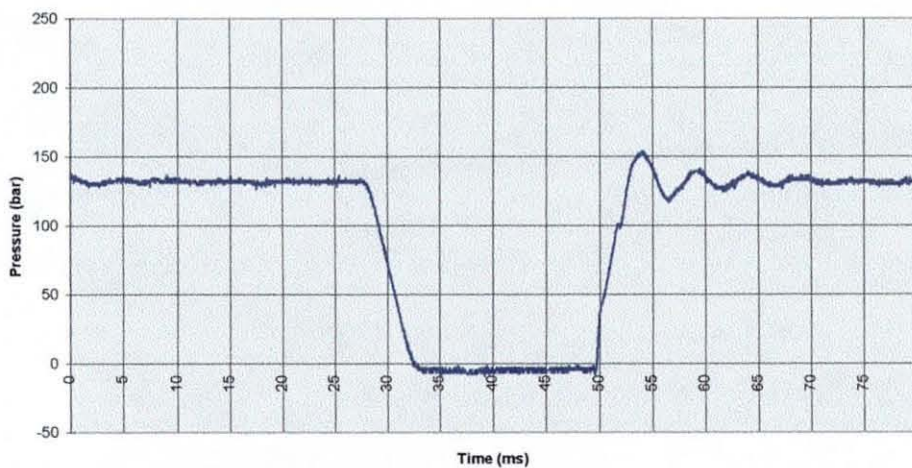


Figure 6.19b Tranducer signal trace for optical brass fitting or test cell, with MOOG frequency of 16Hz.

### Non Optical Brass Fitting

Pressure - 170 bar / 2500 PSI Moog Freq - 0.25 Hz Time Base - 10 milli sec

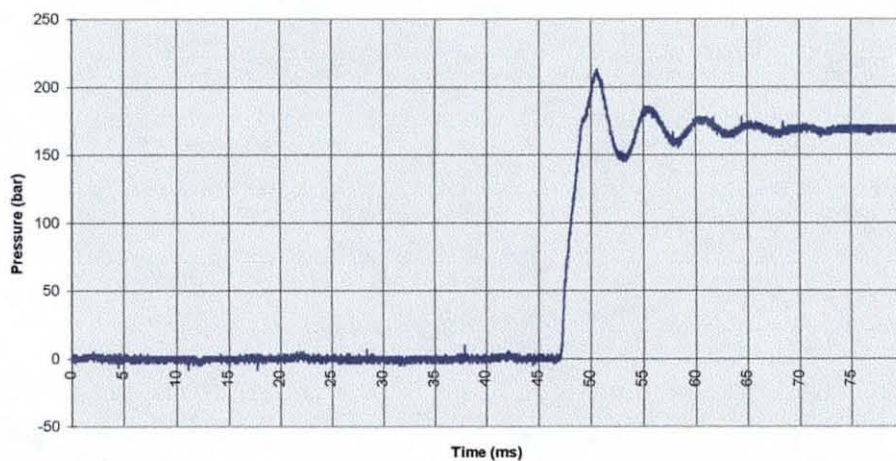


Figure 6.20a Tranducer signal trace for non optical brass fitting or test cell, with MOOG frequency of 0.25Hz.

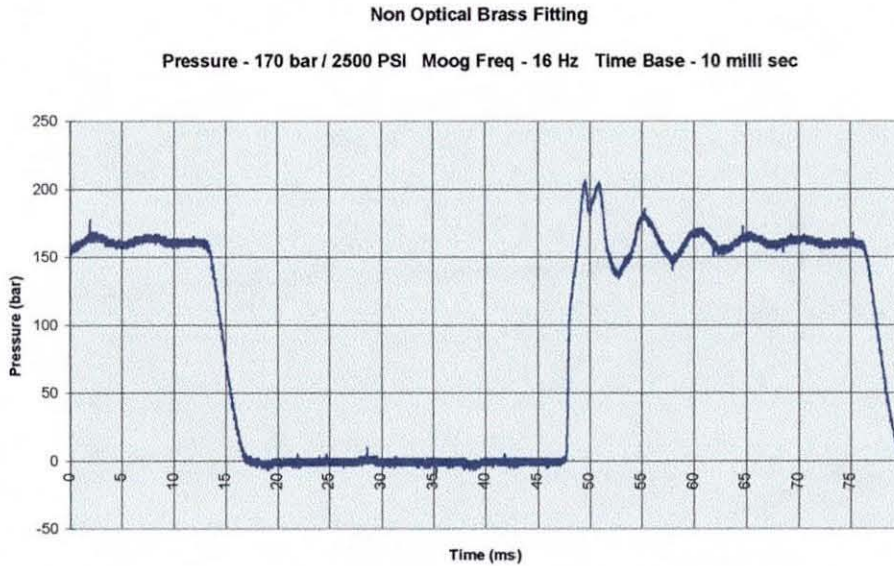


Figure 6.20b Tranducer signal trace for non optical brass fitting or test cell, with MOOG frequency of 16Hz.

All four traces show a typical WH trace characteristic, which is overshoot of the power pack supply pressure. Following this is a diminishing sinusoidal oscillation about the supply pressure. The velocity of sound and therefore WH waves in oil is approximately 1500 m/s. The distance from the transducer face, along the hose to the valve is approximately 1m so the WH wave has 2m to travel. At 1500 m/s the wave should therefore take just 1.33 ms to travel the 2m. However the time period of the WH oscillations on the traces is 5 ms, which is almost 4 times longer than expected and gives a WH wave speed of 400 m/s. This can be accounted for by the fact that the velocity of sound in a liquid can go from 1400 m/s, when containing no gas, linearly down to 150 m/s, when containing only 10% by volume of gas [6.5].

Numerous attempts were made to degas the oil and boil off any water. The oil was removed from the power pack system, pipes and fittings by running the power pack at a very low pressure and the oil was collected in glass beakers. The beakers of oil were then heated to just over 100 degrees Celsius, to boil off any water and put under a vacuum, to suck the air out, in a sealed chamber/oven.

Figure 6.19a shows the steady conditions of mild WH caused by the valve operation. Figure 6.19b shows that high frequency valve operation can cause some of the air to come out of solution and increase the WH characteristics. Figure 6.20a shows that by decreasing the cross sectional area of the test cell, more air comes out of solution and increases the WH characteristics further. Finally Figure 6.20b shows that the combination of smaller cross sectional area and high frequency valve operation causes much more air to come out of solution, with much more severe WH characteristics and resultant damage to the transducer.

The cross sectional area of the fitting or test cell was already extremely small (3mm diameter) and assumptions that a substantial amount of air was in the system when the transducer was damaged led to testing with increasing volumes of air in the system.

### **6.5.3 Increase in Air Volume in the System**

The original Optical brass fitting or test cell was refitted to the end of the hydraulic hose. The system was run at a low pressure of approximately 300 to 400 PSI and air was purged from the system using the same procedure as described in Chapter 5. The test cell was held with the transducer at the highest part of the system. The transducer was unscrewed and a pipette was used to extract some oil until the visible chamber of the test cell was entirely filled with air. The transducer was then replaced and the system was run at just over 1500 PSI with the MOOG servovalve frequency set to 0.25Hz. On the first cycle of the valve there was a large flash of light in the optical test cell window and the corresponding pressure trace was substantially different from previous testing. The transducer was damaged on the 3rd valve cycle and further testing of more transducers at the same valve frequency of 0.25Hz and later 16Hz, resulted in the same outcome.

Figure 6.21 shows the pressure traces for the valve at 0.25Hz and 16Hz. Although the supplied power pack pressure is only 1500 PSI the initial rate of change of the pressure pulse is as high as 233000 bar/s, a 70 bar rise in 300 $\mu$ s. The trace is almost identical at 16Hz, but the maximums and minimums on the curves are slightly sharper and the initial rate of increase of pressure is almost 267000 bar/s, 80 bar rise in 300 $\mu$ s.

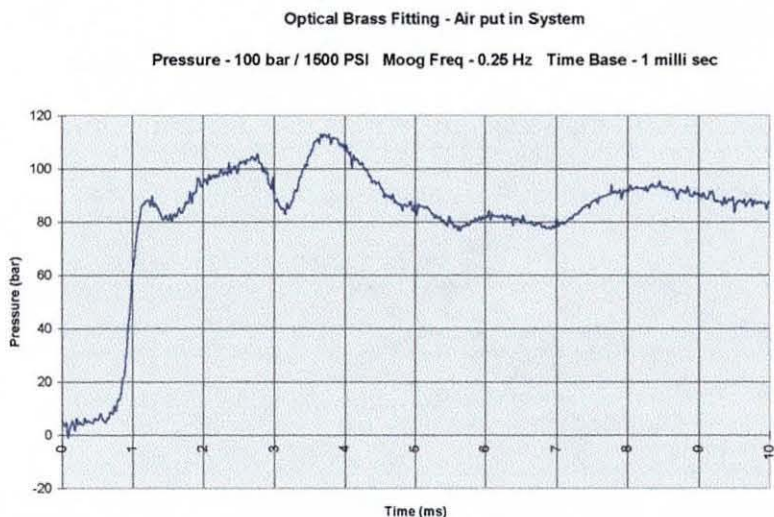


Figure 6.21a Tranducer signal trace for optical brass fitting or test cell filled with air. MOOG freq. = 0.25Hz.

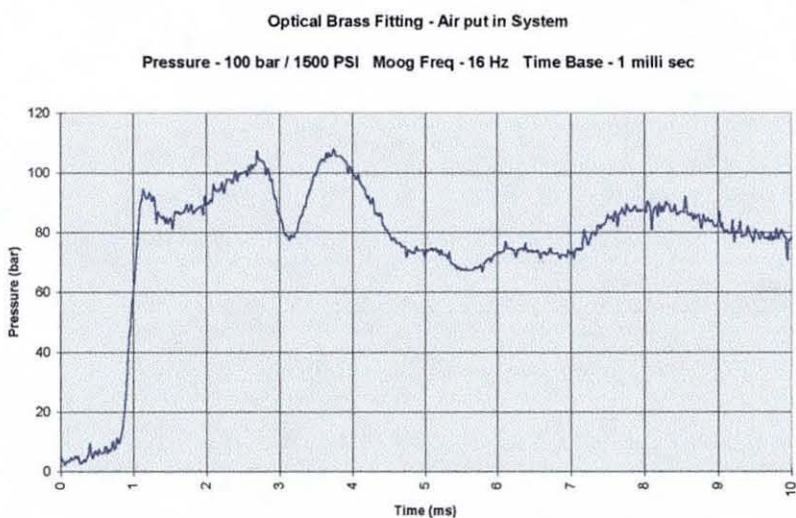


Figure 6.21b Tranducer signal trace for optical brass fitting or test cell filled with air. MOOG freq. = 16Hz.

Figure 6.22 shows traces for the small non optical test cell, containing air, with valve frequencies of 0.25Hz and 16Hz and a power pack supply pressure of 2500 PSI. The pressure pulses are very similar to the ones obtained with the optical test cell. Figure 6.22 portrays pressure changes of 600000 bar/s (120 bar / 200 $\mu$ s) and just over 700000 bar/s (120 bar / 170 $\mu$ s) for valve frequencies of 0.25Hz and 16 Hz respectively. As with the optical fitting the maximums and minimums are sharper at the higher frequency.

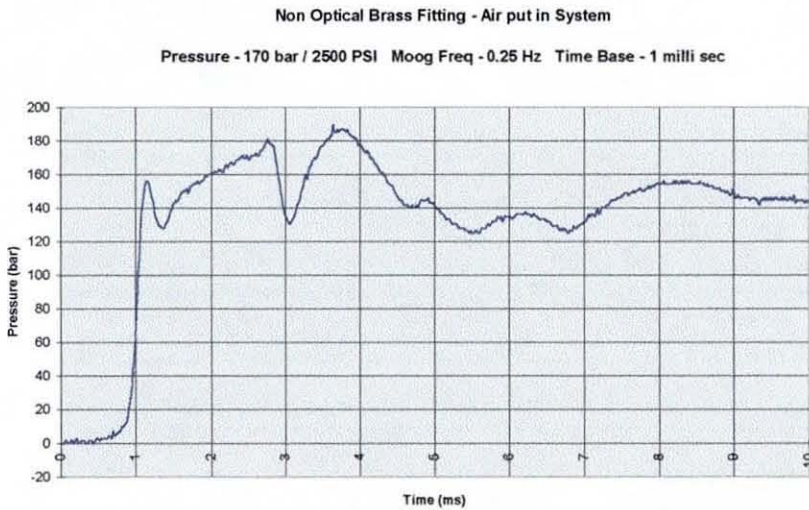


Figure 6.22a Tranducer signal trace for non optical brass fitting or test cell filled with air. MOOG freq. = 0.25Hz.

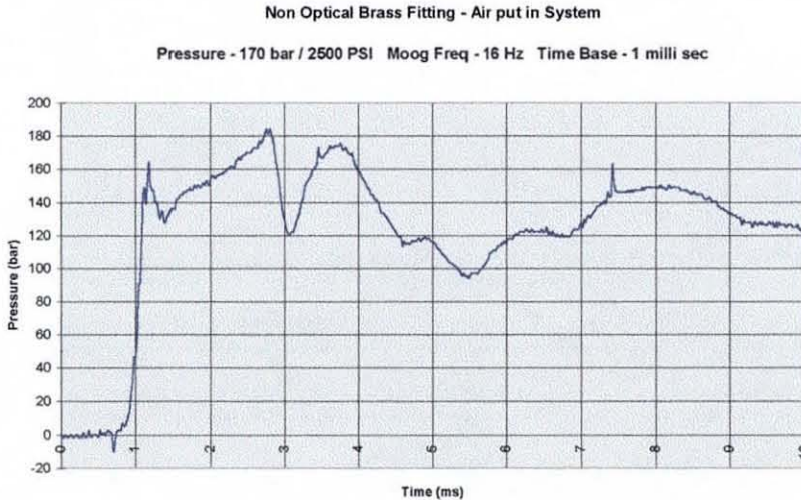


Figure 6.22b Tranducer signal trace for non optical brass fitting or test cell filled with air. MOOG freq. = 16Hz.

With both cells or fittings and at both frequencies, damage to the transducers was observed both electrically and mechanically. In all four cases the wire bonds behind the diaphragm were ripped off causing electrical failure of the module. Slight pitting of the diaphragm occurred with the lower pressure rise rates experienced with the larger optical test cell. With the smaller non optical test cell the very high pressure rise rates caused more extensive pitting and even large indentations of the surface of the transducer diaphragm. The damage on the surface seems to suggest that the pressure wasn't evenly distributed.

The WH noise, heat and vibration features are much more noticeable with much air in the system and with the small non optical test cell, at 16Hz valve frequency, the hydraulic hose was almost too hot to hold. The temperatures created by the compression of air inside the hose must be extremely high. These temperatures were high enough to create dieseling or ignition of the oil, that produced the flashes or sparks of light. Sparking continued on most valve cycles until all the oxygen in the air or gas was burnt out. The sparks varied in size depending on the magnitude of the bubble and examples of these can be seen in Figures 23a, 23b and 23c. The image in Figure 23d shows a very intense and almost perfectly circular flash of light.

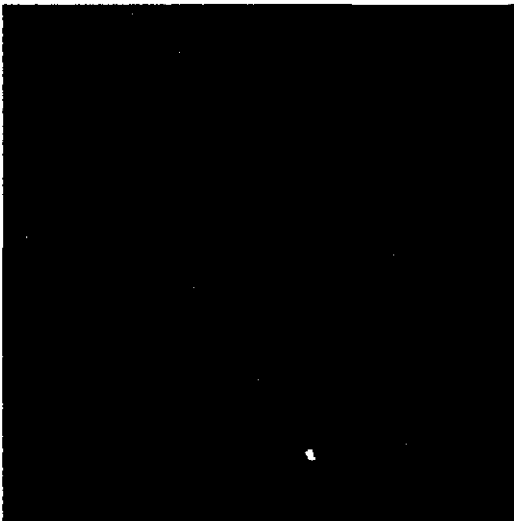


Figure 6.23a Image of sparking within the oil



Figure 6.23b Image of sparking within the oil

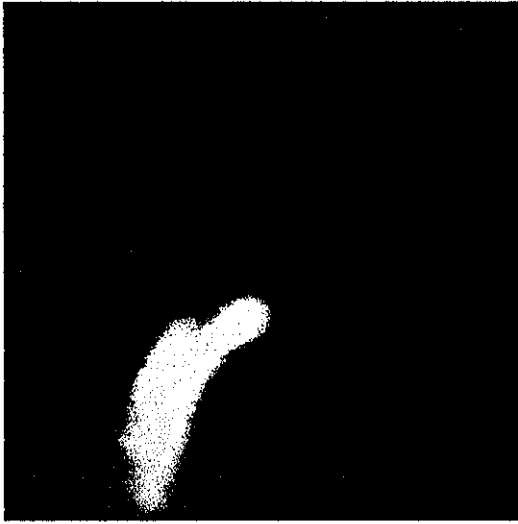


Figure 6.23c Image of sparking within the oil

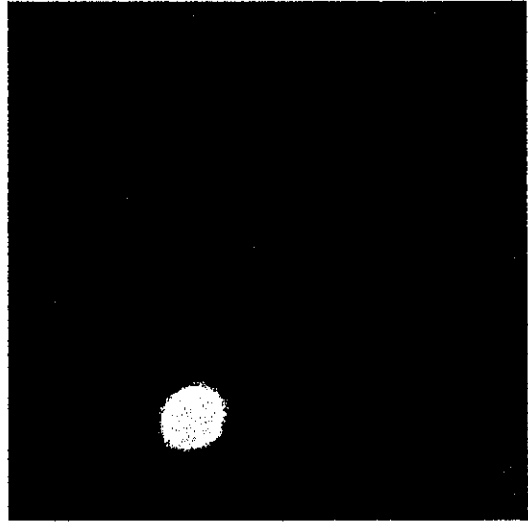


Figure 6.23d Image of sparking within the oil

The following section describes the diesel cycle as opposed to the otto cycle and in the section following this there is also a detailed proof, which can be used to calculate the typical compression ratios, temperatures and energies involved in the diesel cycle due to the compression of the air.

## **6.6 The Air-Standard Cycles**

### **6.6.1 The Diesel and Otto Cycles - A Brief Description**

The Compression Ignition (CI) and Spark Ignition (SI) engines follow the Diesel and Otto cycles respectively [6.6]. Although very similar the cycles have one main difference. In the diesel or CI engine the combustion process is achieved by raising the fuel-air mixture above the temperature at which the mixture will ignite. On the other hand SI engines need an external energy source, for example a spark plug, to

ignite the fuel. Both the air standard Diesel (Figure 6.24a) and Otto (Figure 6.24b) cycles can be seen below.

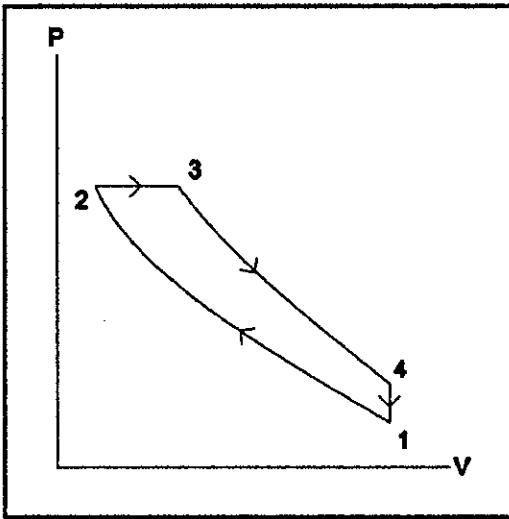


Figure 6.24a The Air-Standard Diesel Cycle

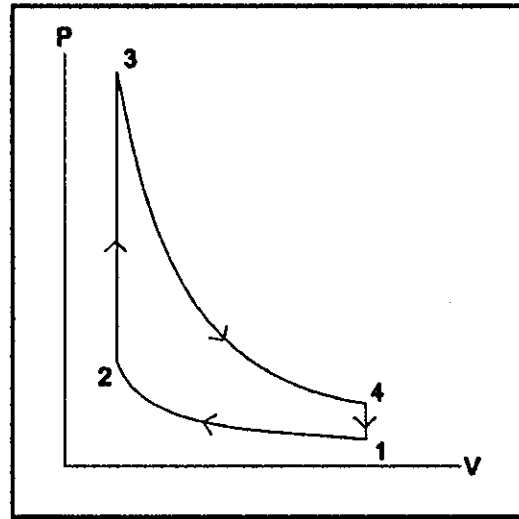


Figure 6.24b The Air-Standard Otto Cycle

The sparking events that occurred during the experimental work on the transducer can be explained by the diesel cycle as no external energy source was used to ignite the fuel. Therefore the following describes the diesel engine in more detail.

### 6.6.2 The Diesel Cycle

Normally diesel engines have an air fuel mixture between 14:1 and 24:1 and diesel fuel is used instead of gasoline. This combination means that the air temperature within the cylinder will surpass the ignition temperature at the end of the compression stroke. In a SI (Otto cycle) engine the fuel is premixed with the air and the point of combustion is determined by the sparking of the spark plug. If in the CI (Diesel cycle) engine the fuel was premixed with air, then there would be no control on the timing of the combustion process and combustion would begin throughout the mixture, as soon as the ignition temperature was reached. Therefore the diesel fuel is injected into the cylinder when combustion is required.

Although Figure 6.24a shows the air-standard diesel cycle an actual CI diesel engine cycle can be represented by Figure 6.25 [6.7]. This is actually a four stroke cycle of compression, expansion, exhaust and induction as described below.

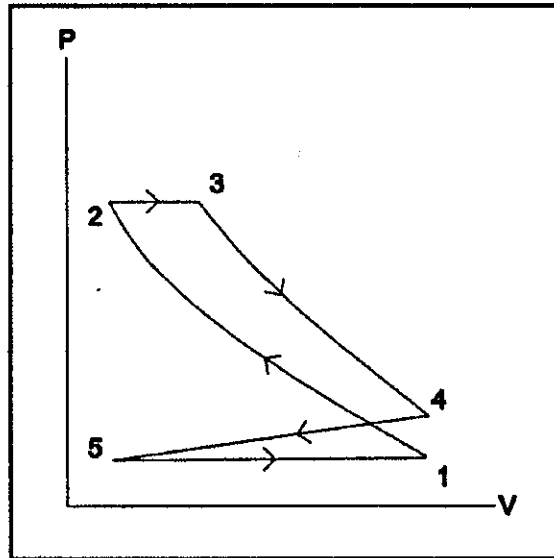


Figure 6.25 The Typical Diesel Engine Cycle

- 1-2 This is the compression stroke and the atmospheric pressure air in the diesel engine cylinder is compressed. The diesel fuel is injected just before point 2 and the temperature of the air is high enough for the fuel droplets to vapourise and ignite upon entering the cylinder.
- 2-3 This is the start of the expansion or working stroke. The pressure remains constant during combustion, because the fuel is sprayed into the cylinder at a constant rate.
- 3-4 The combustion process is now complete and the pressure falls almost back to atmospheric pressure, until an exhaust valve is opened and blow-down begins.
- 4-5 Any products that haven't escaped during blow-down are displaced by the cylinder piston during the exhaust stroke.
- 5-1 During the induction stroke just air is drawn into the cylinder so the engine is ready to begin the compression stroke.

## 6.7 Pressure, Temperature, Volume and Work Done due to Air Compression in a Dieseling Process

The experimental work carried out showed sparking of the oil. This is due to compression of air that produces the very high temperatures required to produce self ignition. The calculations show the kind of pressures, temperatures, volume compressions and work done that would be produced due to the compression of an air bubble typically found in the dieseling that occurred in the experimental work. Initially the equation for an adiabatic (no heat is transferred to or from the system) process for an ideal gas needs to be proved [6.8]:

$$pV^\gamma = K \quad \text{where } p = \text{pressure, } V = \text{volume, } K = \text{constant and } \gamma = \mathfrak{C}_p/\mathfrak{C}_v$$

$\mathfrak{C}_p$  = molar heat capacity at constant pressure  
 $\mathfrak{C}_v$  = molar heat capacity at constant volume

This would mean that  $p_i V_i^\gamma = p_f V_f^\gamma$  where  $p_i$  = initial pressure,  $p_f$  = final pressure  
 $V_i$  = initial volume,  $V_f$  = final volume

Applying the First Law of Thermodynamics to the adiabatic process gives:

$$dQ = 0 = dU + p dV \quad (1) \quad \begin{array}{l} dQ = \text{Change in heat} \\ dU = \text{Change in internal energy} \end{array}$$

If at constant volume a system has heat added to it, no work ( $dW$ ) is done so  $dW = p dV = 0$ . Therefore according to (1)  $dQ = dU$ , which means the heat solely increases the internal energy. Also the heat added at constant volume is related to the molar heat capacity at constant volume by the following equation:

$$dQ = n \mathfrak{C}_v dT \quad \begin{array}{l} n = \text{Number of moles in system} \\ dT = \text{Change in temperature} \end{array}$$

From  $dU = dQ$  we have  $dU = n \mathfrak{C}_v dT$  so substituting this into (1) gives:

$$0 = n \mathfrak{C}_v dT + p dV$$

$$dT = - p dV / n \mathfrak{C}_v \quad (2) \quad \text{For an adiabatic process}$$

Another representation of dT can be gained by taking the differential of the ideal gas equation of state  $pV = nRT$  (R is the universal gas constant) which is:

$$p dV + V dp = nR dT$$

$$dT = (p dV + V dp) / nR \quad (3) \quad \text{For an ideal gas}$$

Cancelling dT and n in (2) and (3) leads to:

$$p dV + V dp = -pR dV / \vartheta_v$$

For an ideal gas,  $\vartheta_p - \vartheta_v = R = \text{Universal gas constant}$ . Substituting this gives:

$$p dV + V dp = -p dV (\vartheta_p - \vartheta_v) / \vartheta_v = -p dV (\gamma - 1) \quad \text{Where } \gamma = \vartheta_p / \vartheta_v$$

$$p dV + V dp = p dV - \gamma p dV$$

$$V dp = -\gamma p dV$$

$$dp / p = -\gamma dV / V$$

By integrating indefinitely and using constant = the constant of integration this gives:

$$\int dp / p = -\int \gamma dV / V + \text{constant}$$

$$\ln p + \gamma \ln V = \text{constant} \quad \text{Assuming } \gamma \text{ doesn't change over the range of integration}$$

$$\ln pV^\gamma = \text{constant}$$

$$pV^\gamma = K$$

Having proved this relationship for an ideal gas under adiabatic conditions it is now possible to calculate how much the air is compressed by, when the system pressure increases from atmospheric pressure (1 bar = 101 KPa) to 200 bar = 20.2 MPa. If the air bubble within the oil is  $1\text{cm}^3 = 1 \times 10^{-6} \text{m}^3$  we have the following:

$$p_i V_i^\gamma = p_f V_f^\gamma \quad p_i = 1.01 \times 10^5 \text{ Pa}, p_f = 2.02 \times 10^7 \text{ Pa} \\ V_i = 1 \times 10^{-6} \text{ m}^3, \gamma = 1.4 \text{ for air.}$$

$$(1.01 \times 10^5) (1 \times 10^{-6})^{1.4} = (2.02 \times 10^7) (V_f)^{1.4}$$

$$(V_f)^{1.4} = 1.991 \times 10^{-11}$$

$$V_f = 2.272 \times 10^{-8} \text{ m}^3 \text{ or } 0.0272 \text{ cm}^3$$

$$V_i / V_f = 1 / 0.0272 = 44$$

Therefore when the air bubble pressure increases 200 fold the volume decreases by a factor of 44. From the ideal gas equation of state it is possible to calculate the increase in air temperature of the bubble due to the 200 times increase in pressure. The ideal gas equation of state is given by:

$$pV = nRT \quad \text{Where } n \text{ and } R \text{ are constant so:}$$

$$p_i V_i / T_i = p_f V_f / T_f$$

$$T_f = T_i p_f V_f / p_i V_i$$

$$T_f = 293 (2.02 \times 10^7) (2.272 \times 10^{-8}) / (1.01 \times 10^5) (1 \times 10^{-6})$$

$$T_f = 1331 \text{ K}$$

The temperature increases from 293 K (20 degrees C) to 1331 K (1058 degrees C) which shows for a 200 times increase in pressure the temperatures increases approximately by 4.5 times. The temperature of 1331 K is extremely high and would explain the self ignition of the diesel oil.

Finally it is possible to calculate the work done during an adiabatic compression of air using the following equation:

$$dW = p dV$$

$$W = \int p dV = \int_{V_i}^{V_f} (p_i V_i^\gamma / V^\gamma) dV$$

$$= p_i V_i^\gamma \int_{V_i}^{V_f} dV / V^\gamma$$

$$= (p_i V_i^\gamma / 1 - \gamma) ((1 / V_f^{\gamma-1}) - (1 / V_i^{\gamma-1}))$$

$$\begin{aligned}
&= (p_i V_i^\gamma / 1 - \gamma) ((V_i^{\gamma+1} / V_f^{\gamma+1}) - (V_f^{\gamma+1} / V_i^{\gamma+1})) \\
&= (p_i V_i^\gamma / 1 - \gamma) (1 - (V_i / V_f)^{\gamma+1})
\end{aligned}$$

Inserting the values  $p_i = 1.01 \times 10^5$ ,  $V_i = 1 \times 10^{-6}$ ,  $V_f = 2.272 \times 10^{-8}$ ,  $\gamma = 1.4$  gives:

$$W = ((1.01 \times 10^5) (1 \times 10^{-6}) / 0.4) (1 - (1 \times 10^{-6} / 2.272 \times 10^{-8})^{0.4})$$

$$W = -0.895 \text{ J}$$

This value is quite low as it is the work done by the almost incompressible oil on the  $1 \text{ cm}^3$  air bubble whereas the work done by the hydraulic system on the oil would be much greater, due to the greater volume and lower compressibility of the oil.

## 6.8 Discussion of Results and Conclusion

If as previously suggested oil jets, from bubble collapse, were able to cause damage, then the larger quantities of air would inevitably produce oil jets of greater severity. This could result in larger, faster rising, pin point pressures and thus more damage would occur. The problem is that the transducer wouldn't detect pin point pressures, because as previously mentioned in Chapter 4, the transducer measures the average pressure across the diaphragm.

From the testing of the transducers we can see that the combination of smaller cross sectional areas of fittings and increased valve frequencies lead to air coming out of solution. Compression of these air pockets induces sparking, WH noise, heat and vibration and most noticeably swift pressure rises that are the cause of transducer damage after numerous cycles. Moreover the intentional act of putting air in the system gives rise to more extensive sparking, heat, noise and vibration along with extremely swift pressure rises. The latter being the cause of greater and almost instant transducer damage.

The experiments have shown that damage appears to be associated with air in the system. Damage is most severe when large quantities of air are introduced artificially. Even though steps were taken to purge the air, it is forced out of solution by the compression and rarefaction cycles of the pump. Sparking was seen and could be due to fast compression and heating of the air or due to self ignition of the oil vapour/air mixture, essentially the process which occurs in the diesel cycle. Finally the calculations showed that the type of pressures involved in the hydraulic system cause a large compression ratio and extremely high temperatures in the air, the latter causing self ignition of the air / oil mixture.

# CHAPTER 7

## Study II of Hydraulic System Fluid Pulses

### 7.1 Introduction

As long as the power pack supply pressure and the MOOG servovalve frequency remain constant the same trace is produced with every cycle of the valve. The effect of each pressure pulse was the same and so the experiment is known to be reproducible. The idea, therefore, was to obtain an image of the transducer face, using a delayed laser flash as the light source, during consecutive pulses, each photograph at a slightly different stage of the pressure pulse, (Figure 7.1) to see if the occurrence of diaphragm indentations could be recorded.

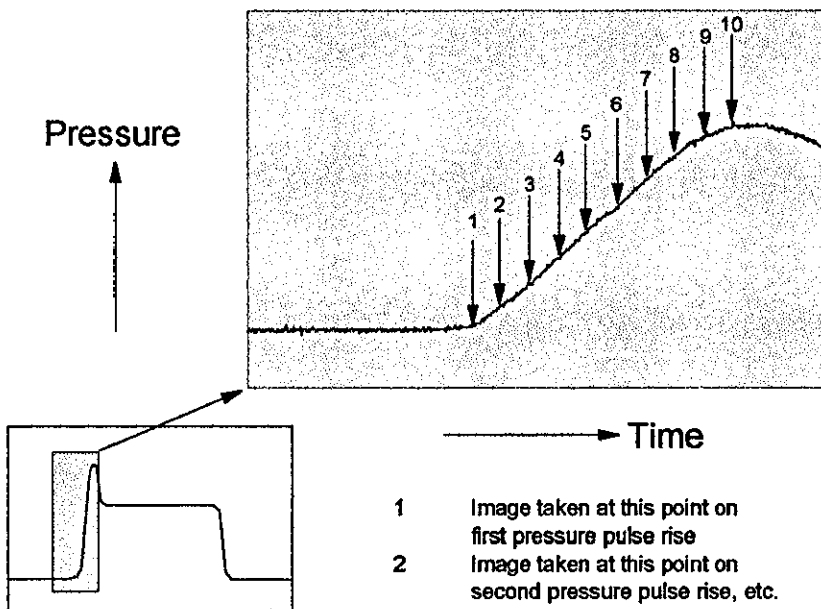


Figure 7.1 Example Trace to Explain the Recording of a Reproducible Pressure Pulse.

The video recorder that was used for the experimental work described in Chapter 6 records 25 frames a second, which equates to 40ms a frame. The rise times involved with the pressure transducer were of the order of  $100\mu\text{s}$  to 1ms so another method of recording was required. This problem was to be solved with the use of the CCD camera and a suitable light source. The source would be used to illuminate the transducer diaphragm for as short a duration as possible, i.e. less than  $1\mu\text{s}$ . It was decided that a Q switch Ruby laser would be suitable with a flash duration of the order of 50ns (nano seconds). However the laser would have to be triggered.

## 7.2 Testing of Laser Triggering

### 7.2.1 TTL Monostable

The Ruby laser could be triggered by a 5V TTL signal via an existing delay unit. The function generator used to drive the MOOG Servovalve had a suitable TTL output that was in phase with the output to the valve. However the TTL output was converted by a TTL monostable circuit and the reasons for this are explained below. The circuit is shown in Figure 7.2 and the conversion of the TTL signal is conveyed in Figure 7.3.

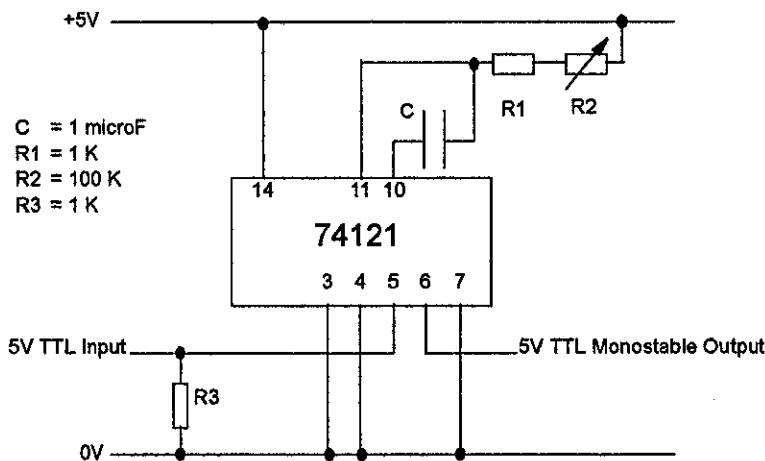


Figure 7.2 TTL Monostable Circuit

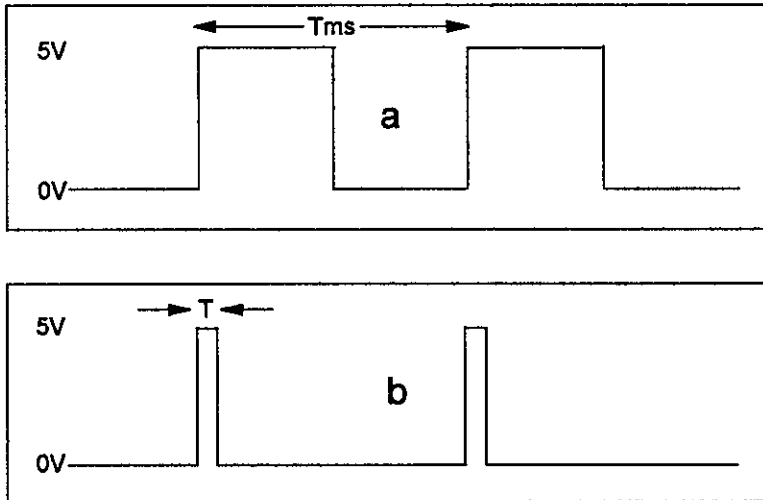


Figure 7.3 Conversion of (a) TTL Output to (b) TTL Monostable Output

The TTL output signal time period is defined as  $T_{ms}$  and this is also the time period of one cycle of the MOOG Servovalve. Ideally the  $T$  time length in Figure 7.3b should be as small as possible. This is because if the laser delay unit was switched on whilst the function generator TTL output was at 5V, the laser would instantly trigger. Also the laser is only ready to trigger every 1.8 seconds so for the lowest function generator frequency of 0.25Hz the laser could trigger prematurely. By altering the variable resistor  $R_2$  in Figure 7.2, it was possible to produce a  $T$  value of just  $600\mu s$ , which is a fraction of the 1.8 seconds taken for the laser to power up time. Hence, the chance of switching on the laser control unit whilst the TTL output was at 5V was extremely remote.

### 7.2.2. Equipment Assembly

Figure 7.4 shows a diagram of the equipment assembly used and Figure 7.5 is a picture of this setup, although the delay unit, laser, spatial filter, lens and mirrors are out of view. Also not shown is a photodiode to detect the laser flash.

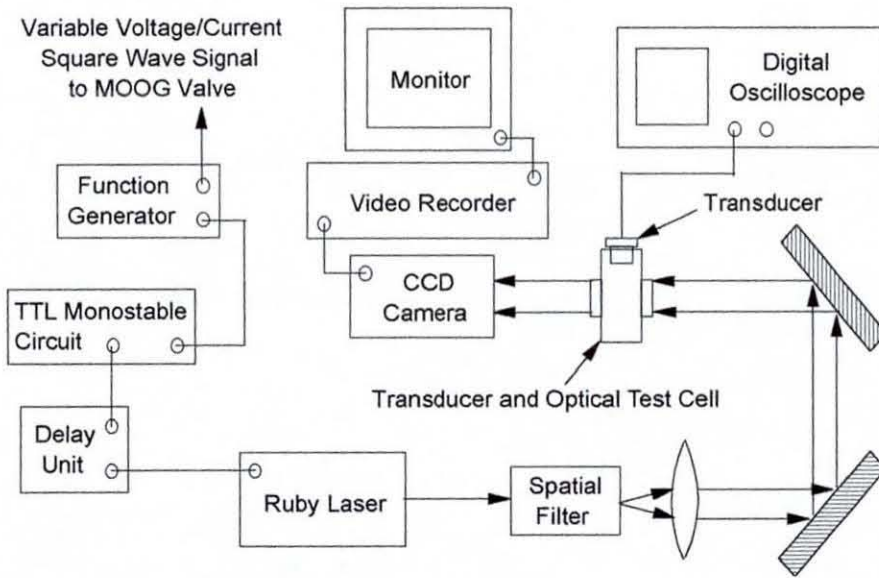


Figure 7.4 Diagram of the experimental set up.

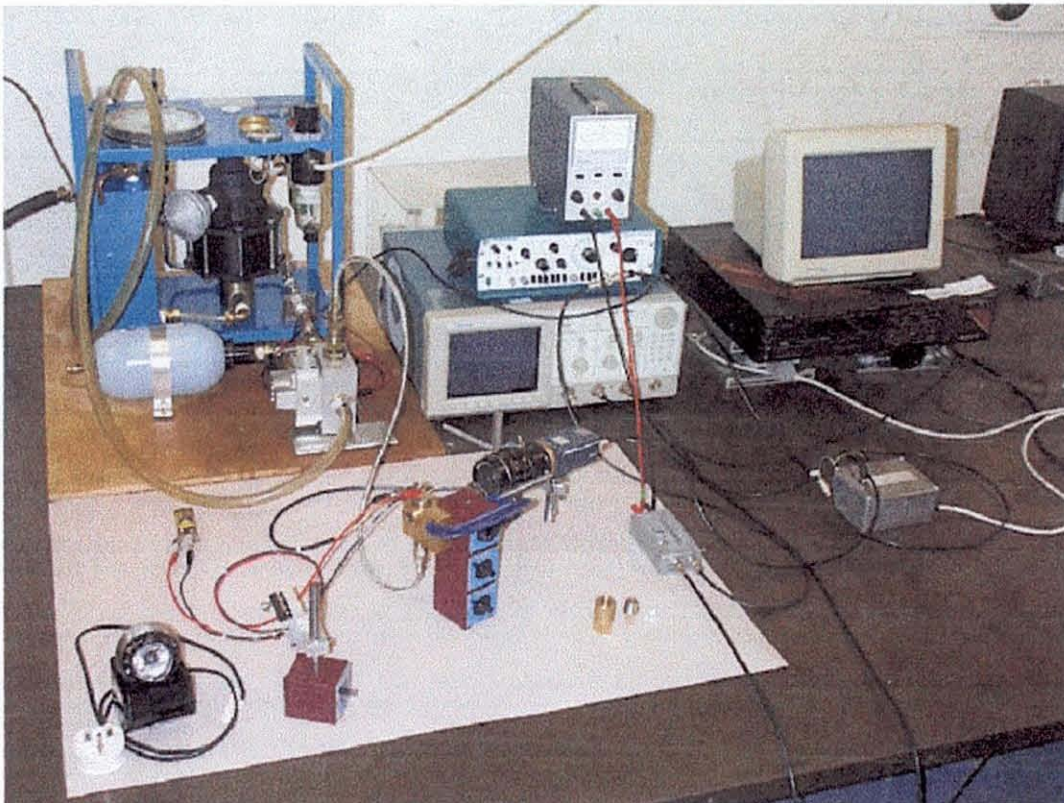


Figure 7.5 Photograph of experimental setup

This photodiode was connected to the digital scope so that the laser flash, the 5V TTL monostable signal and the pressure pulses, as detected by the transducer, could be viewed simultaneously. The power pack was set to approximately 2000 PSI and the function generator set to 0.25 Hz. By alteration of the scope time base the laser flash, the 5V TTL monostable rise and the pressure rise from the transducer could be seen on the screen. The nominal delay between the 5V TTL monostable signal rise and the laser flash was 1.2ms. So setting the delay unit to 1ms would produce an actual delay of 2.2ms. The delay unit value was altered until the laser flash, as detected by the diode and the start of the pressure pulse were both visible on the scope with a time base setting of just 1ms.

### **7.3 Sequence of Images of the Transducer Diaphragm**

Initially there was no air in the system so that the pressure pulse produced would have a smooth rise of over 5ms. The delay unit was controlled by analogue dials and wasn't very accurate so the trigger point shifted randomly over a range of approximately 100 $\mu$ s. Therefore incorrect delays were produced. However the dial was carefully adjusted until the laser flash and the initial pressure rise were at the same instant. Gradual turning of the dial after consecutive pressure pulses produced longer delayed laser flashes so that a sequence of 8 pictures was produced. Therefore the images were of 8 consecutive pulses each at a slightly later stage than the previous pulse. Figure 7.6 contains these images at times of 0, 200, 1000, 1500, 2900, 4000, 4200 and 4800  $\mu$ s after the start of the pressure pulse rise. As with some of the images in Chapter 6 the pictures were rather dark so manipulation of the "curves" facility lead to the images in Figure 7.7. Slight deformation of the transducer could be seen and thus no damage occurred under the influence of the steady pressure rise.

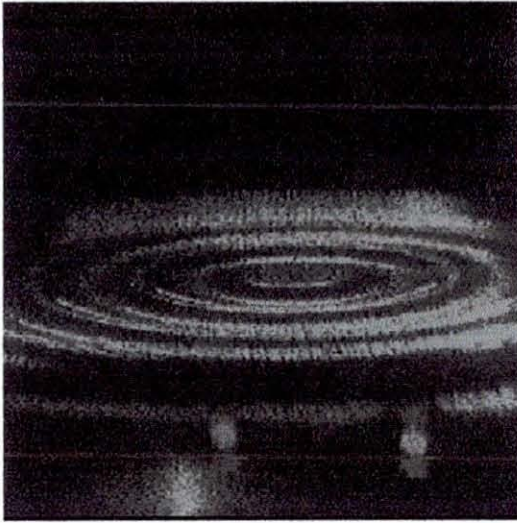


Figure 7.6a Photograph of the transducer at the start of the pressure pulse ( $0 \mu s$ ).

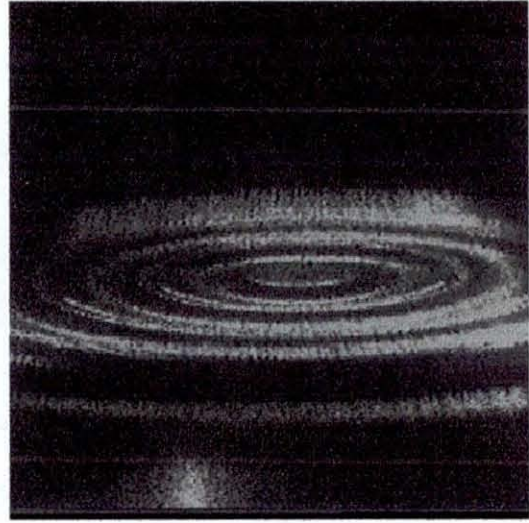


Figure 7.6b Photograph of the transducer at  $200 \mu s$  after the start of the pressure pulse.

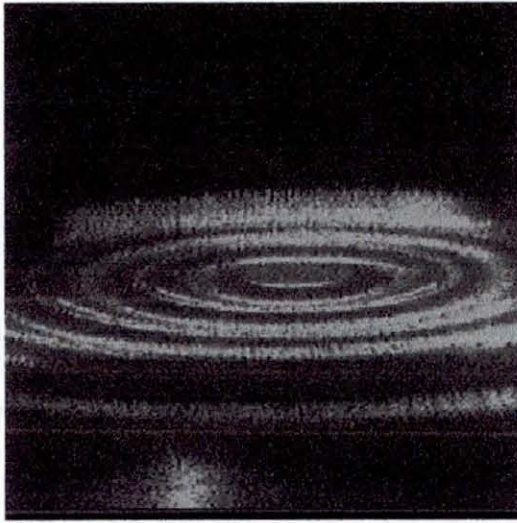


Figure 7.6c Photograph of the transducer at  $1000 \mu s$  after the start of the pressure pulse.

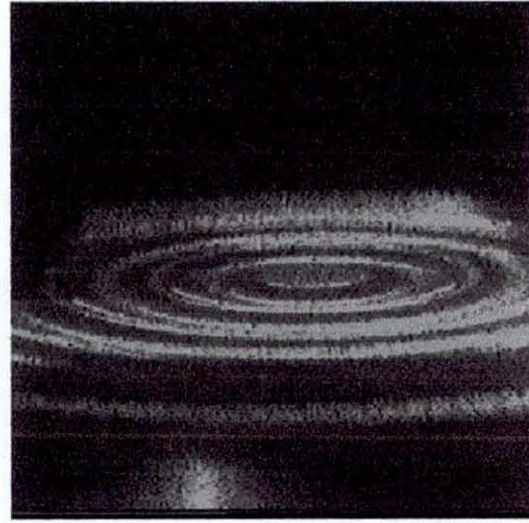


Figure 7.6d Photograph of the transducer at  $1500 \mu s$  after the start of the pressure pulse.

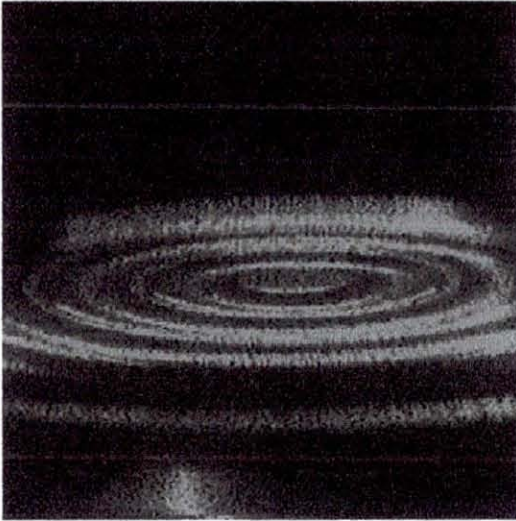


Figure 7.6e Photograph of the transducer at 2900  $\mu\text{s}$  after the start of the pressure pulse.

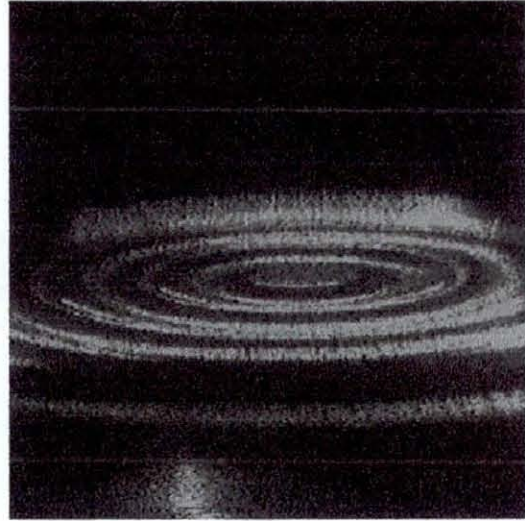


Figure 7.6f Photograph of the transducer at 4000  $\mu\text{s}$  after the start of the pressure pulse.

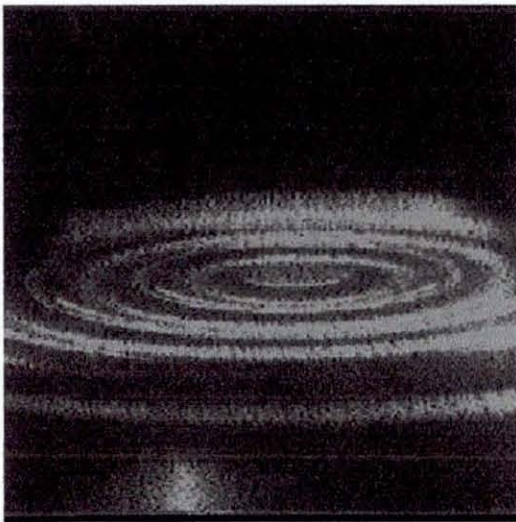


Figure 7.6g Photograph of the transducer at 4200  $\mu\text{s}$  after the start of the pressure pulse.

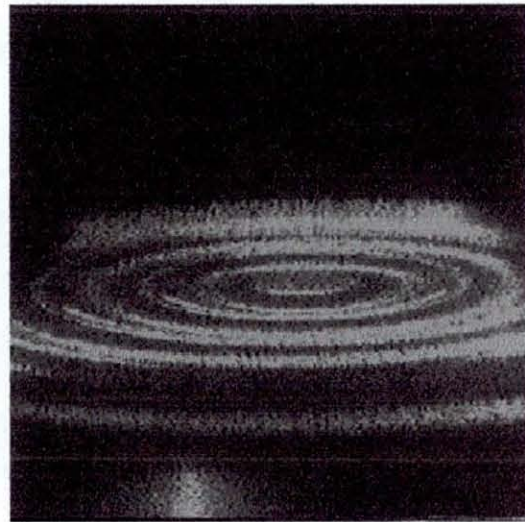


Figure 7.6h Photograph of the transducer at 5000  $\mu\text{s}$  after the start of the pressure pulse.

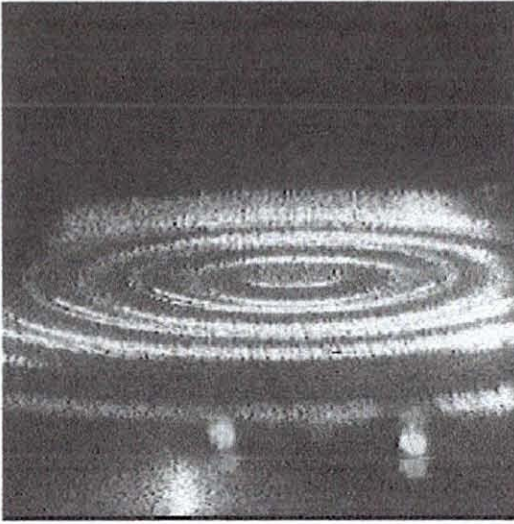


Figure 7.7a Image of the transducer at the start of the pressure pulse ( $0 \mu\text{s}$ ).

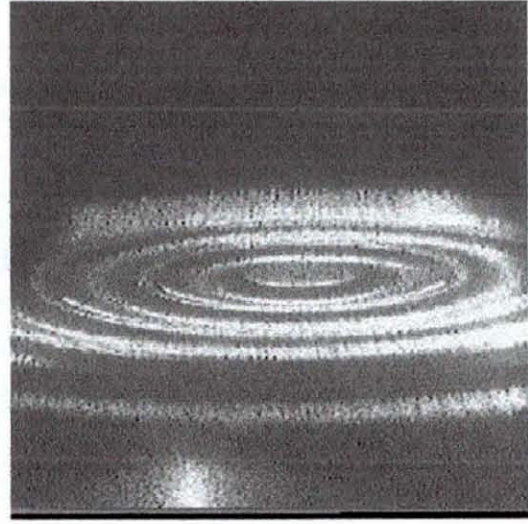


Figure 7.7b Image of the transducer at  $200 \mu\text{s}$  after the start of the pressure pulse.

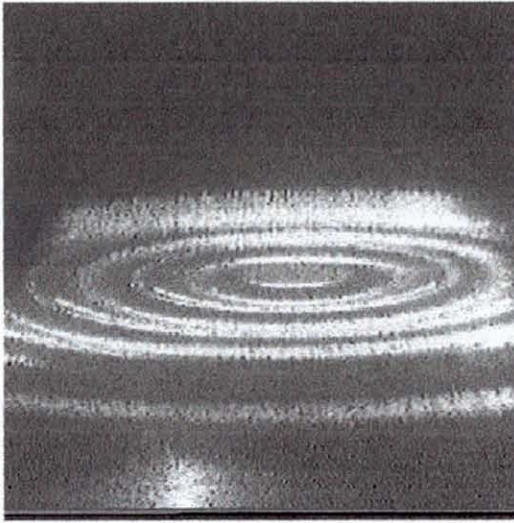


Figure 7.7c Image of the transducer at  $1000 \mu\text{s}$  after the start of the pressure pulse.

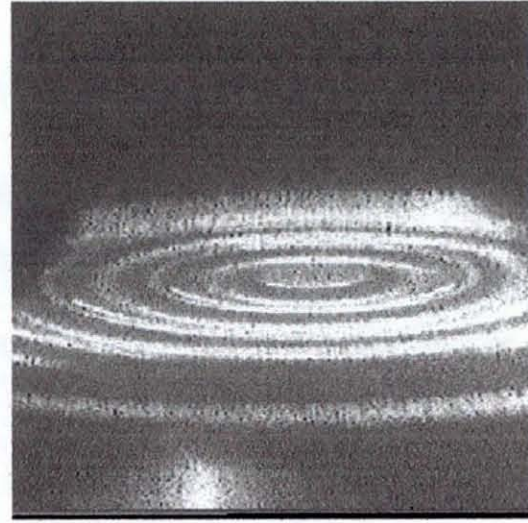


Figure 7.7d Image of the transducer at  $1500 \mu\text{s}$  after the start of the pressure pulse.

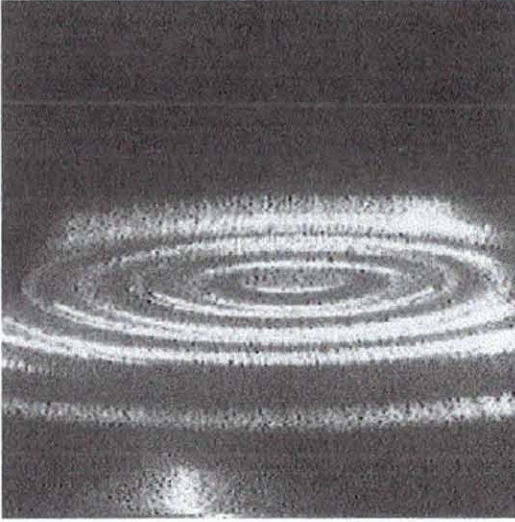


Figure 7.7e Image of the transducer at 2900  $\mu\text{s}$  after the start of the pressure pulse.

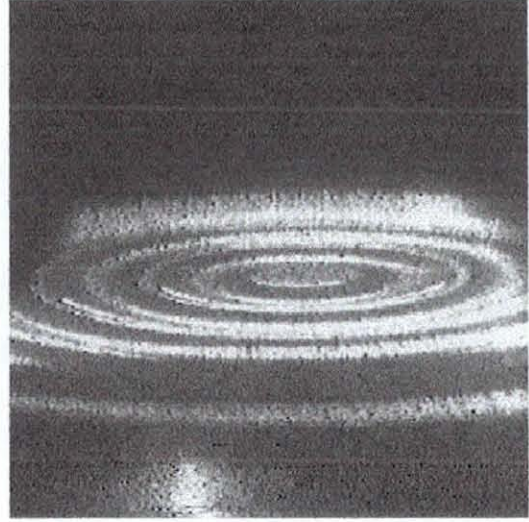


Figure 7.7f Image of the transducer at 4000  $\mu\text{s}$  after the start of the pressure pulse.

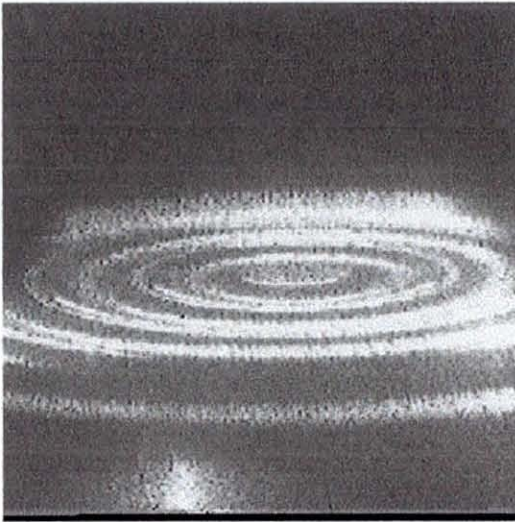


Figure 7.7g Image of the transducer at 4200  $\mu\text{s}$  after the start of the pressure pulse.

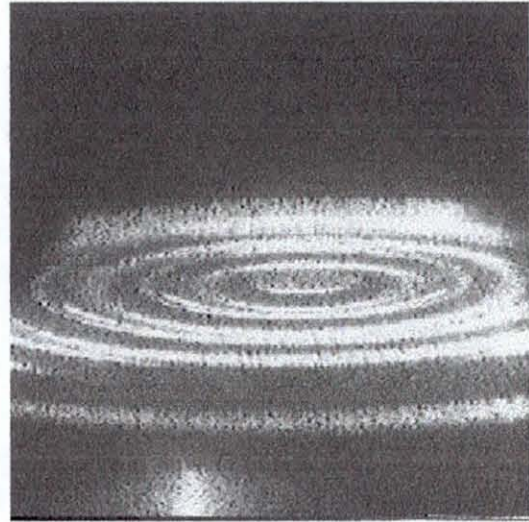


Figure 7.7h Image of the transducer at 5000  $\mu\text{s}$  after the start of the pressure pulse.

If air was to be put in the system the transducer face wouldn't be visible during the whole of the pressure rise. Perhaps the air would compress enough so that most of the pressure rise could be visualized. Figure 7.8 contains original photographs and manipulated images. However, these suggest that even with a little air in the system a clear transducer face image is only really possible when the pressure is near it's maximum. Indeed further observations showed that with more air in the system these compressed air bubbles slightly obstructed the field of view even at the maximum pressure. This indicates that they were not completely compressed or driven into solution. Figures 7.8d, 7.8e and 7.8f are images of the transducer at the beginning, middle and end of the pressure rises respectively. Even a small trace of a bubble is visible at the end of the pressure rise in Figure 7.8f. Unfortunately due to the air's visual obstruction it wasn't possible to get a clear sequence of images during a damaging pressure pulse and air was even present at the maximum pressure.

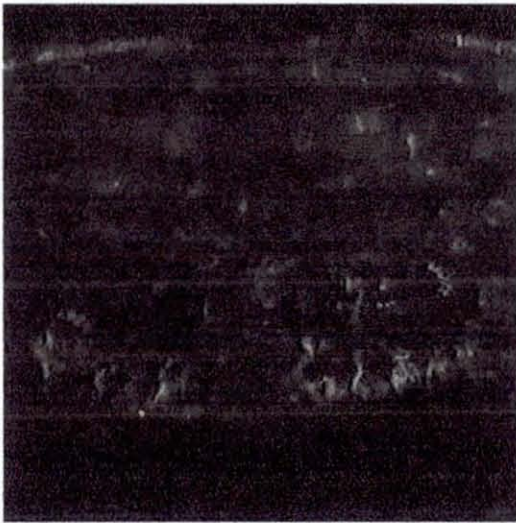


Figure 7.8a Photograph of the transducer at the start of the pressure pulse, with air artificially introduced into the system.

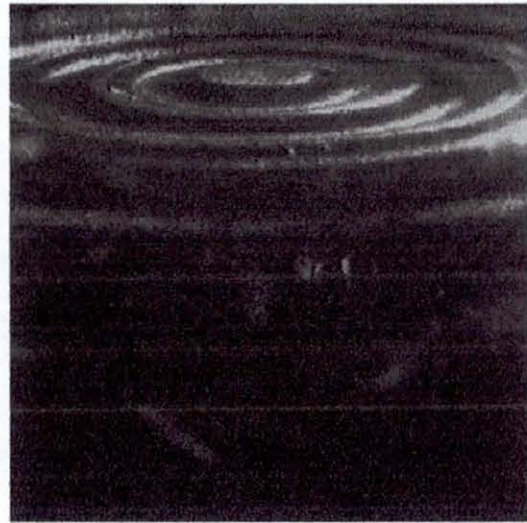


Figure 7.8b Photograph of the transducer at the middle of the pressure pulse, with air artificially introduced into the system.

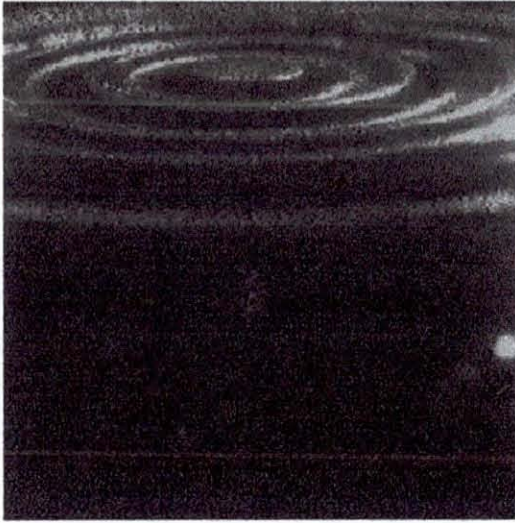


Figure 7.8c Photograph of the transducer at the end of the pressure pulse, with air artificially introduced into the system.

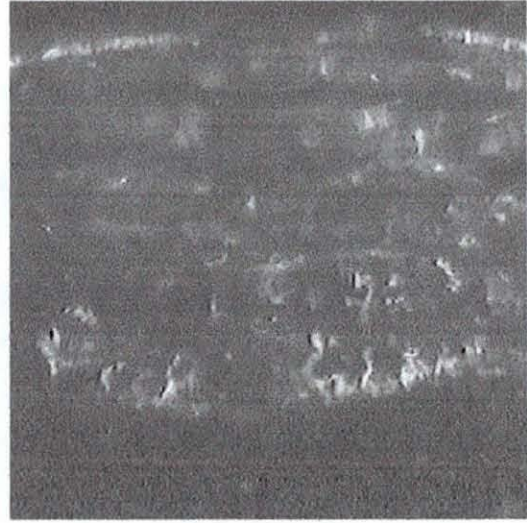


Figure 7.8d Image of the transducer at the start of the pressure pulse, with air artificially introduced into the system.



Figure 7.8e Photograph of the transducer at the middle of the pressure pulse, with air artificially introduced into the system.

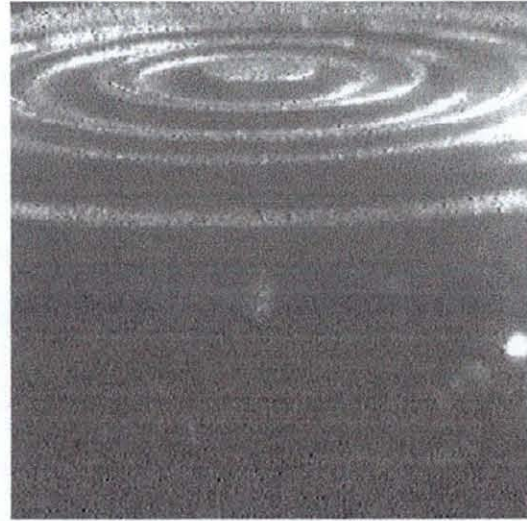


Figure 7.8f Photograph of the transducer at the end of the pressure pulse, with air artificially introduced into the system.

# CHAPTER 8

## Conclusions and Possible Future Work

### 8.1 Conclusions

The work in Chapters 6 and 7 has shown that with the use of an optical test cell, which housed the transducer, it was possible to observe the movement of small suspended particles in the hydraulic fluid immediately next to the transducer diaphragm at low frequency operation of the pressure switching MOOG Valve.

Before studying the transducer diaphragm under the 200 bar pressure fluctuations it was necessary to become accustomed to the equipment. Initially, without the use of the hydraulic power pack, accumulator and Moog valve the transducer was tested and calibrated to ensure accurate recording of pressures. Prior to the delivery of the main equipment, an experiment was carried out and monitored to test the transducers. The experiment consisted of a weight impacting onto a water surface which created small scale pressure pulses which were similar in type to the ones produced later, using the power pack. Therefore it was essential to become familiar with the oscilloscope, function generator and other laboratory electrical equipment. Various pressure pulse traces with pressures changes of 20 bar over a period of just 200 $\mu$ s were recorded.

Once the hydraulic equipment was available it was connected using the high pressure rated fittings and pipes. The air was then purged from the system by running the power pack at a low pressure and slightly releasing the transducer fitting until no more air was seen to escape. This was only possible with the transducer at the highest point in the system. With the power pack running observation using the CCD camera showed that the oil contained random impurity particles. However these were difficult

to detect and consistently sized particles were required to trace the movement of the oil during the pressure pulses.

Once selected as the seeding, the polystyrene spheres were injected into the oil and again air was purged from the system. With slow operation of the MOOG valve, for example 1 Hz, uniform movement of the particles would be expected as shown in Figure 8.1a below. Please note that the transducer is represented by the grey section to the right hand side of the window. Also note that A1 and A2 are the positions of particle A before and after the pressure pulse respectively. Finally the distances from A1 and B1 to the transducer face, are 3 times and twice the distance from C1 to the transducer face respectively.

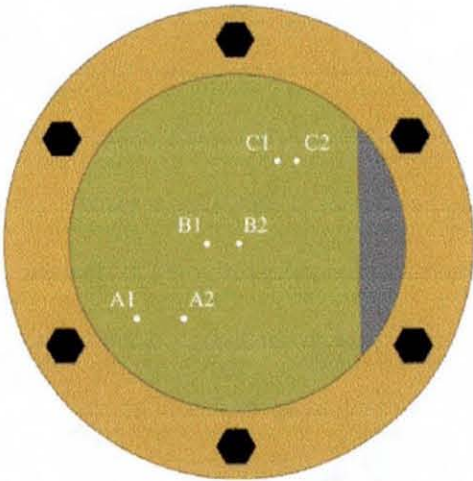


Figure 8.1a Side view drawing of the test cell to show expected position of the particles before and after a pressure pulse.

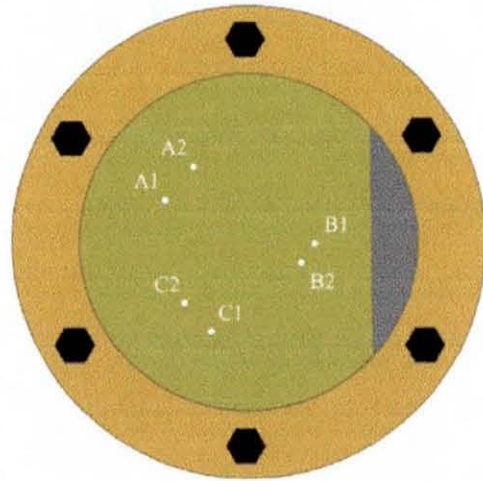


Figure 8.1b Side view drawing of the test cell to show the actual position of the particles before and after a pressure pulse.

Still looking at Figure 8.1a, if the particle A moves a distance 6mm from A1 to A2, particle B moves 4mm from B1 to B2 and particle C moves 2mm from C1 to C2. However Figure 8.1b, which is based on the particle movement in Figure 6.16, conveys the fact that in reality swirling of the oil takes place with random magnitudes of particle movement. The problem was that transducer damage wouldn't occur under these conditions. Increase of the MOOG valve frequency to 16 Hz sharpened the

pressure pulse trace and decreased the rise time. It was only then that air contained within the oil was seen to come out of solution. However transducer damage still didn't arise so more air was put into the system.

The test cell, that housed the transducer, was held at the highest point in the system and oil was extracted from the cell, thus producing a larger air pocket which filled the field of view in the test cell window. It wasn't until this stage that transducer damage occurred. However, under these conditions it wasn't possible to track the particle movements or obtain a clear image of the transducer face. Figure 8.2 shows the type of bubble compression that occurred due to a pressure pulse.

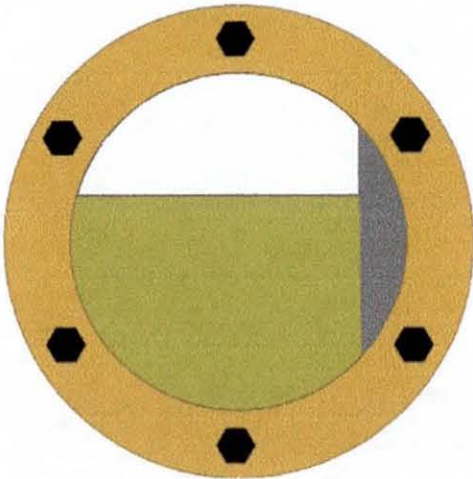


Figure 8.2a Side view drawing of the test cell to show the air bubble before the pressure pulse.

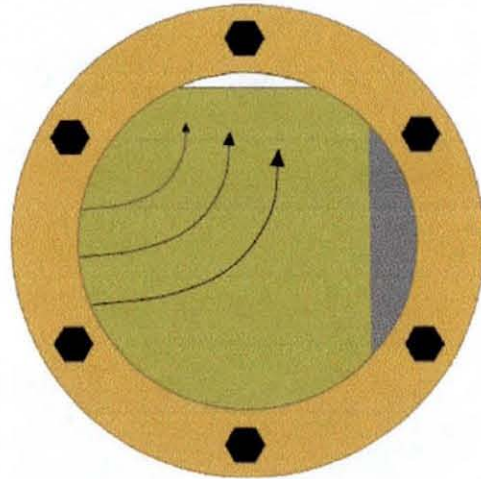


Figure 8.2b Side view drawing of the test cell to show the air bubble after the pressure pulse.

The large air bubble in Figure 8.2a was compressed from atmospheric pressure to a much smaller high pressure air pocket shown in Figure 8.2b. From the calculations in Chapter 6 for an increase in pressure of 200 fold the volume of the air bubble or pocket would decrease in volume by 44 times. The experimental work showed that high pressure fluctuations make the air go in and out of solution quite easily. Even though the oil used was degassed using a vacuum chamber, there was still a sufficient amount of air that came out of solution at higher frequency, high pressure changes.

The compression of the air bubble produced very high temperatures and also sparking within the oil that was visible to the naked eye. The fact that damage, via the swift rising pressure transients, only occurred when air was present suggests that air in the system was the reason for the transducers failing. As mentioned in Chapter 6 it could be that when pressure was applied, the air bubbles collapsed and resultant jets of oil impinged on and damaged the surface of the transducer. The transducer was damaged both electrically, via breakage of the wire bonds and mechanically, through pitting and large indentation of the surface associated with the shorter duration pressure rises. Although it wasn't possible to get a sequence of images of these pressure transient rises, the events were recorded by the 25 frames per second CCD camera and video assembly.

It was thought that by using a triggered laser as the light source it would be possible to obtain images of more substantial transducer face deformation. However clear images were only possible with no air bubbles in the system and as previously mentioned no transducer damage took place under these conditions. Images of the transducer face were obtained during the quicker rises associated with having air in the system. Unfortunately as seen in Chapter 7 these pictures show that the face was visible towards the middle and end of the pulse and even then the air slightly obstructs the field of view.

## **8.2 Possible Future Work**

Further work could be carried out to determine for definite if the air in the system causes damage and if so, why? There could be work to discover if oil jets are formed and whether they cause the faster rise times to be produced. The levels of damage could be monitored to see why sometimes just small pitting of the surface occurs and other times large indentations were formed.

Another aspect could be to monitor the pressure for longer or shorter lengths of hydraulic hose to see if the pipe length affects the results in anyway. Instead of the flexible hydraulic hose a solid steel pipe could be used to connect the MOOG servovalve to the transducer fitting. The effects of the hydraulic hose expansion and contraction, could be compared to the steel pipe effects to see if the hydraulic hose excites the air out of solution.

The main problem with the laser was that light illumination can only take place every 2 seconds or so, due to the low repetition rate of the laser. A suitable light source of shorter pulse separation (of the order of 10-20 $\mu$ s) could be utilized to obtain a sequence of images over a duration of just 100 $\mu$ s, then the damaging rise times could be optically monitored.

Finally a laser beam could be directed on to the transducer face at a fixed angle and the shift of the reflected beam captured and monitored as a function of time. The shift (deflection of diaphragm) for steady pressure rises could be compared to other shifts resulting from faster damaging pressure rises, to give an idea of how the transducer moves prior to being damaged.

# REFERENCES

## CHAPTER 1

[1.1] Tabor, D., "Gases, liquids and solids", Second edition, Cambridge University Press, Cambridge, 1979.

[1.2] Munson, B.R., Young, D.F. and Okiishi, T.H., "Fundamental of Fluid Mechanics", John Wiley & Sons, Inc., New York, 1990.

[1.3] Massey, B.S., "Mechanics of Fluids", Sixth edition, Chapman & Hall, London, 1989.

[1.4] Williams, J. and Elder, S.A., "Fluid Physics for Oceanographers & Physicists", Pergamon Press plc, Oxford, 1989.

[1.5] Fox, R.W. and McDonald, A.T., "Introduction to Fluid Mechanics", Fourth edition, John Wiley & Sons, Inc., New York, 1994.

[1.6] Shames, I.H., "Mechanics of Fluids", Third Edition, McGraw-Hill, Inc., New York, 1992.

[1.7] (Edited by) Tennent, R.M., "Science Data Book", Twentieth impression, Oliver & Boyd, Harlow, 1995.

[1.8] Boyle, H.B., "Transducer Handbook", Newnes of Butterworth-Heinemann Ltd, Oxford, 1992.

## CHAPTER 2

- [2.1] Lomas, C.G., "Fundamentals of Hot Wire Anemometry", Cambridge University Press, Cambridge, 1986.
- [2.2] Perry, A.E., "Hot-wire Anemometry", Oxford University Press, Oxford, 1992.
- [2.3] Takami, T., "Three-component velocity measurements in turbulent flow using a technique of rotating probe with and inclined hot-wire", JSME International Journal Series B-Fluids and Thermal Engineering, Vol. 41, pp. 145-150, 1998.
- [2.4] Rosemann, H., Staeger, R. and Kreplin, H-P., "Development and application of a quadruple hot-wire technique for turbulent flows", Measurement Science and Technology, Vol. 7, pp. 1477-1491, 1996.
- [2.5] Vukoslavcevic, P. and Wallace, J.M., "A 12 sensor hot-wire probe to measure velocity", Measurement Science and Technology, Vol.7, pp. 1451-1461, 1996.
- [2.6] Khoo, B.C., Chew, Y.T. and Li, G.L., "Time resolved near-wall hot-wire measurement", Measurement Science and Technology, Vol.7, pp. 564-575, 1996.
- [2.7] Internet Page - [tnh.phys.tue.nl/pages/hw1/roger/verslag/node5.html](http://tnh.phys.tue.nl/pages/hw1/roger/verslag/node5.html)
- [2.8] Zhoo, M., "Particle image velocimetry applied to non-reacting and reacting flows within cylindrical combustion chambers", PhD Thesis, Loughborough University, May 1996.
- [2.9] Durst, F., Melling, A. and Whitelaw, J.H., "Principles and Practice of Laser-Doppler Anemometry", Second edition, Academic Press Inc., London, 1981.

[2.10] Drain, L.E., "The Laser Doppler Technique", John Wiley & Sons Ltd., Chichester, 1980.

[2.11] Goldstein, R.J. and Hagen, W.F., "Turbulent flow measurements utilizing the Doppler shift of scattered laser radiation", Phys. Fluids, Vol. 10, pp. 1349, 1967.

[2.12] Lewis, R.D., Foreman, J.W., Watson, H.J. and Thornton, J.R., "Laser Doppler velocimeter for measuring flow-velocity fluctuations", Phys. Fluids, Vol. 11, pp. 433, 1968.

[2.13] Durst, F. and Whitelaw, J.H., "Integrated optical units for laser anemometry", J. Phys. E: Sci. Instrum., Vol. 4, pp. 804, 1971.

[2.14] Durst, F. and Whitelaw, J.H., "Measurements of mean velocity, fluctuating velocity and shear stress using a single channel anemometer", DISA Inf., Vol. 12, pp. 11, 1971.

[2.15] Kim, C.H., Randall, R.E., Members, ASCE, Boo, S.Y. and Krafft, M.J., "Kinematics of 2-D transient water waves using laser doppler anemometry", Journal of Waterway, Port, Coastal, and Ocean Engineering, Vol. 118, pp. 147-164, 1992.

[2.16] Jentink, H.W., Stieglmeier, M. and Tropea, C., "In-flight velocity measurements using laser doppler anemometry", Journal of Aircraft, Vol. 31, pp. 444-446, 1992.

[2.17] Durst, F., Jovanovic, J. and Sender, J., "LDA measurements in the near wall region of a turbulent pipe-flow", Journal of Fluid Mechanics, Vol. 295, pp.305-335, 1995.

[2.18] Kassab, S.Z., Bakry, A.E. and Warda, H.A., "Laser doppler anemometry measurements in an axisymmetric turbulent jet", *Rev. Sci. Instrum.*, Vol. 67, pp. 1842-1849, 1995.

[2.19] Lawson, N.J., "The application of particle image velocimetry to high speed flows", PhD Thesis, Loughborough University, 1995.

[2.20] Internet Page - [www.lerc.nasa.gov/WWW/OptInstr/piv.html](http://www.lerc.nasa.gov/WWW/OptInstr/piv.html)

[2.21] Internet Page - [esapub.esrin.esa.it/pff/pffv5n3/beckv5n3.htm](http://esapub.esrin.esa.it/pff/pffv5n3/beckv5n3.htm)

[2.22] Kurada, S., Rankin, G.W. and Srihar, K., "A new particle image velocimetry technique for three-dimensional flows", *Optics and Lasers in Engineering*, Vol. 28, pp. 343-376, 1997.

[2.23] Hassan, Y.A., and Philip, O.G., "A new artificial neural network tracking technique for particle image velocimetry", *Experiments in Fluids*, Vol. 23, pp.145-154, 1997.

[2.24] Scherer, J.O. and Bernal, L.P., "In-line holographic particle image velocimetry for turbulent flows", *Applied Optics*, Vol. 36, pp. 9309-9318, 1997.

[2.25] Trolinger, J.D., Lal, R.B., McIntosh, D. and Witherow, W.K., "Holographic particle-image velocimetry in the first international microgravity laboratory aboard the space shuttle Discovery", *Applied Optics*, Vol. 35, pp. 681-690, 1996.

[2.26] Vogel, A. and Lauterborn, W., "Time resolved particle image velocimetry used in the investigation of cavitation bubble dynamics", *Applied Optics*, Vol. 27, pp. 1869-1876, 1988.

[2.27] Chen, R.C. and Fan, L. -S., "Particle image velocimetry for characterizing the flow structure in three-dimensional gas-liquid-solid fluidized beds", Chemical Engineering Science, Vol. 47, pp. 3615-3622, 1992.

[2.28] Magness, C., Robinson, O. and Rockwell, D., "Unsteady crossflow on a Delta wing using particle image velocimetry", Journal of Aircraft, Vol. 29, pp. 707-709, 1992.

### CHAPTER 3

[3.1] Internet Page - [www.lascofittings.com/effects.htm](http://www.lascofittings.com/effects.htm)

[3.2] Internet Page - [www.water-hammer.com/liquid-dyn/graphics/shock.htm](http://www.water-hammer.com/liquid-dyn/graphics/shock.htm)

[3.3] Internet Page - [sellensr.me.queensu.ca/sellens/451/hammer.htm](http://sellensr.me.queensu.ca/sellens/451/hammer.htm)

[3.4] Clarke, D., "Introduction to water hammer", Chemical Engineer, No. 449, pp. 44-45, 1988.

[3.5] Kroon, J.R., Stoner, M.A. and Hunt, W.A., "Water hammer: Causes and effects", Journal American Water Works Association, Vol. 76, pp. 39-45, 1984.

[3.6] Weis, F., "Dispelling common misconceptions about water-hammer", Water Engineering and Management", Vol. 143, pp. 24-30, 1996.

[3.7] Kremers, J., "Avoid water-hammer", Hydrocarbon Processing, Vol. 62, pp. 67-68, 1983.

[3.8] Lobo, C.A.O.C. and Griffith, P., "Avoiding steam bubble collapse-induced water-hammer in the auxiliary piping of steam power plants", *Journal of Pressure Vessel Technology*, Vol. 116, pp. 49-56, 1994.

[3.9] Nakagawa, M. and Takenaka, T., "Damping and peak period shortening of water-hammer in collapse of a cooling cavity", *JSME International Journal Series B - Fluids and Thermal Engineering*, Vol. 38, pp. 300-307, 1995.

[3.10] Mortimer, S. and Edwards, D.C., "Avoiding water hammer in steam systems", *Specialist Inspector Reports*, No. 5, 1988.

[3.11] Mayhew, Y.R. and Rogers, G.F.C., "Thermodynamic properties of fluids and other data", *British Thermal Units*, Basil Blackwell, Oxford, 1965.

[3.12] Gruel, R.L., Huber, P.W. and Hurwitz, W.M., "Piping response to steam generated water hammer", *Journal of Pressure Vessel Technology Transactions of the ASME*, Vol. 103, pp. 219-225, 1981.

[3.13] Stephenon, D., "Effect of air valves and pipework on water hammer pressures", *Journal of Transportation Engineering-ASCE*, Vol. 123, pp. 101-101, 1997.

[3.14] Zhong, P., Chuong, C.J., Preminger, G.M., "Propagation of shock waves in elastic solids caused by cavitation microjet impact :2 Application in extracorporeal shock-wave lithotripsy", *Journal of Acoustical Society of America*, Vol. 94, pp. 29-36, 1993.

[3.15] Hammond, D.A., Amateau, M.E. and Queeney, R.A., "Cavitation erosion performance of fiber-reinforced composites", *Journal of Composite Materials*, Vol. 27, pp. 1522-1544, 1993.

[3.16] Perusich, S.A. and Alkire, R.C., "Ultrasonically induced cavitation studies of electrochemical passivity and transport mechanism: 1", *Journal of Electrochemical Society*, Vol. 138, pp. 700-707, 1991.

[3.17] Clarke, D., "Water-hammer: 2", *Chemical Engineer*, No. 457, pp. 14-15, 1989.

[3.18] "Air spring cushion water-hammer", *Machine Design*, Vol. 67, pp. 58, 1995.

[3.19] Azoury, P.H., Baasiri, M. and Najm, H., "Effect of valve closure schedule on water hammer", *Journal of Hydraulic Engineering-ASCE*, Vol. 112, pp. 890-903, 1986.

## CHAPTER 5

[5.1] *Hydratron Power Pack Manual*, Hydratron Ltd. Broadheath.

[5.2] *Fawcett Christie Accumulator Manual*.

[5.3] *MOOG E760 Series Servovalve Manual*, MOOG Controls Ltd., Tewkesbury.

## CHAPTER 6

[6.1] Internet Page - [www.mech.ed.ac.uk/~ally/thesis/node84.html](http://www.mech.ed.ac.uk/~ally/thesis/node84.html)

[6.2] Lawson, N.J., "The application of particle image velocimetry to high speed flows", PhD Thesis, Loughborough University, 1995.

[6.3] Drain, L.E., "The Laser Doppler Technique", John Wiley & Sons Ltd., Chichester, 1980.

[6.4] Ashby, M.F. and Jones, D.R.H., "Engineering Materials 2", Elsevier Science Ltd., Oxford, 1994.

[6.5] Clarke, D., "Introduction to water hammer", Chemical Engineer, No. 449, pp. 44-45, 1988.

[6.6] Work, K., "Thermodynamics", Third Edition, McGraw-Hill Book Co., NY, 1977.

[6.7] Rogers and Mayhew, "Engineering Thermodynamics".

[6.8] Keller, F.J., Gettys, W.E. and Skove, M.J., "Physics Classical and Modern", Second Edition, McGraw-Hill, Inc., NY, 1993.

